STABLE ISOTOPE AND GEOCHEMICAL SOURCE-TRACKING OF GROUNDWATER AND SURFACE WATER POLLUTION TO KĀNE‘OHE BAY, HAWAI‘I

A THESIS SUBMITTED TO THE GRADUATE DIVISION OF THE UNIVERSITY OF HAWAI‘I AT MĀNOA IN PARTIAL FULFILLMENT OF THE REQUIREMENTS FOR THE DEGREE OF

MASTER OF SCIENCE

IN

GEOLOGY AND GEOPHYSICS

AUGUST 2018

By

Daniel E. Dores

Thesis Committee:

Craig R. Glenn, Chairperson

Brian Popp

Robert Whittier

Keywords: groundwater, onsite sewage disposal systems, local meteoric water line, nitrogen, stable isotopes, submarine groundwater discharge, wastewater, dissolved inorganic carbon

ACKNOWLEDGMENTS

I thank advisor and committee chair Craig Glenn for conceiving and developing this project and securing its funding, and my committee members Brian Popp and Robert Whittier for their support and expertise over the past two years. Their knowledge and guidance has elevated the content and presentation of the research herein.

We thank Michael Mathioudakis, Trista McKenzie, and Daniel Litchmore for help in the field, and Natalie Wallsgrove, Danilo Licudine, and Catherine Rong for help in the lab. Special thanks are offered to the community members of Kahaluʻu, especially Ken LeVasseur, for assistance with the project, as well as private land owners and those who offered groundwater well access. We also thank the Honolulu Board of Water Supply, Lyon Arboretum, Division of Land and Natural Resources, Honolulu Botanical Gardens, Waimanalo Wastewater Treatment Plant, Hawaiʻi Department of Health, Waimea Valley, Hawaiʻi Agriculture Research Center for land use permissions. This research was supported by grants to C.R. Glenn from the Hawaiʻi Department of Health, the U.S. Geological Survey State Water Resources Research Institutes Program, and a grant/cooperative agreement from the National Oceanic and Atmospheric Administration, Project R/WR-2, which is sponsored by the University of Hawaiʻi Sea Grant College Program, SOEST, under Institutional Grant No. NA14OAR4170071 from NOAA Office of Sea Grant, Department of Commerce. The views expressed herein are those of the author and do not necessarily reflect the views of NOAA or any of its sub-agencies UNIHI-SEAGRANT-XM-16-03. It is also supported by grants to D.E. Dores from the Geological Society of America, University of Hawaiʻi Harold T. Stearns Fellowship, and L. Stephen Lau Research Scholarship.

Ultimately, I thank my family and loved ones who supported me for the duration of this research and the years leading to it, and for all they have done to give me this opportunity.

ABSTRACT

Improved understanding of water resources and their contamination is an emerging priority for Pacific Islands to protect limited freshwater supplies, prevent environmental degradation in coastal environments, and improve public health. This study addresses these concerns through understanding island-wide groundwater recharge and pollution pathways to groundwater and the coastal ocean on the island of Oʻahu, particularly in the Kahaluʻu region of Kāneʻohe Bay of east Oʻahu. We investigate delivery and differentiation of contaminated groundwater to streams and nearshore coastal waters in the Kahaluʻu region as a system representative of pollution dynamics in Pacific Islands. In this region, nutrient pollution is primarily sourced from onsite sewage disposal system (OSDS) release of untreated wastewater to the environment. OSDS usage is a widespread wastewater management practice in the U.S. and Pacific Islands, and OSDS coverage (unites per area) in the Kahaluʻu region is one of the densest in the State of Hawaiʻi, creating a marquee study for dynamics of raw sewage inputs to groundwater in aquifers of volcanic rock and valley fill sediments.

A multi-tracer investigation of water contamination in the Kahaluʻu region, including nutrient concentrations, stable nitrogen and oxygen isotopic compositions of nitrate, boron concentrations and isotopic composition, and common ion concentrations, identified locations of nutrient pollution to groundwater, streams, and nearshore environments. OSDS leachate is the primary source of nutrient pollution in the region, followed by agriculture. Shallow groundwater flow transports wastewater-derived nutrients to streams and submarine groundwater discharge (SGD), which in turn transports these nutrients to coastal environments and Kāneʻohe Bay. In coastal settings, our isotopic measurements of nitrogen in *Rhizophora mangle* (red mangrove) foliage suggest further investigations are merited in *R. mangle* as a potentially promising new method of coastal pollution monitoring. In sum, the Kahaluʻu–Kāneʻohe Bay study presents a "type example" of transportation schematic of Pacific Island OSDS-sourced nutrient delivery through groundwater aquifers to fresh and saline surface waters as a function of OSDS density, unit distance to the water body, geochemical mixing and transformation dynamics, and local and regional subsurface variations that can exist between deep and shallow groundwater.

Congruent and ancillary to the above, an island-wide study of the stable hydrogen and oxygen isotopic compositions of precipitation was completed in order to better understand

relationships between groundwater, seasonality of precipitation, and locations of recharge. Results from a network of 16 precipitation collectors deployed for 1 year reveal that O‘ahu’s groundwater recharge is dominated by wet season precipitation and high altitudes, as opposed to dry season rainfall and the island’s coastal plains. In addition, we catalogue the first geospatial distribution of hydrogen and oxygen isotopic compositions of rainfall for O‘ahu and create the first local meteoric water line for O‘ahu. Combined with $\delta^{2}H$ and $\delta^{18}O$ values of groundwater, we derive localized groundwater recharge to regional aquifer storage. Results align with flow regimes interpreted in previous studies of O‘ahu’s hydrogeology.

CONTENTS

LIST OF FIGURES

LIST OF TABLES

CHAPTER 1. INTRODUCTION

Fresh water and coastal system resources are a management priority in light of global climate change and localized urban development, particularly in Pacific Island settings. Threats of saltwater intrusion from sea level rise, pollution from land-use practices, and lack of adequate wastewater treatment threaten the sustainability of fresh groundwater and surface water resources on these islands. This project focuses on two scientific priorities of water resource management on the island of Oʻahu, Hawaiʻi: (1) evaluating the scale of wastewater pollution to a coastal watershed-aquifer system and ensuing nutrient attenuation in the natural environment and (2) understanding the precipitation patterns that contribute to aquifer recharge.

Chapter 2 encompasses the study of aquatic wastewater-borne nutrient pollution in the Kahaluʻu region of windward Oʻahu, a location identified by the Hawaiʻi Department of Health (HDOH) as a cesspool upgrade priority 1 location (HDOH, 2018). Usage of onsite sewage disposal systems (OSDS), including cesspools, is common worldwide in areas with limited municipal wastewater treatment capacity, and the Hawaiian Islands are no exception. Pacific Island communities utilize OSDS like cesspools and septic tanks where geographic isolation, economic challenges, and geologic barriers prevent installation of a sewer collection system for delivery to wastewater treatment plant where sewage receives a higher level of treatment. The Kahaluʻu region of Kāneʻohe Bay is one of Oʻahu's most OSDS-dense regions and dominated by cesspool usage and groundwater and surface water quality are now at risk of pollution from minimally treated cesspool leachate as recognized by the HDOH. In all these regards, the Kahaluʻu study area is a prototypical example of a coastal volcanic island watershed representative of OSDS-wastewater management challenges.

Coastal submarine groundwater discharge (SGD) and surface runoff fed by groundwater base flow to streams are the two primary transport mechanisms of terrestrially sourced nutrients to coastal environments and estuaries of Kāneʻohe Bay in the Kahaluʻu study region. Understanding effects that nutrient-rich wastewater leachate will have on natural nutrient cycling informs us of avenues to maximize the natural environment's potential to attenuate excessive nutrient loading in coastal environments. The study interprets the three major pathways for groundwater flow throughout a tropical volcanic aquifer in a coastal environment, the nutrient transport pathways in each system, and the impact of wastewater-borne nutrient loads from

OSDS. These three dominant flow paths include: (1) base flow from the deep aquifer to the upper reaches of the stream, (2) coastal SGD to the nearshore environment, and (3) shallow groundwater contributions to lower reaches of streams, including riparian zone buffering and hyporheic zone interactions. Through the assessment of these three delivery mechanisms, we highlight the effects of nutrient loads from wastewater leachate on the natural environment (Chapter 2). All data from Chapter 2 is available in Appendix 1.

Chapter 3, in turn, evaluates island-wide aquifer recharge on Oʻahu through a comparison of the isotopic composition of local groundwater and precipitation. As a state, Hawaiʻi sources 99% percent of its domestic water from groundwater (Gingerich and Oki, 2000). Therefore, knowledge of aquifer recharge locations and identification of sources of seasonal recharge to groundwater reservoirs is necessary for improved management of Oʻahu's freshwater resources. The results of this study delineate spatial and temporal recharge dynamics for the major aquifers of Oʻahu, as well as the general subsurface flow paths that dictate groundwater flow throughout the island. Such subsurface flow paths are important information for land-use management in the prevention of contaminant propagation throughout a watershed during groundwater flow. Chapter 2 illustrates this utility with a case study concerning flow paths in windward Oʻahu's Kahaluʻu region, which Chapter 2 expands upon to include wastewater leachate as the primary contaminant of concern. All data from Chapter 3 is available in Appendix 2.

The findings presented in Chapter 3 develop the first catalogue of precipitation δ^2H and $\delta^{18}O$ values on Oʻahu. Such data exist for many drinking and monitoring wells throughout the central and southeastern portion of the island from the United States Geologic Survey National Water-Quality Assessment (USGS NAWQA) Program. By pairing our network of precipitation δ^2H and $\delta^{18}O$ values with existing δ^2H and $\delta^{18}O$ data from the USGS NAWQA program, this study demonstrates the ease at which our precipitation isotopic data can be coupled with cost-effective analysis of the hydrogen and oxygen isotopic composition of groundwater to evaluate recharge potential and seasonal influence at any point on the island. In this work, documentation of a local meteoric water line (LMWL) for Oʻahu contributes to a growing body of work worldwide known as the global meteoric water line (GMWL). These meteoric water lines are linear relationships between the two hydrogen and oxygen isotope ratios measured in water (δ^2H and $\delta^{18}O$) and show local variations in comparison to the global trend.

CHAPTER 2. GEOCHEMICAL AND STABLE ISOTOPE SOURCE-TRACKING OF WASTEWATER CONTAMINATION PATHWAYS TO PACIFIC ISLAND COASTAL ENVIRONMENTS: EAST O‘AHU AND KĀNE‘OHE BAY, HAWAI‘I

Abstract

Onsite sewage disposal systems (OSDS) are a common wastewater management practice in Pacific Islands, but their widespread use has caused public health hazards and environmental degradation in these communities. Nutrients found in wastewater leachate, including effluent from properly functioning cesspools and malfunctioning septic tanks, are transported through groundwater to streams and nearshore coastal waters. The wet coastal watersheds, volcanic aquifers, and sedimentary fill of the Kahaluʻu region of Oʻahu, Hawaiʻi present an ideal setting in which to typify the natural biogeochemical cycling and fate of wastewater effluent on many Pacific Islands. A multi-tracer approach to distinguish nutrient pollution sources and distribution was employed, including DIN concentrations, $\delta^{18}O_{nitrate}$ and $\delta^{15}N_{nitrate}$ values, common ion concentrations, and boron (B) concentrations with $\delta^{11}B$ values. High NO_3^- concentrations and elevated $\delta^{15}N_{nitrate}$ values reveal wastewater presence in multiple streams and nearshore surface waters. High $\delta^{15}N$ values of mangrove foliage where local groundwater and surface water with elevated NO_3^- concentrations and $\delta^{15}N_{nitrate}$ values suggest *R. mangle* can incorporate wastewater-borne N species into plant biomass. B concentrations and $\delta^{11}B$ values were also used to differentiate agricultural and wastewater pollution, isolating one stream to be experiencing enriched nutrient loads from agricultural discharge. This study demonstrates the transportation schematic of OSDS-sourced nutrient delivery through the groundwater aquifer to fresh and saline surface waters of the study area as a function of OSDS density, unit distance to the water body, and regional subsurface hydrogeological variations between deep and shallow groundwater.

1. Introduction

Nutrient-rich wastewater leachate with high total nitrogen and phosphorus can reach the groundwater of Pacific Islands and increases pristine baseline concentrations, posing a serious environmental hazard and public health risk. Dissolved nitrate is a known contaminant to drinking water aquifers, regulated to concentrations under 10 mg L^{-1} (714 μM) by the World

Health Organization (WHO, 2011) and U.S. Environmental Protection Agency (U.S. EPA, 2018) due to adverse health effects such as methemoglobinemia. In the presence of agricultural fertilizer inputs and leachate of untreated or minimally treated wastewater, nitrate concentrations in drinking water aquifers become at risk of exceeding this threshold. High-nutrient groundwater resulting from contamination by these sources is transported to streams and estuaries as base flow and to the shoreline as submarine groundwater discharge (SGD) (Giblin and Gaines, 1990). Such elevated nutrient content in nearshore waters can in turn result in environmental degradation and marine eutrophication (Anderson et al., 2002; Conley et al., 2009).

Islands across the Pacific struggle with wastewater management, as sewage-derived nutrient pollution to aquifers jeopardize their coastal environments and limited water resources, including aquifers and streams (UNEP, 2011). As municipal sewer systems are not available in many Pacific island communities, many residents use onsite sewage disposal systems (OSDS) including cesspools, septic tanks, aerobic units, and soil treatments, (GWP Consultants, 2007). Cesspools are one of the most common yet least efficient OSDS in wastewater treatment (Whittier and El-Kadi, 2014). The Hawaiian Islands alone have 110,000 OSDS, including 87,900 cesspools, from which an estimated 200.1 million L of cesspool effluent discharges to the subsurface daily (HDOH, 2018). Hawaiian cesspool installation is regulated to a distance of 3 feet (~1 m) between the bottom of the tank and the water table. Improper usage and failed maintenance of cesspools, septic tanks, and other OSDS on Pacific Islands result in leaching of untreated or minimally treated wastewater effluent to coastal aquifers and nearshore environments (Fujita et al., 2013; Rouse, 2013; Shuler et al., 2017; Abaya et al., 2018).

Enriched nutrient concentrations sourced from OSDS can be observable in groundwater, streams, and coastal environments of watersheds with high OSDS density (units per area) where wastewater leachate penetrates the water table, and their source as sewage leachate can be verified via primary and secondary wastewater tracers (Lusk et al., 2017; Aravena et al., 1993). We chose the Kahaluʻu watershed region on the east side of Oʻahu, Hawaiʻi as a "type example" OSDS-dense Pacific Island watershed to quantify and trace pathways and biogeochemical transformation of nutrient-rich wastewater leachate from cesspools and improperly maintained septic tanks (e.g. Babcock et al., 2014) through groundwater and streams to tropical coastal environments. Assessment of hydrologic pathways and geochemical transformations in tropical

volcanic island aquifers from recharge to base flow and SGD determines OSDS leachate delivery and trends in nutrient transport. Nitrogen species transformation throughout this transport plays a critical role in the ultimate nutrient content delivered to fresh groundwater, streams, and coastal environments. We further evaluate environmental efficacy for attenuation of excess nitrogen concentrations through mineralization of wastewater-borne organic nitrogen, nitrification, denitrification, and uptake of ammonium nitrite, and nitrate species into plant biomass. We found dissolved inorganic nitrogen concentrations across the study area in excess of locally defined baseline conditions and were able to successfully differentiate sources of such concentrations as wastewater or agriculture through our multi-tracer approach.

2. Background

2.1. Representative study area

The Kahaluʻu region on the island of Oʻahu, Hawaiʻi well represents a typical setting for biogeochemical cycling of wastewater-derived nitrogen (N) in tropical Pacific Island aquifers in transit to the ocean. Particularly, the region's basaltic aquifer, defined in section 2.3., is representative of the geology of populated Pacific linear volcanic island chains, including Samoa, French Polynesia, and the Cook Islands, excluding atolls (Neal and Trewick, 2008). The Kahaluʻu region is exemplary of the 2-fold geographic isolation categorical of any Pacific Island community that stems from an island's remote location coupled with on-island topographic divides and challenging natural environments, such as tropical jungles. Most importantly, Kahaluʻu's OSDS usage, outlined in section 2.2., is archetypal of municipal wastewater disposal challenges faced by all Pacific Islands (GWP Consultants, 2007; UNEP, 2011).

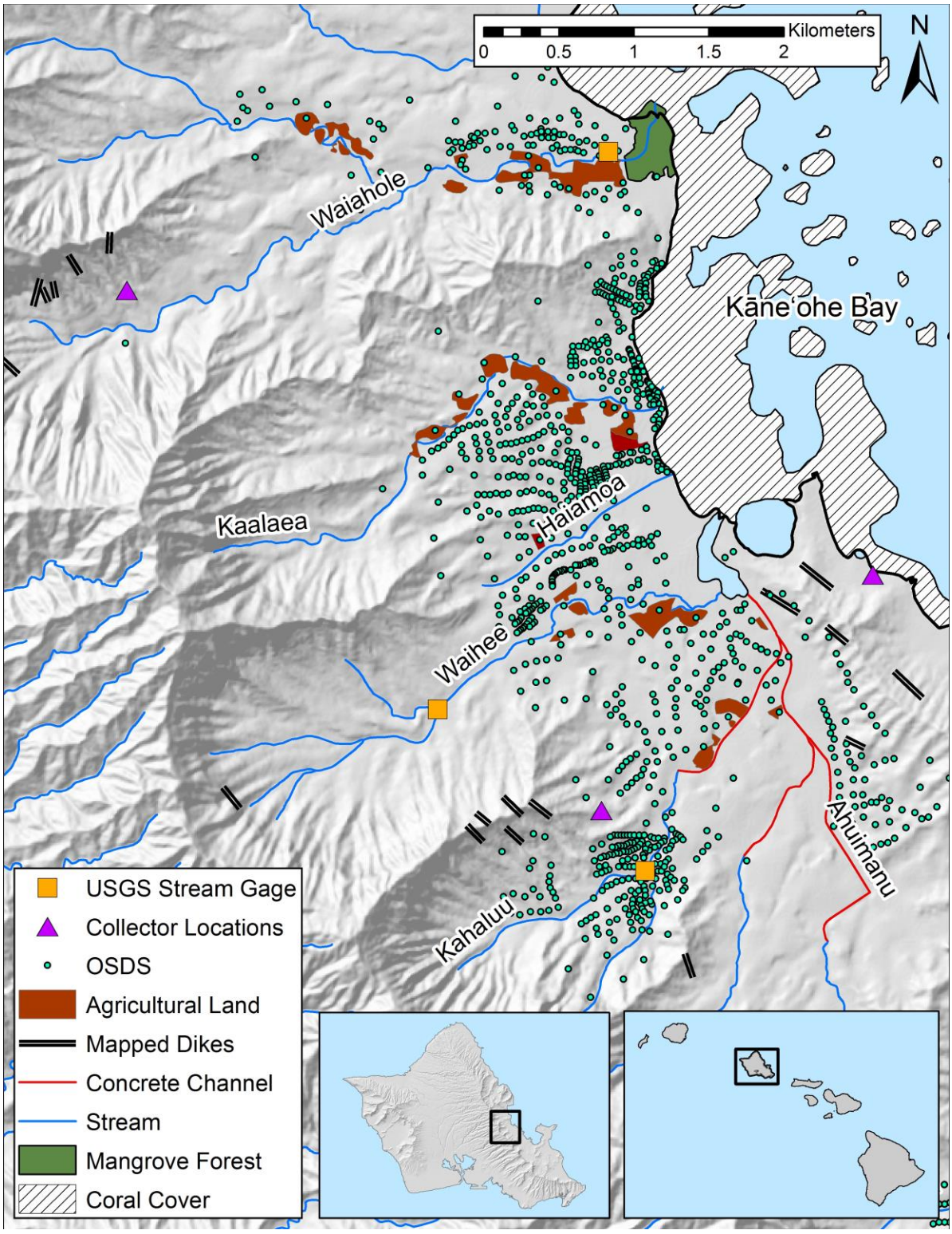

Figure 2.1. Shaded relief map showing land use and OSDS distribution of the Kahaluʻu region study area, as well as coral reef distribution in Kāneʻohe Bay. The study area's 940 OSDS units are shown as circles; density is highest along Kahaluʻu Stream, Kaalaea's coast, and in Haiamoa watershed. Agricultural land adjacent to streams is mapped as land parcels. Precipitation collectors and USGS stream gages are depicted as triangles and squares, respectively.

2.2. Kahaluʻu OSDS usage and historic nutrient pollution

Our study area (**Figure 2.1)** consists of 5 watersheds (Kahaluʻu, Waiheʻe, Haiamoa, Kaalaea, and Waiāhole) flanking Kāneʻohe Bay and contains one of the densest concentrations of suburban OSDS on Oʻahu (Whittier and El-Kadi, 2009). The 26 km^2 land area is one of the Hawaiʻi Department of Health's (HDOH) highest priority regions for cesspool upgrade, containing 940 OSDS, including 675 cesspools, within 3 km of the coast. Beaches in this area have witnessed numerous closures due to high counts of fecal indicator bacteria *Enterococcus* and *Chlostridium Perfringens* in the water, indicative of wastewater pollution (HDOH, 2018).

All groundwater and overland flow in the area discharges into Kāneʻohe Bay, Hawaiʻi's largest embayment at 41 km^2, which is home to a rich and diverse coral ecosystem and recreational waters of high cultural, aesthetic, and economic value (Cesar and van Buekering, 2004; van Beukering and Cesar 2004) containing one of Hawaiʻi's two coral barrier reefs. Sustained dissolved inorganic nutrient loads above baseline concentrations reduce coral vitality in such reefs (Bruno et al., 2003; Fabricius, 2005; Pastorok and Bilyard, 1985; Prouty et al., 2017; Redding et al., 2013; Wiedenmann et al, 2013). Previous direct sewage discharge into Kāneʻohe Bay in the 1960s, for example, resulted in increased dissolved inorganic nutrient concentrations leading to eutrophic conditions, a rise in native invasive macroalga *Dictyosphaeria cavernosa*, and a paradigm shift away from the coral-dominated ecosystem (Stimson et al., 2001; Smith et al. 1981; Hunter and Evans, 1995; Bahr et al., 2015). With an end to direct sewage discharge to Kāneʻohe Bay in 1979, corals recovered quickly, but are currently at risk of chronic stressors including freshwater kills (Bahr et al., 2015) and bleaching events (Bahr et al., 2017), which could be exasperated by high groundwater-derived nutrients to the Bay.

Sewage leachate from the Kahaluʻu region has Kāneʻohe Bay trending toward a potentially renewed tipping point in nutrient contamination. Nutrient concentrations can typically be highly elevated in SGD (e.g. Johannes, 1980, Johannes and Hearn, 1985; Burnett et al., 2003; Slomp and Van Cappellen, 2004; Kroeger and Charette, 2008; Moore, 2010; Bowen et al, 2007; Kim and Swarzenski, 2010; Moosdorf et al., 2015; Rodellas et al., 2015), particularly in the Hawaiian Islands (Garrison et al., 2003; Paytan et al., 2006; Johnson et al., 2008; Knee et al., 2008, 2010a,b; Street et al., 2008; Kelly, 2012; Kelly et al., 2013; Amato et al., 2016; Bishop et al.,

2017). Other Hawaiian volcanic aquifers show the ability to transport wastewater through aquifers to SGD in the coastal environment (Glenn et al. 2012, 2013; Fackrell et al., 2016), specifically in OSDS-dense regions (Richardson et al., 2016; Wiegner et al., 2016). Based on the Kahaluʻu region's modeled water table depth, most cesspools are anticipated to lack the proper 1 m buffer to the water table necessary for remediation of wastewater-borne nutrients (Dawes and Goonetilleke, 2003). With SGD estimates in the Kahaluʻu region of Kāneʻohe Bay being 2-4 times the volume of surface runoff (Dulai et al., 2016), persistent and unmonitored excessive nutrient loading from OSDS to the groundwater could lead to increased nutrient concentrations in the Bay paralleling 1960s sewage pollution conditions.

2.3. Hydrogeology of the Kahaluʻu regional study area

All five of the region's primary watersheds exist within the catchment of the Koʻolau Rift Zone aquifer of Oʻahu's Koʻolau Mountain Range, the erosional remnant of the Koʻolau shield volcano. What remains of the Koʻolau Range is the western half of the shield volcano following the loss of the volcano's eastern half, which slumped catastrophically into the Pacific (Moore, 1964) removing ~40% of the old volcano (Moore and Clague, 2002; Satake et al., 2002). Koʻolau volcanic rocks are comprised of Plio-Pleistocene age basalts, sporadically draped by Pleistocene-Holocene sedimentary deposits that infill valleys (Hunt, 1996), as illustrated in **Figure 2.2**. The volcanic rocks fall into four major categories: lava flows, pyroclastic deposits, dikes, and weathered basalt. Relatively impermeable vertical intrusive dikes greatly limit down-dip groundwater flow in the horizontal direction towards the ocean, creating a series of compartments of dike-impounded water (Takasaki et al., 1969). While laterally uncertain, within the study area dike compartmentalization likely stretches from the Koʻolau summits seaward through the coastal plain wetlands, and into the subsurface offshore (Takasaki and Mink, 1982) (**Figure 2.3**). Individual dikes are typically a meter or so thick and several kilometers in length. The rift zone dikes in this area are densely packed, increase in density towards the summits, and strike roughly NNW, extending along the caldera rift-zone axis (Walker 1986, 1987; Clague and Sherrod, 2014). Coastal sedimentary caprocks that would impede groundwater flow and SGD (e.g. Nichols et al., 1996) are notably lacking within the study area.

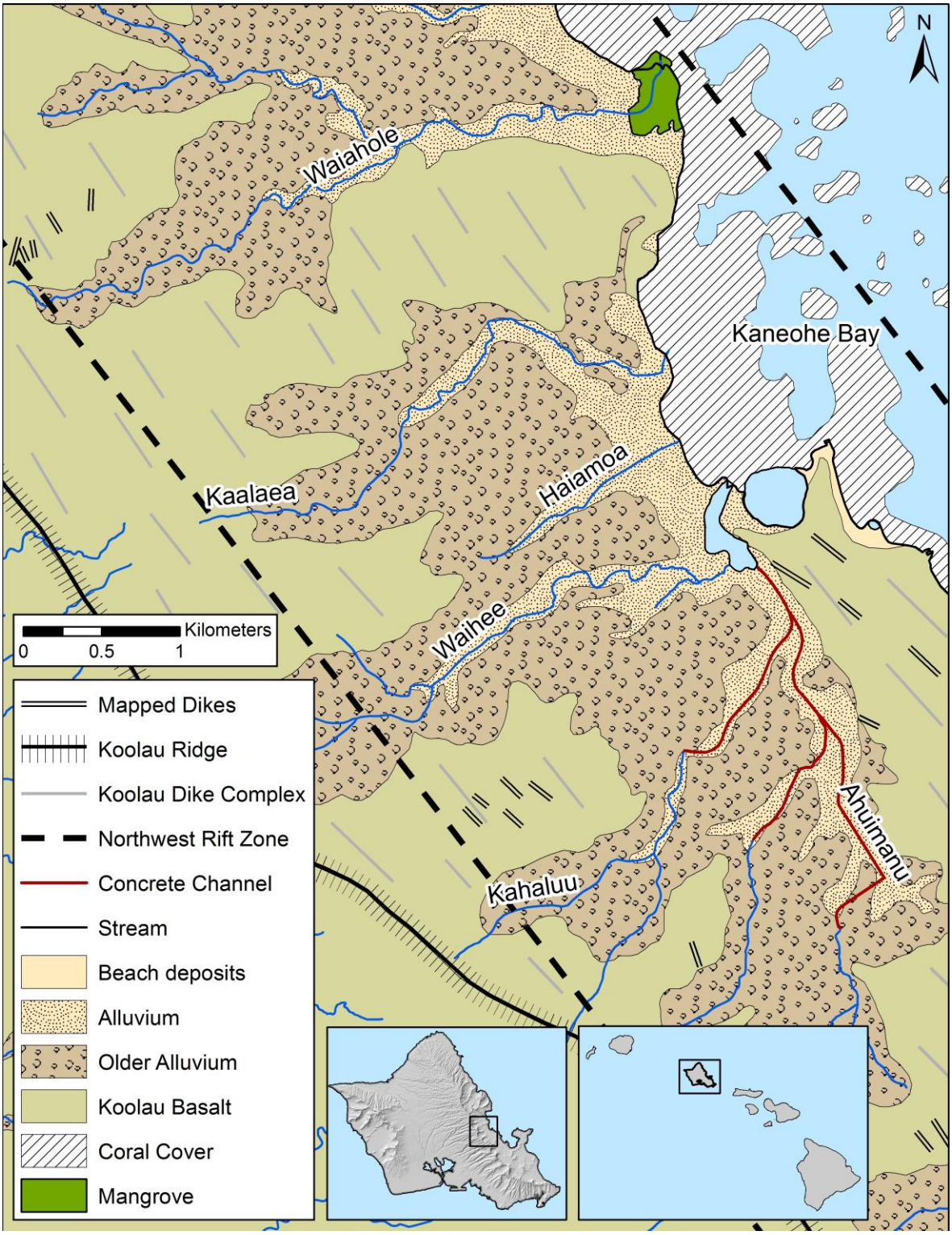

Figure 2.2. Geologic map of the Kahaluʻu region study area, located on the eastern side of the island of Oʻahu in the Hawaiian Island chain. Geologic units include the Koʻolau Basalt, Alluvium, Older Alluvium, and Beach Deposits. Structural units include the dike complex, both mapped and interpreted, in the Northwest Rift Zone. Notable surface features include streams, concrete channels, coral cover in Kāneʻohe Bay, and Waiāhole Mangrove Forest.

Fast infiltration of precipitation to aquifers in the region is aided by the high permeability of basalt (Takasaki and Mink, 1981); a permeable soil layer centimeters to a meter thick is underlain by several meters of weathered basalt, or saprolite (Hunt, 1996). Precipitation infiltrates downward through these layers and collects in dike-impounded reservoirs, which themselves leak down dip along inclination of the regional lava flows towards lower elevations. Groundwater contributes to stream flow as base flow where erosion has cut into the aquifer (Hirashima, 1971; Hunt, 1996). As discussed further below, due to the relative retardation of down-dip flow by the dike-ridden basalts in the area, much of the shallow-level groundwater flow in the Kahaluʻu region is funneled towards the ocean through the intervening valley fill colluvium and alluvium (Figure 2.2).

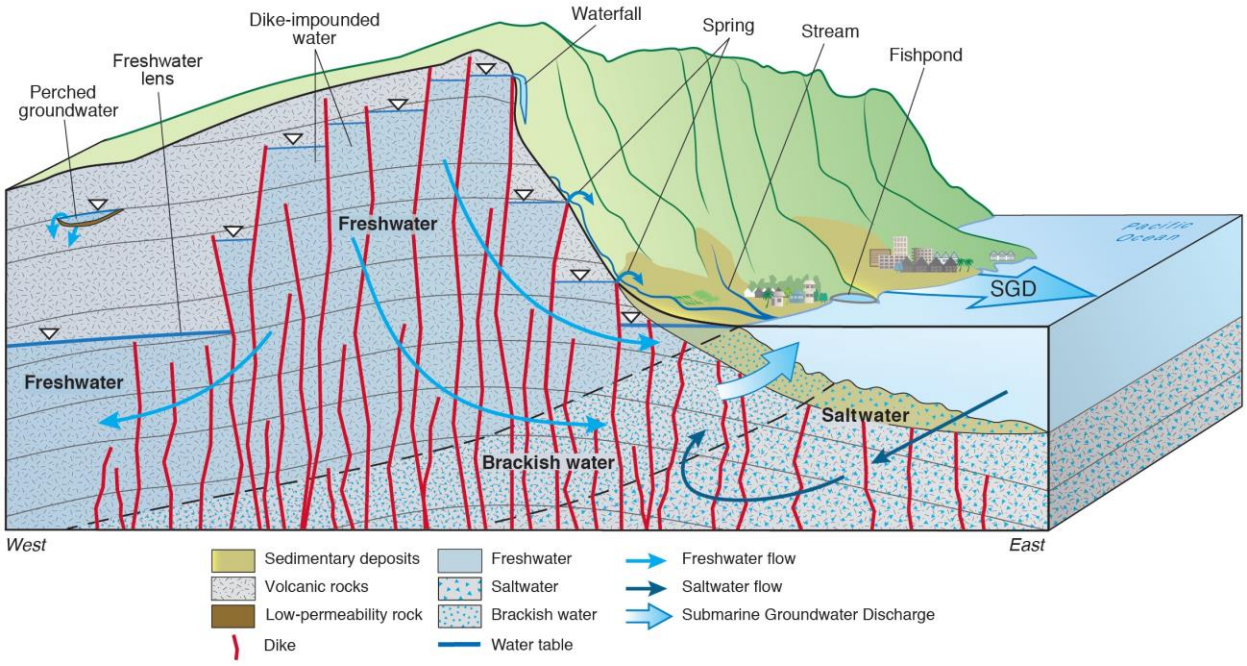

Figure 2.3. Conceptual geologic cross section of the Kahaluʻu regional study area, with Kāneʻohe Bay to the right, located on the eastern side of Oʻahu in the Hawaiian Island chain. Not to scale. After Cox, 1954; Peterson, 1972; Takasaki and Mink, 1981, 1982; MacDonald et al., 1983; Miller et al., 1999; Gingerich and Oki, 2000.

The Kahaluʻu region on windward Oʻahu is analogous to the geology of many shield volcanoes in the tropical Pacific, such as Maui, Hawaiʻi (Stearns and Vaksvik, 1935; Macdonald et al., 1983), and American Samoa (McDougall, 1985; Stearns, 1944). All these islands form from layers of basaltic rock intersected by dike complexes of varying size and density, similar to

those described above for windward Oʻahu (Macdonald et al., 1983; Walker and Eyre, 1995). Other regions of Pacific Islands, including leeward Oʻahu, experienced mass wasting events comparable to Koʻolau Volcano's collapse in the Kahaluʻu study region (Presley et al., 1997).

Tributary streams to Kāneʻohe Bay carry significant dissolved nutrient loads, especially after major rainstorms when streams experience event-based runoff influx (De Carlo et al., 2007; Hoover and Mackenzie, 2009), and together with SGD form the combined total coastal nutrient flux to the Bay (Hoover, 2002). In this study, OSDS-sourced nutrient loading is evaluated across five neighboring watersheds, each with their own centralized stream channel, land uses, and OSDS densities, discharging to four different nearshore and coastal environments: concrete channel, deltaic estuary, direct coastal discharge, and mangrove forest (**Table 2.1)**.

Table 2.1. Summary of watershed size, agricultural land area, number of OSDS, volumetric discharge, and discharge environment (USGS Pacific Islands Water Science Center; State of Hawaii Office of Planning Statewide GIS Program).

Stream	Size (km^2)	Ag. Land (km^2)	OSDS	Discharge (m^3/s)	Discharge Environment
Kahaluʻu	3.38	0.04	207	0.112	Concrete
Waiheʻe	5.86	0.08	155	0.19	Deltaic estuary
Haiamoa	1.66	0.02	222	0.025	Coastal
Kaalaea	4.56	0.14	233	0.043	Coastal
Waiāhole	10.22	0.17	87	1.10	Mangrove forest

2.4. Climate of the Kahaluʻu regional study area

Trade wind weather dominates Oʻahu's climate and the weather of the Kahaluʻu regional study area. Trade winds blow in a northeast to southwest direction and vary seasonally, being strongest from May to September (Blumenstock, 1961, Lyons, 1982; Schroeder, 1993; Giambelluca and Sanderson, 1993). Regional precipitation comes from orographic rainfall, as northeasterly trade winds lift moist air up to condense toward the peaks of the Koʻolau Mountains, the study area's western watershed divide. Resultantly, the Kahaluʻu region experiences two dominant seasons: a 5-month warm, comparatively "dry" summer of May to September and a 7-month cool, "wet" winter from October to April (Giambelluca and Sanderson, 1993). Mid-latitude frontal rain band storms, extratropical cyclones ("Kona storms"), and tropical cyclones comprise Kahaluʻu's additional wet season precipitation (Blumenstock, 1961; Schroeder, 1993). Oʻahu's precipitation is also subject to variability in the El Niño Southern Oscillation System (ENSO) (He and Pacific Climate Team, 2015). ENSO-neutral

conditions were observed by the National Oceanic and Atmospheric Administration (NOAA) in the 2017 dry season, but weak La Niña conditions persisted for at least the start of both the 2016-2017 and 2017-2018 wet seasons. From 1956-1982, the Hawaiian Islands typically receive more wet season rainfall under La Niña conditions. From 1983-2010, however, the Hawaiian Islands receive less wet season rainfall in La Niña conditions (O'Connor et al., 2015).

2.5. Mangroves in Kahaluʻu's coastal estuaries

Mangroves occur in 123 countries and territories globally (Spalding et al., 2010), and throughout Pacific Islands 12 nations and 4 territories host indigenous mangroves (Gilman et al., 2006). Numerous studies show the potential for mangroves to remove excess nutrients present in sewage effluent and serve as a means of wastewater filtration (Boonsong et al, 2003; Ouyang and Guo, 2016; Wong et al., 1997; Wu et al., 2008a; Yang et al., 2008). Mangroves were originally invasive to the islands of Hawaiʻi but today *Rhizophora mangle* trees are a locally dominant component of coastal estuaries in the Kahaluʻu study region and many other coastal environments on Oʻahu (Englund et al., 2000). This study investigates the ability of the red mangrove, *R. mangle*, to serve as a secondary wastewater treatment option in coastal tropical environments of a Pacific Island in response to OSDS-induced nutrient loading.

Mangroves reduce the amount of nitrogen and phosphorous in waters that pass through them by taking up dissolved nutrients (Reef et al., 2010) and trapping particulate nutrients through sediment and water retention (Adame et al., 2010). In regions where dissolved inorganic nutrient concentrations are high, mangrove forests serve as net receptors that trap nutrients within their biomass, resulting in improved water quality (Adame and Lovelock, 2011; Adame et al., 2010; Davis et al., 2003). *R. mangle*'s ability to retain sediment has improved water quality in some estuaries on Hawaiʻi (Allen, 1998; Englund et al., 2000) and in developed areas like Kahaluʻu, mangroves are expected to have substantially high total nitrogen and phosphorus accumulation, as shown in other developed regions by Sanders et al. (2014). Mangrove nutrient uptake is most efficient at salinities near 15, and is still successful at a salinity of 30 (Wu et al., 2008b). This allows mangroves to cover the full marine salinity tidal range in Hawaiʻi and provides them with an adaptive advantage over other wetland ecosystems (Demopoulos and Smith, 2010).

3. Materials and Methods

Water samples were collected from the five primary watersheds of the Kahaluʻu region (**Appendix 1**). Our sampling strategy delineates hydrologic flow paths for nutrient transport, assesses sources of nutrient loading as OSDS or agriculture, and determines the attenuation mechanisms for nutrient pollution in the natural environment. Groundwater samples were collected from municipal and private deep drinking water wells, shallow monitoring wells, riparian and hyporheic zone pore water, and beach face piezometers. Pore waters were accessed via push-point piezometer and peristaltic pump connected via 1.5 m-long silicone Masterflex tubing. Surface water samples were taken from streams, estuaries, and nearshore coastal waters, with coastal samples taken at low tide to increase the propensity of capturing fresh SGD at its maximum seaward flow (cf. Maher et al., 2013; Sadat-Noori et al., 2016). Basic water quality parameters including pH, salinity, total dissolved solids (TDS), specific conductivity (SpC), dissolved oxygen (DO), and temperature (T) were attained in-situ with an YSI EXO multi-parameter sonde. A description of each sampling method is found in sections 3.2. and 3.4.

Reconnaissance sampling occurred during Oʻahu's wet season in 2016 October. The majority of sample collection followed in the dry season from 2017 July to 2017 August. According to NOAA Hawaiian wet season rainfall summaries from 2017-2018, Oʻahu's 2017 dry season was El Niño Southern Oscillation System-normal (ENSO) and drier than normal. Wet season sampling took place in 2017 December and 2018 March. Oʻahu's 2017-2018 wet season had weak La Niña conditions in October 2017 lasting until April 2018. Overall, NOAA considers the 2017-2018 winter to be the 5th wettest seasons in the last 30 years for the Hawaiian Islands.

3.1. Endmembers

Endmembers include seawater, deep groundwater, stream headwaters, raw wastewater, and agricultural drainage. Seawater endmember samples came from two offshore samples in Kāneʻohe Bay free of freshwater influence. Deep groundwater endmember samples were from the municipal wells of the Koʻolau Range that supply drinking water. Stream headwater samples were taken from Kahaluʻu and Ahuimanu Streams where no OSDS exist up-gradient. Sewage endmembers samples were taken from two local septic tanks, and from Waimanalo Wastewater Treatment Plant (WWTP) untreated sewage, final clarifier wastewater, and sand filter effluent.

WWTP final clarifier wastewater is most representative of OSDS effluent because cesspools and septic systems allow suspended solids to settle from wastewater in the same manner as the final clarifier.

Agricultural endmember samples came from the drainage outflow pipe of an inundated Hawaiian taro paddy; these paddies divert water from the stream channels before discharge back to the stream. Other row crops and ornamentals are grown in the region, but taro farming appears to be the widely practiced agricultural activity, largely confined to Waiheʻe, Waiāhole, and Kaalaea watersheds. The primary fertilizer treatment for taro and row crops is organic material, with synthetic fertilizer being reported for some ornamental crops. The common organic fertilized consists of a fish bone meal (~60% fish scraps and 40% animal bone) (Reppun, 2016). The common "synthetic" fertilizer option for local agriculture is conventional urea fertilizer, not classified in organic fertilizer category by previous research in Hawaiʻi (Deenik, 2008).

3.2. Control watershed

Surface and pore water samples collected from Waiāhole Stream in Waiāhole watershed, the northernmost watershed of our study area (Figure 2.2), represent undisturbed N cycling dynamics and were thus chosen to represent a relatively un-impacted control stream for this study. Waiāhole watershed is separated from the southern watersheds of our study area by a dike-intruded basaltic ridge that serves as both a topographic divide for overland flow as well as a hydrogeologic barrier that we propose impedes groundwater flow between Waiāhole and the southern watersheds. Low OSDS usage and low OSDS density in Waiāhole watershed, coupled with the stream's high volumetric flux and limited development in the forest reserve, reduces the impact of wastewater leachate on stream water quality in the Waiāhole stream channel.

3.3. H and O isotopes for recharge assessment

Similar to that employed by Scholl et al. (2002) for East Maui, we constructed a local meteoric water line (LMWL) for the Kahaluʻu study area to aid in identifying areas of recharge using hydrogen and oxygen isotopic composition of precipitation and groundwater. A LMWL is a regional aspect of the global meteoric water line (GMWL), which relates δ^2H and $\delta^{18}O$ values measured in precipitation (Craig, 1961). LMWLs account for regional variation (Dansgaard,

1964) in the H and O isotopic composition of rainfall, creating an expected trend between δ^2H and $\delta^{18}O$ values in local precipitation at a site. The volume-weighted average (VWA) of precipitation samples was used to provide the annual estimate of the isotopic composition of regional recharge according to the equation

$$Volume\ Weighted\ Average = \frac{\sum_{i=1}^{n}(P_i * \delta_i)}{\sum_{i=1}^{n} P_i} \quad \textbf{(Equation 2.1)}$$

where δ_i represents the $\delta^{18}O$ or δ^2H value of the sample, *P* is the volume in mL of the sample, and *n* is the total number of samples utilized in the summation (Jaeschke et al., 2011).

We compared VWA δ^2H values in precipitation to δ^2H values of Kahaluʻu groundwater to confirm local precipitation as the source of regional aquifer recharge (cf. Scholl et al., 1996; Scholl et al., 2015). Similarly, δ^2H values of shallow groundwater and subsurface pore waters were compared to test if the deep aquifer is derived from the shallow groundwater that reaches the streams as base flow and coastline as SGD. Lastly, we use regional stream δ^2H values to link surface flow back to base flow from both the deep and shallow groundwater of Kahaluʻu.

Precipitation collectors designed after Scholl et al. (1996) were installed in 2017 February in the upper reaches of Waiāhole and Kahaluʻu watersheds. An additional collector was installed in September 2017 at the coast of Kahaluʻu watershed to capture nearshore precipitation. Precipitation collectors consist of a 20 L HDPE bucket with lid and attached 110 mm diameter plastic Buchner funnel deployed on a small wooden platform with three metal legs (e.g. Scholl et al., 1996) with a spigot at the base to drain the collector. A 1-cm thick mineral oil layer prevents evaporation from the collector. Collectors were sampled every 3 months for seasonal resolution.

Groundwater samples for isotopic analysis were collected in HCl-washed 60 mL HDPE bottles from deep drinking water wells and shallower monitoring wells, springs, streams, beach-face piezometers, and estuaries. Isotopic composition of samples was determined at the University of Hawaiʻi School of Ocean and Earth Science and Technology (UH SOEST) Biogeochemical Stable Isotope Facility using a fully automated Picarro L2130-*i* WS-CRDS cavity ring down mass spectrometer with results expressed as δ-values in per mil (‰) relative to VSMOW. Sample precision for terrestrial water samples at 1 standard deviation was 0.45‰ for

δ^2H values and 0.15‰ $\delta^{18}O$ values from 10 duplicate pairs. Sample precision for precipitation samples at 1 standard deviation was garnered from a larger, island-wide data set with 0.39‰ for δ^2H values and 0.12‰ $\delta^{18}O$ values from at 1 standard deviation from 19 duplicate pairs.

3.4. Geochemical source-tracking

A multi-tracer approach was utilized in source tracking nutrient-borne wastewater contamination to identify pathways for environmental attenuation of dissolved inorganic nutrient loads throughout the watershed-aquifer system. Each approach and method is detailed separately below. The stable isotopic composition of NO_3^- was used to indicate presence or absence of wastewater leachate in the observed water body. To supplement these results, dissolved common ion concentrations of chloride (Cl^-), sulfate (SO_4^{2-}), and potassium (K^+) were used as secondary pollution indicators. Apart from the nutrient-rich leachate of OSDS present throughout the Kahaluʻu region, other causes of elevated dissolved inorganic nutrient loads include continuous drainage from agricultural plots and storm event-based runoff from urbanized regions and the aforementioned agriculture. Boron (B) concentrations and isotopic composition were used to distinguish wastewater sources from agricultural inputs in streams. Additionally, DIN composition and DO content were used to identify areas of high organic matter input and resultant degradation to delineate nutrient contributions from natural processes.

3.4.1. Nutrient concentrations

Concentrations of total nitrogen (TN), ammonia (NH_3), ammonium (NH_4^+), nitrate (NO_3^-), nitrite (NO_2^-), total phosphorus (TP), orthophosphate (PO_4^{3-}), and silicate (SiO_2) (cf. Hem, 1985) were analyzed in samples from across the study area collected from groundwater, streams, and coastal waters. NH_3+NH_4^+, NO_3^-+NO_2^-, and NO_2^- concentrations were the reported dissolved inorganic nitrogen (DIN) species, expressed in units of μM. Samples were collected in HCl-washed 500 mL HDPE screw top bottles and frozen until analysis at the HDOH State Lab with an AutoAnalyzer III (Seal Analytical, AA3). Sample precision at 1 standard deviation based on 14 duplicate pairs was as follows: 4.86 μM TN, 0.56 μM NH_3+NH_4^+, 1.27 μM NO_3^-+NO_2^-, 0.07 μM NO_2^-, 0.11 μM TP, 0.76 μM PO_4^{3-} and 44.45 μM SiO_2.

3.4.2. Dual isotopic composition of NO_3^-

$\delta^{15}N_{nitrate}$ and $\delta^{18}O_{nitrate}$ values were used to infer NO_3^- source through the dual isotope approach (Xue et al., 2009; Liu et al., 2006), with endmembers being OSDS-sourced wastewater, degrading organic matter, and agricultural drainage/runoff. $\delta^{15}N$ and $\delta^{18}O$ of NO_3^- values can be used to approximate NO_3^- from wastewater, agricultural fertilizers, and natural soil inputs (Kendall and McDonnell, 1998; Kendall et al., 2007). For example, Kendall and McDonnell (1998) report that most NO_3^- sourced from NH_4^+ in fertilizer, which in our area would be the "synthetic" urea option, have $\delta^{15}N_{nitrate}$ values between -7 and 5‰, soil has $\delta^{15}N_{nitrate}$ values between 3 and 8‰, and wastewater has $\delta^{15}N_{nitrate}$ values between 0‰ and 25‰. In our study region, organic fertilizers, like the fish blood meal, are common and thus potentially have a large range of $\delta^{15}N_{nitrate}$ values (2 to 20‰) (Kendall et al., 2007). As the N transformations in flooded taro fields characteristic of this region are both complex and intensive (Penton et al., 2012; Penton et al., 2014), this study therefore focused on quantifying the agricultural drainage discharge of the agroecosystem as effluent released to streams as an endmember. We assume atmospheric deposition of NO_3^- has little impact on NO_3^- concentration and resulting isotopic composition in the area due to high NO_3^- content and prevalence of other sources, including OSDS, agricultural drainage, and high-vegetation land cover. Thus, isotopic composition of NO_3^- serves as one important proxy to identify the source of the measured NO_3^- load.

Samples for stable isotopic composition of NO_3^- were collected in HCl-washed 60 mL HDPE bottles, filtered (0.45 μm), and frozen prior to analysis. NO_3^- isotopic compositions were determined at UH SOEST Biogeochemical Stable Isotope Facility using a Finnigan Mat252 coupled to a GasBench II with denitrifying bacteria for N_2O gas analysis as described in Sigman et al., 2001 with USGS and NIST calibration standards. $\delta^{18}O_{nitrate}$ values are expressed in ‰ against VSMOW with sample precision of 0.63‰ determined as 1 standard deviation based on 26 duplicate pairs; $\delta^{15}N_{nitrate}$ is listed against AIR with sample precision of 0.32‰ determined as 1 standard deviation based on 26 duplicate pairs.

3.4.3. Boron concentrations and isotopic compositions for agricultural differentiation

The concentration of B and $\delta^{11}B$ values help distinguish NO_3^- sources as B behaves conservatively and NO_3^- and B are often transported together in aquatic systems (Seiler, 2005).

To be used as a tracer for NO_3^- sources, $\delta^{11}B$ values must be measured in all endmembers and each mixed pool sample. With a wide range of $\delta^{11}B$ values distinct for each source, the $\delta^{11}B$ value is uniquely suited to partition appropriate contributions of wastewater NO_3^- against agricultural NO_3^- (Widory et al., 2005). Four samples were taken for endmember analysis, and 10 locations were sampled for B and $\delta^{11}B$ for wastewater source-tracking, with 1 duplicate. Samples were collected in HCl-washed 250 mL HDPE screw top bottles and refrigerated. Analyses were performed at Stony Brook University Isotope Laboratory on NU ICP-MS. $\delta^{11}B$ values are reported in ‰ against NIST 951. Sample precision determined as 1 standard deviation was 0 ppb for B concentration and 0.39‰ $\delta^{11}B$ values based on 1 duplicate pair.

3.4.4. Dissolved common ions for pollution trends

Several ions serve as useful tracers of NO_3^- sources in water to augment the results of the dual isotope technique. These include Cl^-, SO_4^{2-}, and K^+, which are all elevated in domestic sewage (Xue et al., 2009). Samples were collected in HCl-washed 60 mL HDPE screw top bottles from deep and shallow groundwater wells, the five perennial streams of the study area, coastal waters including Kahaluʻu estuary, beach face piezometers, and streambed hyporheic zone. Concentrations of major common ions species were determined by ion chromatography at the Water Resources Research Center Analytical Chemistry Laboratory at UH Mānoa using a Dionex ICS-1100s(IC). Sample precision determined as 1 standard deviation was as follows: 12514 μM Cl^- based on 11 duplicate pairs, 680 μM SO_4^{2-} based on 11 duplicate pairs, 11170 μM Na^+ based on 11 duplicate pairs, 225 μM K^+ based on 10 duplicate pairs, 1594 μM Mg^{2+} based on 11 duplicate pairs, and 321 μM Ca^{2+} based on 11 duplicate pairs.

3.5. Aqueous carbonate geochemistry denitrification assessment

To assess the extent of organic matter degradation in the shallow subsurface, dissolved inorganic carbon concentration (DIC), $\delta^{13}C_{DIC}$ values, and total alkalinity (TA) were measured in groundwater. Carbon dioxide (CO_2) is a byproduct of organic matter oxidation (Froelich et al., 1979) and increases the DIC of the carbon pool (Manahan, 2010). Carbonate (CO_3^{2-}), bicarbonate (HCO_3^-), and aqueous CO_2 contribute to DIC. CO_3^{2-} is negligible in our system based on pH (Nascimento et al., 1997), and the absence of carbonate rocks makes HCO_3^- the

dominant species. Subsurface suboxic to anoxic systems where denitrification occurs have low NO_3^-, low DO, low $\delta^{13}C$ values of DIC, and high DIC due to increases in CO_2 produced during organic matter degradation (Ding et al., 2014). Effectively, TA consists of HCO_3^- and CO_3^{2-} concentrations in the water where other dissolved species such as $B(OH)_4$ ions are negligible (Libes, 2009; Manahan, 2010). $CO_{2(aq)}$ does not directly contribute to TA and is therefore indicative of excess CO_2 produced by organic matter decomposition. Thus, if DIC values exceed expected concentrations, the difference is predicted to be the undissociated CO_2 produced by organic matter degradation. For this degradation, reduction of oxygen is the preferred metabolic pathway, followed by the reduction of NO_3^-, or denitrification, as per the simplified reaction

$$5CH_2O + 4NO_3^- \rightarrow CO_2 + 2N_2 + 3H_2O + 4HCO_3^- \quad \textbf{(Equation 2.2)}$$

where "CH_2O" represents a simple organic molecule oxidized by NO_3^- (Berner, 1980).

Samples for dissolved carbonate geochemistry were taken from subsurface waters including deep groundwater wells, monitoring wells, shallow wells, and stream bank and beach face piezometers. DIC and TA samples were collected in 500 mL HCl-washed borosilicate bottles combusted at 500 °C. Samples for inorganic carbon isotope analysis were collected in 40 mL borosilicate vials sealed with septa and aluminum crimp-top. All samples were filtered to 0.45 μm, preserved with 3 μL saturated $HgCl_2$ solution, and stored in a cool dry location until analysis. DIC and TA was analyzed at the UH SOEST Laboratory for Analytical Biogeochemistry (S-LAB) using a Metrohm 905 Titrando for TA and UIC Coulometer and Marianda VINDTA3D acidification unit for DIC. $\delta^{13}C$ values of DIC were determined at the University of Utah Stable Isotope Ratio Facility for Environmental Research using a Thermo Scientific Gas Bench II coupled to a Thermo Scientific MAT 253 IRMS via Thermo Scientific Conflo IV device. Marble calibrated against NSB-19, Carrara, and LSVEC carbonate standards were used to normalize samples with $\delta^{13}C_{DIC}$ results reported in ‰ relative to PDB. Sample precision at 1 standard deviation was as follows: 19.74 μmol kg^{-1} DIC based on 3 duplicate pairs, 19.5 μmol kg^{-1} TA based on 3 duplicate pairs, and 0.32‰ $\delta^{13}C_{DIC}$ based on 2 duplicate pairs. The 3rd duplicate pair for $\delta^{13}C_{DIC}$ was 7.8‰ different from the primary sample, leading the authors to

believe mishandling occurred during sample analysis, as no other parameters (i.e. DIC concentration, NO_3^- concentration) showed such variability in this duplicate.

3.6. $\delta^{15}N$ of mangrove leaves for biomass uptake

Foliar nitrogen (N) isotopic compositions serve to represent N-cycling in plants and localized ecosystems that may be indicative of the source of N incorporated into plant tissues (Mayor et al., 2014). Similar to the use of $\delta^{15}N$ values in marine macroalgae as potential wastewater tracer (e.g. Dailer et al., 2010; Amato et al., 2016), recent studies show mangrove foliage in agricultural drainage canals of Florida (Fry et al., 2000) and other coastal wetland plants across Hawai‘i subject to wastewater leachate (Bruland and MacKenzie, 2010) to have $\delta^{15}N$ values higher than those plants growing in the absence of anthropogenic effluent.

In the study area, mangrove coverage includes a forest at the coastal discharge point of Waiāhole Stream, a dense thicket in Kahalu‘u estuary at the Waihe‘e Stream discharge point, and shoreline mangrove coverage south of Kaalaea outlet, continuing south of Haiamoa Stream, providing a range of up-gradient OSDS densities. Mature *R. mangle* leaves were taken from the lower crown of adult mangrove trees in areas of new growth and stored in sterile airtight plastic bags at room temperature. Samples were devoid of disease, biological or structural damage, and sediment encrustation. Leaf clippings from *R. mangle* were analyzed for carbon (C) content, N content, $\delta^{15}N$, and $\delta^{13}C$ values. Nutrient concentrations and $\delta^{15}N_{nitrate}$ values were measured in pore water and surface water from the mangrove forest (e.g. Bruland and Mackenzie, 2010). *R. mangle* samples were dried at 57 °C for 2 hours, ground, and homogenized. Foliar $\delta^{15}N$ and $\delta^{13}C$ values were measured at the UH SOEST Biogeochemical Stable Isotope Facility using a ThermoFinnigan Delta^{Plus} XP. Sample precision at 1 standard deviation was as follows: 1.30 μg N, 34.26 μg C, 0.28‰ $\delta^{15}N$, and 0.11‰ $\delta^{13}C$ based on 5 duplicate pairs.

3.7. Salinity corrections

To compare nutrient concentrations among individual samples collected with varying amounts of seawater dilution, samples were normalized to the fresh groundwater endmember as:

$$C_{source} = \frac{C_{sample} + (C_{sample} - C_{marine}) * (S_{sample} - S_{fresh})}{(S_{marine} - S_{sample})} \quad \textbf{(Equation 2.3)}$$

as "C" is concentration and "S" is salinity (Hunt and Rosa, 2009). Freshwater endmembers are water from Koʻolau Range groundwater wells and oceanic endmembers are regional seawater.

4. Results

A complete list of sample details, results, locations, and sampling times can be found in Appendix 1 of this thesis. In most samples, NO_2^- is negligible at less than .071±0.07 µM, allowing the reported NO_2^-+NO_3^- value to serve as a proxy for NO_3^- (mapped in **Figure 2.4**), which is hereafter referred to simply as NO_3^-. A combined NH_3+NH_4^+ concentration was reported for all samples. Based on measured pH and the known pKa value for the conjugate acid-base pair (~9.25), NH_4^+:NH_3 was calculated for all samples. 140 out of 177 samples indicate NH_4^+ > 90% of the measured NH_3+NH_4^+ concentration, and another 21 have at NH_4^+ > 80%. Only five samples have NH_3 > 50%. Thus, we hereafter refer to the combined NH_3+NH_4^+ measured concentration simply as NH_4^+.

Table 2.2. Geochemistry of the wastewater nutrient concentrations and NO_3^- isotopic composition for the wastewater endmembers of this study. Indicated uncertainties are plus or minus 2 standard deviations.

Sample	$\delta^{15}N$ NO_3^- ‰	$\delta^{18}O$ NO_3^- ‰	PO_4^{3-} µM	TP µM	NH_4^+ µM	NO_3^- µM	TN µM	SiO_2 µM
WWTP Sand Filter	26.0±0.3	11.8±0.6	48.9±0.8	50.3±0.1	315.2±0.6	188.9±1.3	558.6±4.9	1078±44.5
WWTP Final Clarifier	24.1±0.3	5.7±0.6	31.3±0.8	35.4±0.1	202.1±0.6	271.0±1.3	474.9±4.9	1070±44.5
WWTP Raw Influent	--	--	134.3±0.8	151.2±0.1	3534.7±0.6	0.4±1.3	3855.4±4.9	1023±44.5
Septic Tank 1	--	--	249.5±0.8	262.9±0.1	4620.9±0.6	0.9±1.3	5484.7±4.9	469±44.5
Septic Tank 1 (D)	--	--	253.5±0.8	262.6±0.1	4719.9±0.6	1.1±1.3	5606.2±4.9	500±44.5
Septic Tank 2	--	--	290.9±0.8	341.9±0.1	5506.2±0.6	3.3±1.3	5878.8±4.9	389±44.5

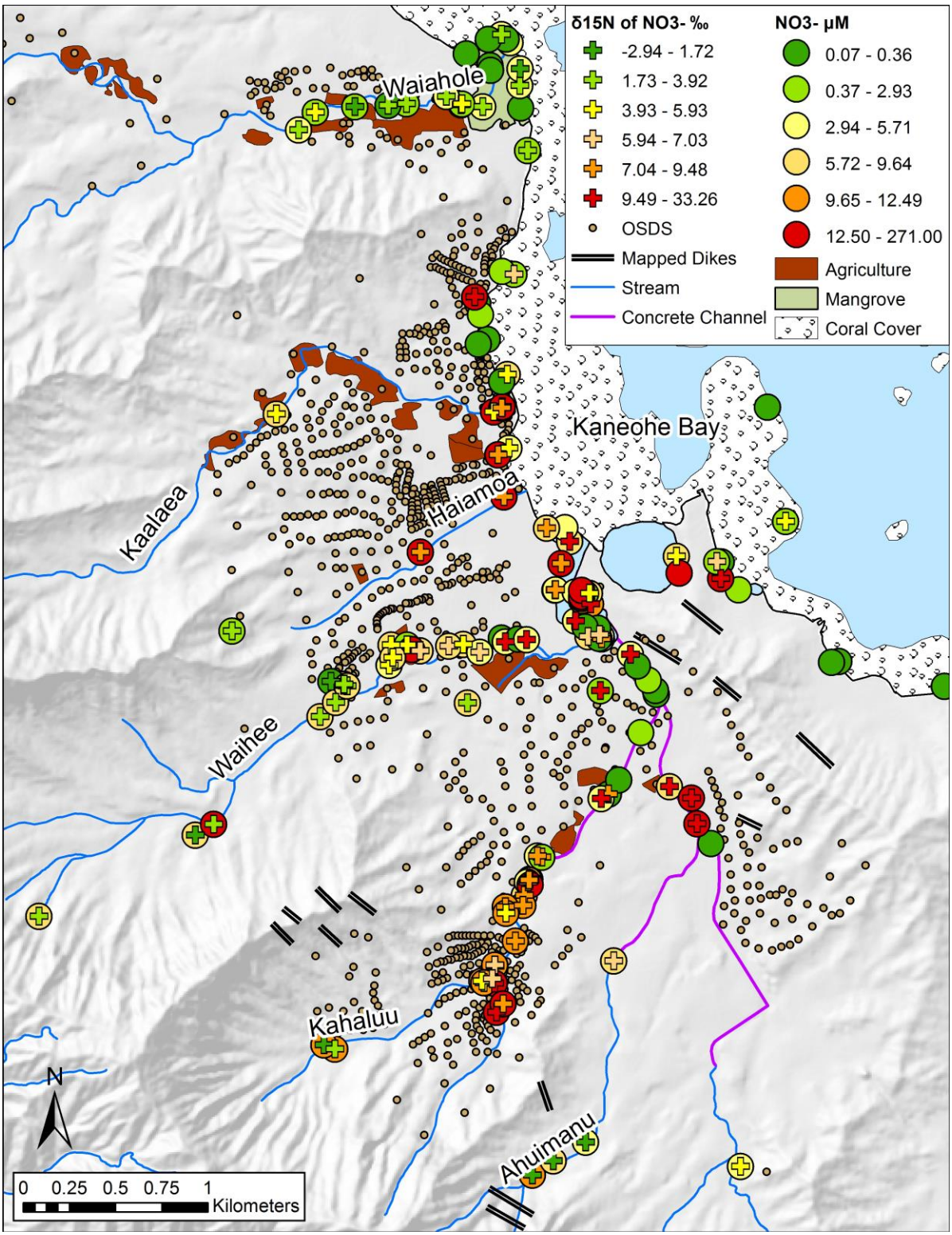

Figure 2.4. Map of color-coded NO_3^- concentration (as circles) and $\delta^{15}N_{nitrate}$ values (as crosses) for the study area. Higher NO_3^- concentration and $\delta^{15}N_{nitrate}$ values are displayed in red, and lower NO_3^- concentration and $\delta^{15}N_{nitrate}$ values are displayed in green.

Table 2.3. Summary of averaged nutrient concentrations, nitrate isotopic composition, salinity, and dissolved oxygen for all endmembers in the study and Waiāhole control watershed. Indicated uncertainties are plus or minus 2 standard deviations. The data for this table is in Appendix 1.

Type	N	$\delta^{15}N$ NO_3^- ‰	$\delta^{18}O$ NO_3^- ‰	ODO (% sat)	PO_4^{3-} µM	TP µM	NH_4^+ µM	NO_3^- + NO_2^- µM	TN µM	SiO_2 µM
Agriculture	1	9.5±0.3	9.0±0.6	--	21.1±0.8	19.5±0.1	7.1±0.6	23.2±1.3	38.8±4.9	536±44.5
Deep Groundwater	7	2.9±0.3	1.5±0.6	84.3	1.5±0.8	1.6±0.1	0.2±0.6	8.8±1.3	12.1±4.9	466±44.5
Ocean	2	4.1±0.3	5.1±0.6	128.9	0.2±0.8	0.23±0.1	1.4±0.6	0.5±1.3	4.61±4.9	8±44.5
Wastewater	6	25.0±0.3	8.8±0.6	38.6	168.1±0.8	184.0±0.1	3149.8±0.6	77.6±1.3	3643.1±4.9	755±44.5
Waiāhole Control Stream	10	2.3±0.3	1.4±0.6	99.1	1.1±0.8	0.6±0.1	1.2±0.6	3.0±1.3	7.0±4.9	503±44.5

4.1. Nutrient pollution endmembers and the control watershed

Sewage-source endmembers are heavily enriched in TN and TP from all wastewater sources, with high concentrations of common ions Cl^-, SO_4^{2-}, K^+, Ca^{2+}, and Mg^{2+}. **Table 2.2** displays the full array of nutrient concentration and NO_3^- isotopic composition for wastewater sources. The majority of TP is PO_4^{3-} at all three stages of the WWTP and both tanks of the Kahaluʻu septic system. Both tanks have TN an order of magnitude greater than any field location. NO_3^- is low in the raw sewage component of both the WWTP and OSDS while NH_4^+ concentration is extremely high. Secondary and tertiary treatments at the WWTP substantially reduce NH_4^+ by an order of magnitude while increasing NO_3^-. Both septic tanks have high NH_4^+ and low NO_3^-. $\delta^{15}N_{nitrate}$ values are high in the secondary and tertiary WWTP stages. $\delta^{18}O_{nitrate}$ values increase from the final clarifier to the sand filter, with sand filter $\delta^{15}N_{nitrate}$:$\delta^{18}O_{nitrate}$ aligning closer with the literature "denitrification trend" ratio (Kendall and McDonnell, 1998; Kendall et al., 2007). In wastewater, TP and PO_4^{3-} concentrations are 1 order of magnitude higher than any other endmember, TN concentration is 2 orders of magnitude higher than any other endmember, and NH_4^+ concentration is 3 orders of magnitude higher than any other endmember (**Table 2.3**).

Our agriculturally-sourced endmember comes from water sampled from taro paddy drainage effluent high in all nutrient concentrations except $Si(OH)_4$. This discharge has very low concentrations of all common ions. The full record of average geochemical composition of all other naturally occurring endmembers used in this study is found in Table 2.3, including Kāneʻohe Bay seawater and water from deep Koʻolau Range drinking water wells.

Waiāhole watershed is used as a relatively "pristine" comparative control watershed for the study area (Table 2.3) based on its low total OSDS (87), low OSDS density (8.5 units per km^2),

and its generally undeveloped landscape in which a forest reserve occupies the upper half of the watershed. NO_3^- concentrations in the Waiāhole control stream range from 0.1-4.7±1.3 μM, with an average of 3 μM; $\delta^{15}N_{nitrate}$ values range from 0.5-4.4±0.3‰, with an average of 2.3‰.

4.2. H and O isotopes for recharge assessment

The 12-month VWA of δ^2H value in precipitation is -9‰ at the Kahaluʻu ridgeline and -7.4‰ in Waiāhole watershed, with a propagated error of 0.8‰ based on the VWA calculated from 4 samples over 12 months. The 6-month VWA of wet season precipitation in Kahaluʻu at the coastline is -14.5‰, with a propagated error of 0.6 for two samples in 6 months. There is substantial change in δ^2H values across the study area based on sample type (n = 99). Stream average δ^2H is -9.2±0.5‰ (n = 28) and the concrete channel average δ^2H is -9.6±0.5‰ (n = 10). Deep groundwater average δ^2H value is -11.0±0.5‰ (n = 6), while shallow groundwater average δ^2H is -10.1±0.5‰ (n = 5) and fresh pore water average δ^2H is -9.0±0.5‰ (n = 17). As δ^2H values were far more variable across sample populations than $\delta^{18}O$ values, δ^2H values were the primary source tracker in these isotopic analyses of recharge and groundwater flow.

Table 2.4. Average nutrient concentrations, nitrate isotopic composition, salinity, and dissolved oxygen for all water bodies in the study. Indicated uncertainties are plus or minus 2 standard deviations. N includes duplicates.

Type	N	$\delta^{15}N$ NO_3^- ‰	$\delta^{18}O$ NO_3^- ‰	Sal.	ODO (% sat)	PO_4^{3-} μM	TP μM	NH_4^+ μM	$NO_3^- + NO_2^-$ μM	TN μM	SiO_2 μM
Estuary	18	8.8±0.3	3.8±0.6	5.9	87.8	0.9±0.8	1.3±0.1	23.2±0.6	10.0±1.3	22.9±4.9	377±44.5
Shallow Groundwater	9	6.8±0.3	3.4±0.6	0.3	47.2	1.8±0.8	2.8±0.1	37.8±0.6	4.5±1.3	57.5±4.9	487±44.5
Coastal	21	5.9±0.3	5.5±0.6	28.5	94.0	0.4±0.8	1.0±0.1	2.4±0.6	1.8±1.3	12.1±4.9	63±44.5
Fresh Pore water	19	12.9±0.3	6.5±0.6	0.2	46.8	0.7±0.8	1.4±0.1	8.9±0.6	13.2±1.3	41.2±4.9	569±44.5
Saline Pore water	16	19.8±0.3	10.7±0.6	14.9	37.6	1.0±0.8	2.1±0.1	33.3±0.6	2.8±1.3	22.4±4.9	344±44.5
Stream	70	6.4±0.3	3.7±0.6	0.2	93.9	1.0±0.8	1.1±0.1	4.2±0.6	11.9±1.3	22.8±4.9	479±44.5
Concrete Channel	10	8.8±0.3	7.2±0.6	0.1	118.7	0.5±0.8	0.4±0.1	3.3±0.6	5.5±1.3	44.1±4.9	421±44.5

4.3. Geochemical source-tracking

4.3.1. Nutrient concentrations

174 nutrient samples were collected and analyzed (Appendix 1) (**Table 2.4**). Overall, NO_3^- was the dominant DIN species in freshwater, deep oxygenated groundwater, hyporheic zone samples well connected to flowing stream water, and estuarine waters with a strong freshwater

influence. NH_4^+ was the dominant DIN species in shallow groundwater and pore water, oceanic samples, and estuarine samples dominated by seawater. In surface-groundwater sample pairs, NO_3^- was the greater DIN species in surface samples but NH_4^+ dominated in groundwater. Septic tank and WWTP DIN is dominated by NH_4^+; only in the final clarifier and sand filter of the WWTP do increased NO_3^- concentrations accumulate. Thus moving forward, we generally assume variations in NO_3^- concentration are representative of the quantity of nutrients transported to sampled waters, and NH_4^+ concentration as an indicator distance from the N contaminant source.

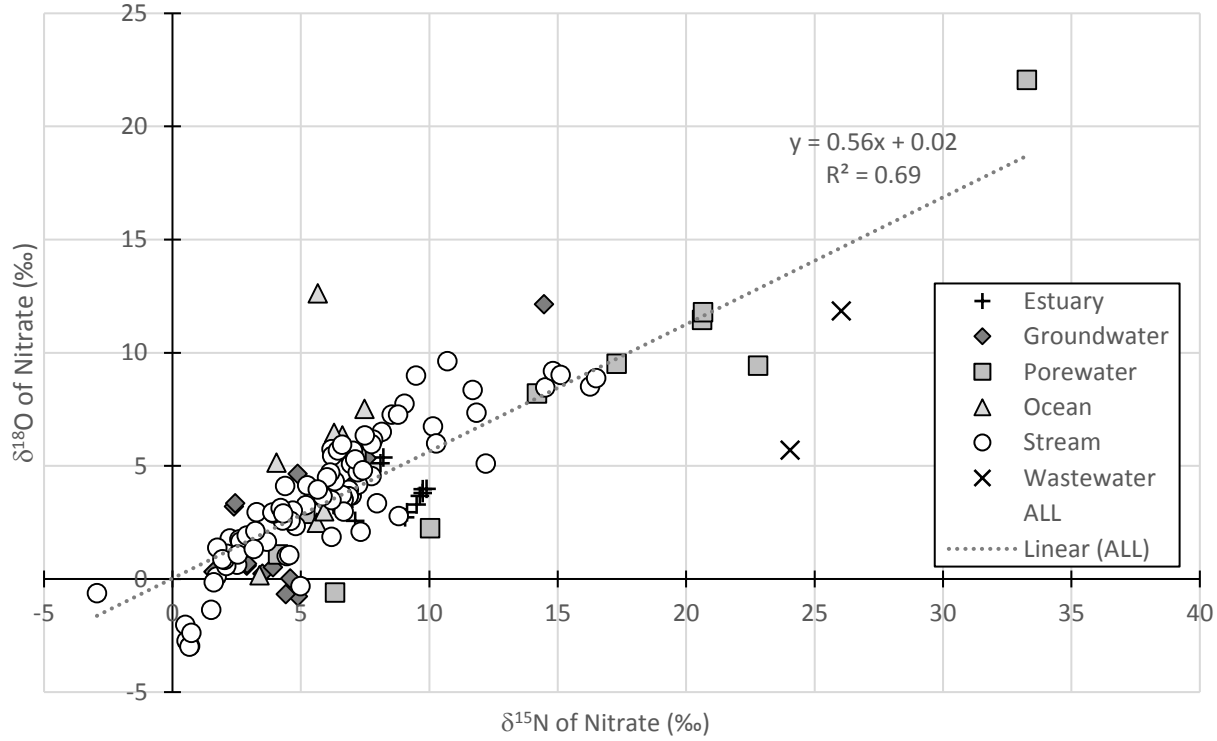

Figure 2.5. Dual isotopic composition of nitrate as $\delta^{15}N_{nitrate}$ vs. $\delta^{18}O_{nitrate}$ for all samples with an observable 0.56 denitrification trend. Stream samples are from Kahaluʻu, Waiheʻe, Waiāhole, Ahuimanu, Kaalaea, and Haiamoa Streams. Ocean samples are from the near shore coastal environment. Groundwater includes deep and shallow wells, while pore water samples come from the shallow subsurface at streams and the coast. Estuarine samples are primarily form Kahaluʻu estuary and Waiāhole Mangrove. Wastewater endmembers are form Waimanalo WWTP.

4.3.2. Dual-isotopic composition of NO_3^-

$\delta^{15}N_{nitrate}$ values (**Figure 2.5**) range from 0.5 to 33.3±0.3‰ (n = 117), with one anomalously low $\delta^{15}N$ value of -2.9±0.3‰; $\delta^{18}O_{nitrate}$ values range from -2.0 to 22.1±0.6‰ (n = 117). Both $\delta^{15}N_{nitrate}$ and $\delta^{18}O_{nitrate}$ values are systematically lower in field samples from Waiāhole watershed relative to other watersheds in the study (Appendix 1). Samples containing $NO_3^- < 0.8$

μM could not be reliably analyzed with available instrumentation, though values are reported for the oceanic endmember where such a threshold had to be tolerated. A slope of 0.56 consistent with the "denitrification trend line" of Kendall and McDonnell (1998) and Kendall et al. (2007) is present in a linear regression of our $\delta^{15}N_{nitrate}$ vs. $\delta^{18}O_{nitrate}$ data. This slope of <1 is interpreted to show effects of anammox in anoxic aquifers (Granger and Wankel, 2016), but is not greatly explored in the remainder of this discussion but rather discussed as a loss of NO_3^- as N_2 gas regardless of the process. The relationship between NO_3^- concentration and $\delta^{15}N_{nitrate}$ value further progress understanding of potential denitrification of sampled NO_3^- sources (**Figure 2.6**).

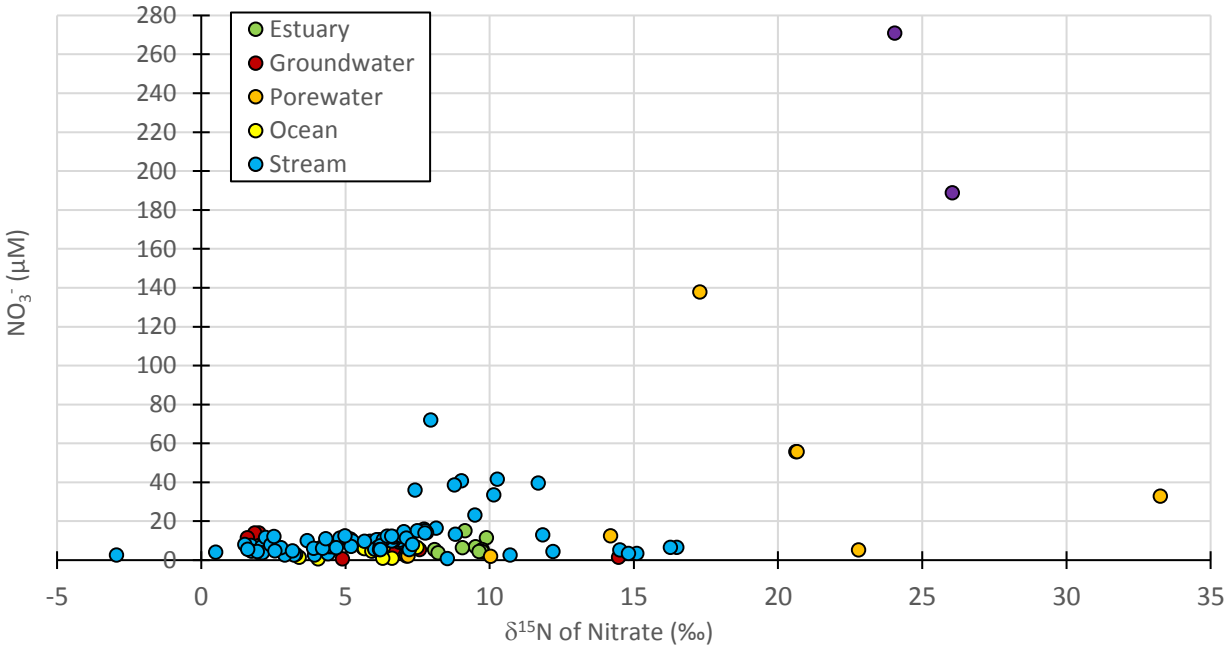

Figure 2.6. NO_3^-concentrations against the $\delta^{15}N_{nitrate}$ (n=143). Samples with low NO_3^- and high $\delta^{15}N_{nitrate}$ are suspected to be the result of denitrification.

4.3.3. Boron concentration and isotopic composition

B concentrations are high in the ocean at 255±0 ppb and in wastewater at 178±0 ppb; B concentrations are low in groundwater at 31±0 ppb and even lower in agricultural discharge at 21±0 ppb, shown in **Table 2.5** and **Figure 2.7**. B concentrations in field samples from all watersheds range from 18 to 32±0 ppb (n = 14). One coastal Kaalaea sample had a B concentration of 141±0 ppb. Wastewater has the lowest $\delta^{11}B$ value at 8.6±0.4‰. Ocean $\delta^{11}B$ value is 39.7±0.4‰, groundwater $\delta^{11}B$ value is 32.9±0.4‰, and agricultural discharge has a $\delta^{11}B$ value of 42.8‰. The range of $\delta^{11}B$ values in all field samples is 27.6 to 47.5±0.4‰ (n = 10).

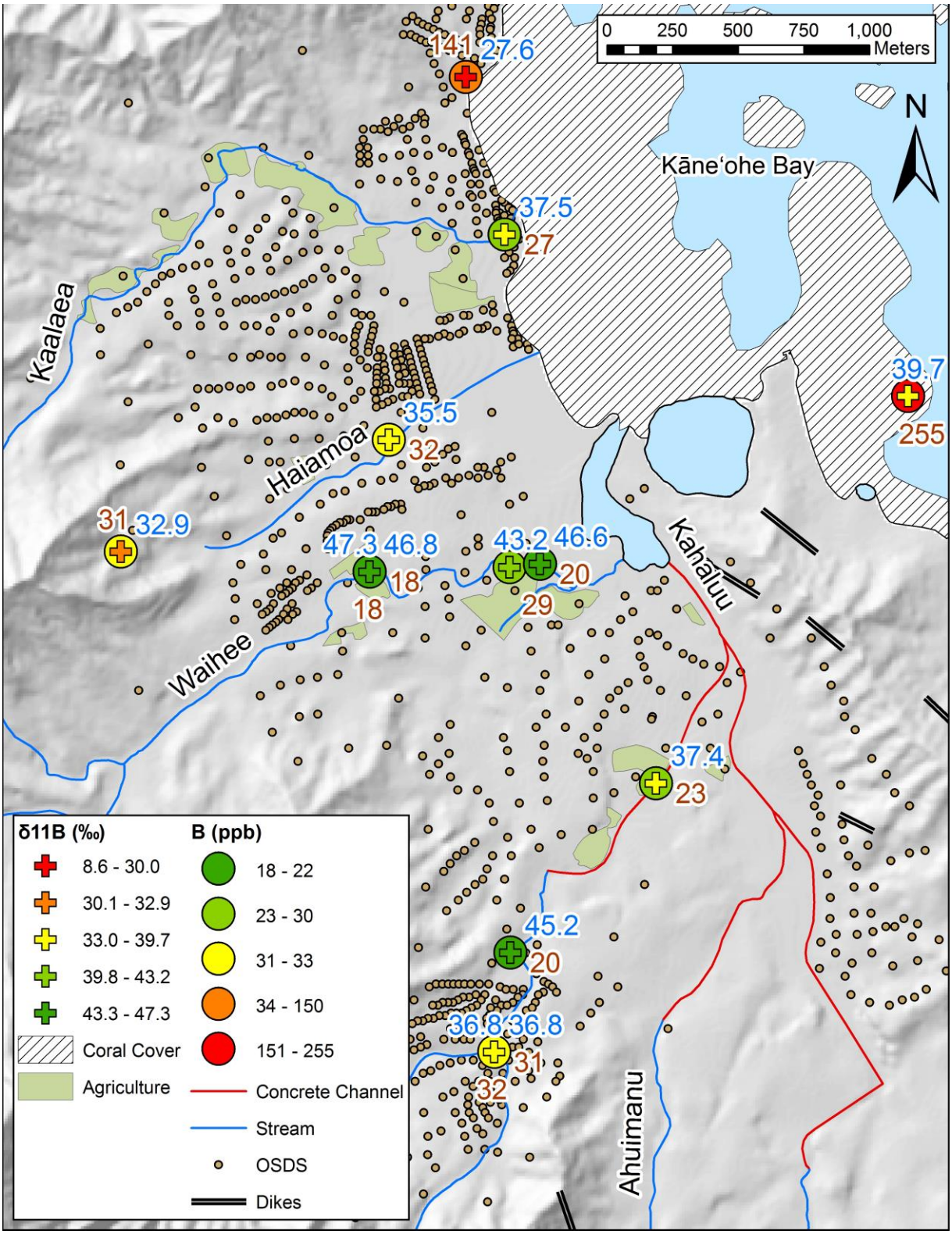

Figure 2.7. Boron concentrations in ppb mapped as circles in the Kahaluʻu study area with $\delta^{11}B$ mapped as crosses. B concentration values are labeled in red, and $\delta^{11}B$ is labeled in blue to 1 decimal place.

Table 2.5. Boron concentrations and isotopic composition for all samples compared with the N species concentrations and isotopic composition of NO_3^-. Indicated uncertainties are plus or minus 2 standard deviations.

Sample	Type	Location	$\delta^{11}B$ ‰	B ppb	$\delta^{15}N$ NO_3^- ‰	$\delta^{18}O$ NO_3^- ‰	NO_3^- + NO_2^- µM	NH_4^+ µM	TN µM
DSWEE01	Stream	Waiheʻe	47.3±0.4	18±0	4.6±0.3	2.6±0.6	5.9±1.3	0.6±0.6	5.93±4.9
DSWEE01(D)	Stream	Waiheʻe	46.8±0.4	18±0	4.4±0.3	2.7±0.6	6.2±1.3	1.3±0.6	6.28±4.9
DSKAH05	Stream	Kahaluʻu	45.2±0.4	20±0	6.4±0.3	3.4±0.6	10.1±1.3	0.3±0.6	10.14±4.9
DSWEE09	Stream	Waiheʻe	46.6±0.4	20±0	12.2±0.3	5.1±0.6	4.4±1.3	0.6±0.6	4.64±4.9
DSWEE10	Agriculture	Waiheʻe	42.8±0.4	21±0	9.5±0.3	9.0±0.6	23.2±1.3	7.1±0.6	24.99±4.9
DSCON03	Concrete Channel	Kahaluʻu	37.4±0.4	23±0	8.5±0.3	7.3±0.6	0.9±1.3	5.9±0.6	--
WSKAL01	Stream	Kaalaea	37.5±0.4	27±0	7.3±0.3	2.1±0.6	8.0±1.3	3.9±0.6	31.84±4.9
DPWEE05	Spring	Waiheʻe	43.2±0.4	29±0	22.8±0.3	9.4±0.6	5.2±1.3	1.9±0.6	5.43±4.9
DSKAH11	Stream	Kahaluʻu	36.8±0.4	31±0	10.3±0.3	6.0±0.6	41.6±1.3	2.4±0.6	41.91±4.9
WWJPR01	Drinking well	Groundwater	32.9±0.4	31±0	3.9±0.3	0.5±0.6	2.7±1.3	0.3±0.6	2.28±4.9
DPKAH11	Hyporheic zone	Kahaluʻu	36.8±0.4	32±0	14.2±0.3	8.2±0.6	12.5±1.3	3.6±0.6	12.85±4.9
WSHAI01	Stream	Haiamoa	35.5±0.4	32±0	8.0±0.3	3.4±0.6	72.1±1.3	4.9±0.6	220.18±4.9
WPKAL05	Coastline	Kaalaea	27.6±0.4	141±0	20.6±0.3	11.5±0.6	55.8±1.3	1.1±0.6	96.45±4.9
WWTP FC	Wastewater	WWTP Final Clarifier	8.6±0.4	178±0	24.1±0.3	5.7±0.6	271.0±1.3	202.1±0.6	474.89±4.9
WOLAE02	Open ocean	Seawater	39.7±0.4	255±0	4.1±0.3	5.1±0.6	0.5±1.3	1.4±0.6	4.61±4.9

4.3.4. Dissolved common ion concentrations for pollution trends

Common ion (Cl^-, SO_4^{2-}, K^+, Ca^{2+}, and Mg^{2+}) concentrations in freshwaters (below 2000 µS m^{-1}) were highest in Kahaluʻu Stream, elevated in Haiamoa, Kaalaea, and Waiheʻe Streams, and lowest in Waiāhole Stream. This trend holds true for Cl^- (n = 129), SO_4^{2-} (n = 129), and K^+ (n = 130) in addition to calcium (Ca^{2+}) (n = 129) and magnesium (Mg^{2+}) (n = 130). Agricultural discharge had low ion concentrations, while wastewater had some of the highest ion concentrations compared to all freshwater samples.

4.4. Aqueous carbonate geochemistry denitrification assessment

DIC of field samples varied between 229 and 11,915±19.7 µmol kg^{-1} (n = 46). Municipal drinking water wells had lowest DIC, ranging from 229 to 676±19.7 µmol kg^{-1}, but the majority of DIC concentrations were between 1,120 and 7,725±19.7 µmol kg^{-1}. The maximum DIC concentrations found were 10,133 and 11,915±19.7 µmol kg^{-1}. TA values range from 798 to 11,532±19.5 µmol kg^{-1} (n = 42) and are lowest in private drinking water wells. DIC and TA co-vary linearly and positively with an R^2 of 0.96. The isotopic composition of DIC varied between

-23.7 and -7.3±0.3‰ $\delta^{13}C_{DIC}$ (n = 46). The lowest $\delta^{13}C_{DIC}$ values are from fresh groundwater wells, while brackish samples typically had higher $\delta^{13}C_{DIC}$.

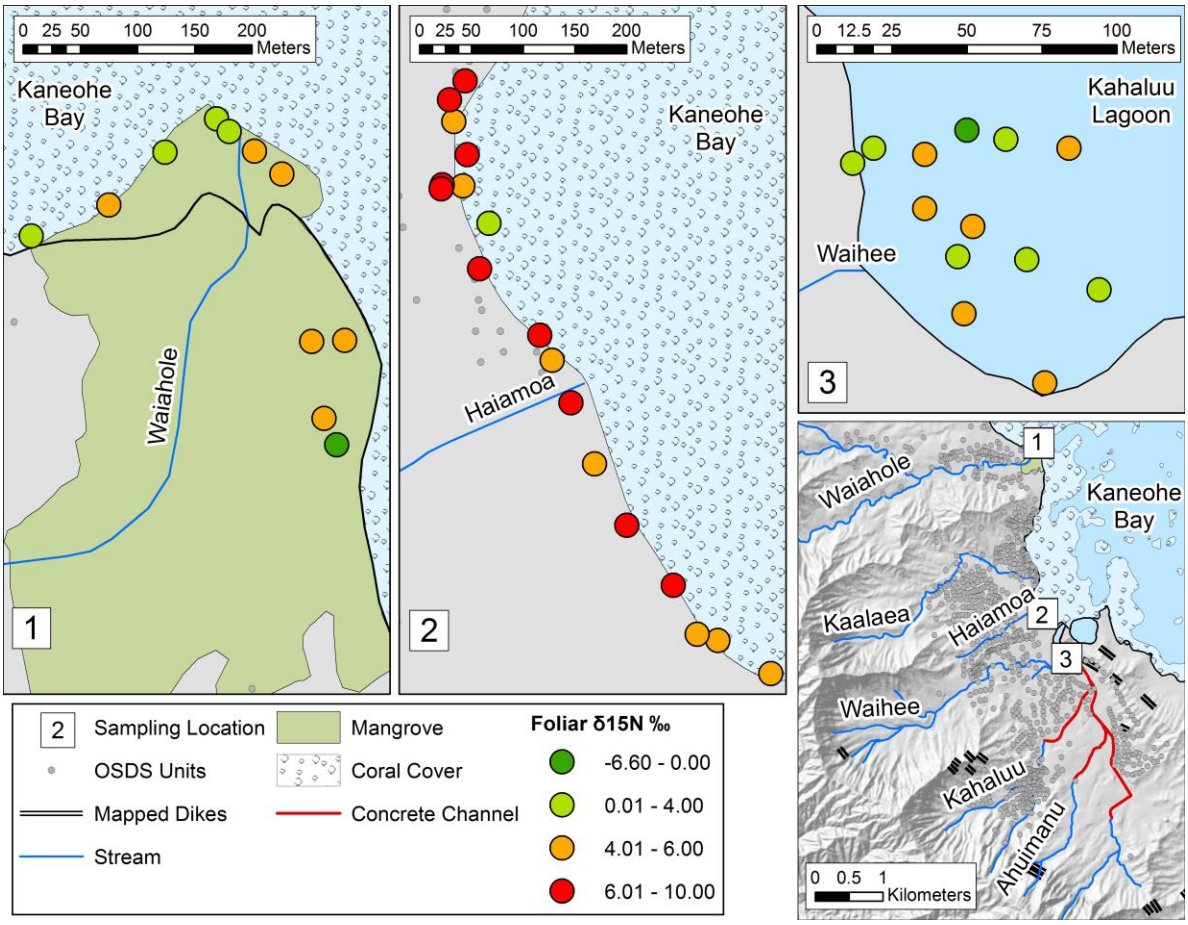

Figure 2.8. Isotopic composition of mangrove leaves mapped across the three regions of *R. mangle* growth in the coastal areas of the Kahaluʻu study region with $\delta^{15}N$ expressed in ‰.

4.5. Foliar C and N sampling

Foliar $\delta^{15}N$ varies from -6.6 to 10±0.3‰ (n = 44) throughout the study area (**Figure 2.8**). Foliar C:N ratios (for C, n = 44; for N, n = 44) and $\delta^{13}C$ (n = 44) vary with salinity in the area. Haiamoa samples have the highest average salinity at 28, Waiāhole mangrove salinity is 22, and Kahaluʻu estuary has the lowest salinity at 11. Both average and maximum values for both C:N and $\delta^{13}C$ in each sampling area decrease with decreasing salinity. Salinity has been shown to affect mangrove functioning (Wu et al., 2008b), and may dictate relationships between C, N, and $\delta^{13}C$ in the study area.

5. Discussion

To establish a hydrologic connection between OSDS and Kahaluʻu regional groundwater, streams, and coastal waters, we compared from these waters DIN concentrations, $\delta^{15}N_{nitrate}$, $\delta^{2}H$, $\delta^{18}O$, common ion concentrations, B concentrations, and $\delta^{11}B$ values. Foliar $\delta^{15}N$ values in mangrove leaves provided new insight on plant N composition, and a combined DIC-TA-$\delta^{13}C_{DIC}$ approach was used to assess N-cycling pathways that could affect DIN concentrations and $\delta^{15}N_{nitrate}$ values used to evidence OSDS leachate presence. This discussion delineates three main pathways for groundwater delivery to surface water in the study area and N-cycling dynamics within each: (1) base flow to streams, (2) shallow riparian drainage to streams, and (3) SGD to the coast. In the following, we propose where wastewater presence may be found in the Kahaluʻu study area, supported by our multi-tracer approach in each watershed to source-track the presence of OSDS leachate.

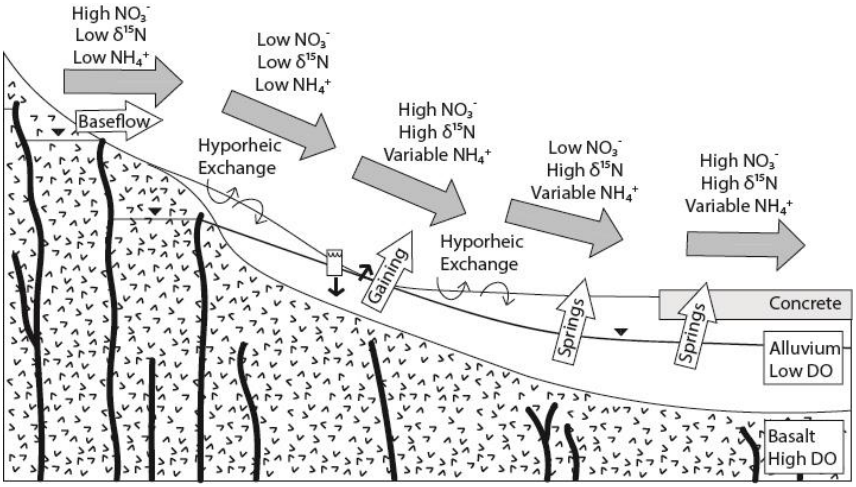

Figure 2.9. Schematic representation of the cycling of N species in the presence of excess nutrient loads from OSDS throughout the streambed, from base flow at headwaters throughout transport to the coast. The position of the groundwater table is marked by solid triangle.

5.1. Primary transport methods for nutrient delivery in the Kahaluʻu region

5.1.1. Nitrogen cycling and transport through stream base flow

Deep groundwater in the Koʻolau Rift Zone aquifer directly flows to the streams of the Kahaluʻu region as spring-fed base flow at the headwaters where the water table has breached dike-impounded reservoirs (Hirashima, 1971; Hunt, 1996), as schematically illustrated in **Figure 2.9**. Shallow groundwater reaches stream channels at varying distances downstream where streambeds intersect the groundwater table, producing seeps or as springs that bring groundwater

to the surface. While overland runoff contributes to stream discharge during rainfall events, groundwater sources perennially feed the streams of the Kahaluʻu region.

The high elevation groundwater feeding Kahaluʻu's streams represented by the deep groundwater well endmember is characterized by high NO_3^- concentration, low NH_4^+, concentration, low $\delta^{15}N_{nitrate}$ values, low $\delta^{18}O_{nitrate}$ values, and high DO concentrations (Figure 2.9, Table 2.3). Headwater compositions of the streams reflect these characteristics. Organic N and NH_4^+ from decomposing organic matter in the dense jungle and soils of high-elevation pristine watershed surfaces contribute to the N species composition of the aquifer beneath it. Thus, we hypothesize partial nitrification and minimal denitrification takes place in the shallow subsurface at the upper elevations of the Koʻolau Range to yield high NO_3^- concentration, low NH_4^+ concentration, and low $\delta^{15}N_{nitrate}$ and $\delta^{18}O_{nitrate}$ values in the presence of high DO concentrations. The lack of urban, agricultural, or industrial development along the ridgeline reduces greatly the possibility of anthropogenic inputs to the higher elevation deep groundwater resources. Once this N pool reaches the well-oxygenated groundwater in the aquifer, rates of nitrification and denitrification should cease, allowing for conservative transport of the current N species composition until groundwater breaches the surface as base flow at lower elevations. The denitrification proposed is evidenced on the ratio of average $\delta^{18}O_{nitrate}$ values to average values $\delta^{15}N_{nitrate}$ at 1:2, comparable to Kendall and McDonnell (1998) and Kendall et al. (2007).

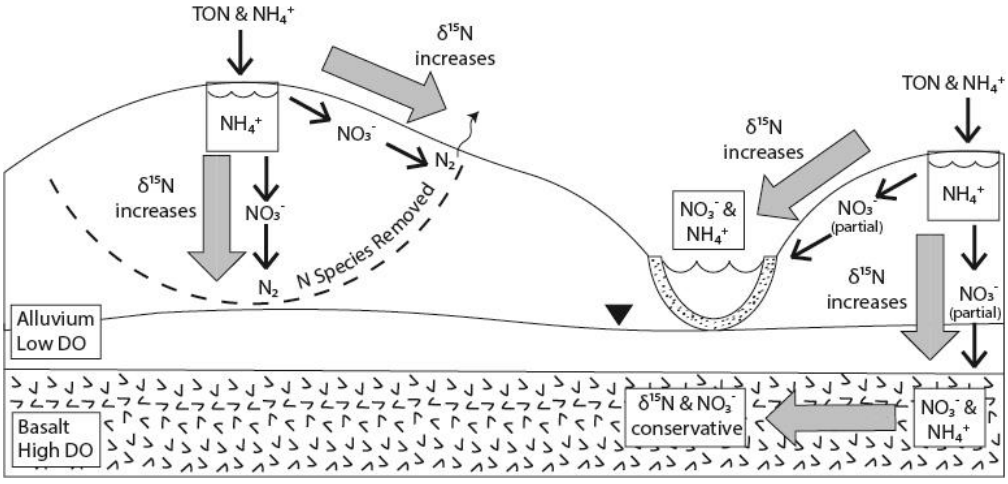

Figure 2.10. Illustration of the N cycling that occurs during nutrient transport to the streambed and delivery varying as a function of distance through the riparian zone. The position of the groundwater table is marked by solid triangle. The right side of this diagram depicts short transport paths between OSDS sources (box with NH_4^+) and both a nearby stream as well as to a relatively shallow water table below. The left half of the diagram illustrates a setting where the OSDS source to stream and underling water table are much greater, thereby resulting in more complete denitrification and conversion to N_2 gas.

5.1.2. Nitrogen transport within the riparian zone

The potential for NO_3^- to reach a stream is controlled by NO_3^- concentration at the source, distance between source and stream bank, and transport time dependent on water table elevation and hydraulic conductivity of subsurface geology. As NO_3^- can be denitrified on its pathway from source to stream (Billy et al. 2010), NO_3^- concentration is expected to decrease and $\delta^{15}N_{nitrate}$ values increase (Kellman and Hillaire-Marcel, 2003). Riparian zones can remove up to 60% of NO_3^- sourced from agricultural soils, lowering NO_3^- concentrations and raising $\delta^{15}N_{nitrate}$ and $\delta^{18}O_{nitrate}$ values in stream waters of large river systems due to denitrification in the riparian zone comparatively dominating denitrification in stream benthic environments (Sebilo et al., 2003). Soils alone can account for significant denitrification before NO_3^- enters a stream (Briand et al. 2017). Therefore, below we evaluate potential NO_3^- delivery to streams based on distance to the riparian zone, depicted by **Figure 2.10**.

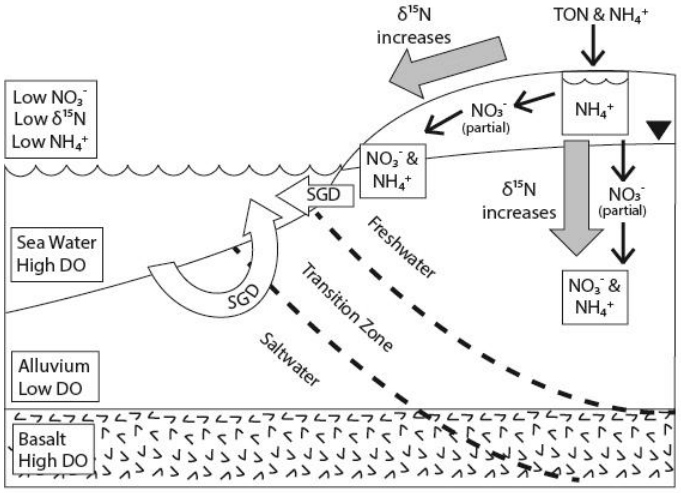

Figure 2.11. Nutrient enrichment that occurs in SGD when leachate from nearshore OSDS units reaches the groundwater table (solid triangle). When OSDS leach nutrient-rich wastewater directly to the phreatic zone, nutrients are efficiently transported to nearshore surface water through shallow SGD. In Kahaluʻu, we observed high NH_4^+ in coastal groundwater in which full nitrification had not yet occurred.

5.1.3. Nitrogen transport in SGD

Ambient ocean water NO_3^- concentration is ~0.5 μM and $\delta^{15}N_{nitrate}$ values near 4‰ (Table 2.3), thus any measurements above these values might indicate presence of OSDS leachate, agricultural discharge, or substantial organic matter degradation and denitrification. Unconsolidated alluvium and beach deposits at the coast provide permeable substrate necessary for efficient discharge of fresh groundwater as SGD. With a narrow distance between the water

table and land surface in the Kahaluʻu region, essentially raw wastewater effluent leaches into the phreatic zone and is transported to nearshore surficial waters through SGD (**Figure 2.11**). Elevated NO_3^- and $\delta^{15}N_{nitrate}$ was found in beach face piezometers tapping shallow pore water along the coastline of the Kahaluʻu regional watersheds. The majority of these samples come from the shorelines of Haiamoa and Kaalaea watersheds where OSDS density is highest and most focused near the coast. Even if denitrification has occurred, it does not attenuate the wastewater influence in SGD. At some nearshore surface sample locations, stream discharge may influence the sample based on proximity to estuaries and bay water circulation patterns.

5.2. Establishing the parameters of the control Waiāhole Stream watershed

5.2.1. Hydrogen and oxygen isotopic evidence for a hydrogeologic boundary connectivity

Waiāhole watershed is hydrogeologically separated from the four southern streams in the study area, and serves as the control watershed for this study. The dike-intruded basaltic ridge between these two watersheds is a topographic watershed divide for surface flow. The 12-month VWA δ^2H value of precipitation at Kahaluʻu ridgeline in Kahaluʻu watershed is more closely related to local groundwater and stream water δ^2H values of the study region than δ^2H values in precipitation from Waiāhole watershed (Section 4.2). This provides isotopic evidence that the ridge serves a hydrologic no-flow boundary for groundwater between Waiāhole and Kahaluʻu watersheds (Figure 2.2). A systematic depletion in ^2H in water as it progresses from precipitation (δ^2H = -9.0±0.8‰) and fresh pore water (δ^2H = -9.0±0.5‰) to shallow groundwater (δ^2H = -10.1±0.5‰), and ultimately deep groundwater (δ^2H = -11.0±0.5‰) suggests local recharge of the Kahaluʻu regional groundwater (Appendix 1). Stream average δ^2H values match Kahaluʻu precipitation with -9.2±0.5‰ in natural streambeds (n = 28) and -9.6±0.5‰ in concrete channels (n = 10), validating the suggestion that stream base flow is sourced from the Kahaluʻu region's local groundwater while experiencing small increases in δ^2H values due to evaporation of stream water in the concrete-lined channel.

5.2.2. Waiāhole Stream watershed nitrogen characteristics

Relatively uncontaminated downstream waters in areas unpolluted by sewage or agricultural drainage have low NO_3^- and NH_4^+ concentrations and low $\delta^{15}N_{nitrate}$ values. Waiāhole Stream

matches these criteria (Table 2.3) and is thus regarded as a pristine reference stream for this study. Low OSDS usage and low OSDS density in Waiāhole watershed, coupled with the stream's high volumetric flux and limited development in the forest reserve, reduces the impact of wastewater leachate on stream water quality in the channel. Thus, we suggest Waiāhole Stream is relatively undisturbed in its N-cycling. Low concentrations of NO_3^- (0-4.7±1.3 μM) and NH_4^+ (0.2- 6.8±0.6 μM), and low $\delta^{15}N_{nitrate}$ values (0.5-4.4±‰) support this interpretation. These parameters are considered baseline concentrations and isotopic ratios for streams free of nutrient-pollution from wastewater or agriculture in the Kahaluʻu region. Additionally, most pore water samples from the coastal mangrove forest shoreline at the coast of Waiāhole control watershed (n = 6) have NO_3^- concentrations and $\delta^{15}N_{nitrate}$ values similar to those measured in Kāneʻohe Bay seawater.

All samples in the study were referenced to the Waiāhole control stream and coastal waters, in addition to sampled endmembers and previously established literature values (Kendall and McDonnell, 1998). Nearshore surface samples were to be analyzed against localized ambient seawater composition. In our study area, we estimate agricultural effluent from taro paddy drainage to have a $\delta^{15}N_{nitrate}$ value of 9.5±0.3‰, but recognize potential variability in N composition under complex and extensive N cycling dynamics in Hawaii's flooded agroecosystems (Penton et al., 2012; Penton et al., 2014). Importantly, all $\delta^{18}O_{nitrate}$ values determined in this study were below 15‰ except one pore water sample. Therefore, all samples show isotopic compositions indicative of soil, wastewater, or nitrification of organic fertilizer as NO_3^- sources (Kendall and McDonnell, 1998). Based on residual NH_4^+ concentrations measured in all samples, complete nitrification is not anticipated, and therefore preferential nitrification of the lighter isotope will lead NO_3^- sourced from nitrified NH_4^+ fertilizer to have lower $\delta^{15}N_{nitrate}$ values than other NO_3^- sources (Kendall and McDonnell, 1998).

5.2.3. Differences in nitrogen characteristics from each watershed

To identify significant differences in stream water across three primary watersheds of our study area of Kahaluʻu, Waiheʻe, and Waiāhole, a Kruskal-Wallis one-way analysis of variance (Kruskal-Wallis H test) was completed to produce the H-statistic. This is a non-parametric test synonymous to a one-way ANOVA on ranks to determine if samples from two independent

populations of equal or different sample sizes are from the same distribution. Significant difference between populations is reported when P > 0.05 (**Table 2.6a, 2.6b**). NO_3^- concentrations and $\delta^{15}N_{nitrate}$ values varied significantly between all three major streams and the concrete channel. NH_4^+ concentrations did not vary significantly between Waiāhole-Waiheʻe and Waiheʻe-Kahaluʻu, $\delta^{18}O_{nitrate}$ values did not vary significantly between Waiāhole-Waiheʻe, and TN concentrations did not vary significantly between Kahaluʻu-Concrete channel. The results of this test are 2-fold. First, significant differences in NO_3^-, NH_4^+, and TN concentrations and both NO_3^- isotopes imply different N sources or cycling for each stream. Second, the greater variance in NO_3^- concentrations and $\delta^{15}N_{nitrate}$ values across the three regions show these parameters can serve as useful tracers in the Kahaluʻu study area.

Table 2.6a. (Top) Krustal-Wallis H-values and P values for the one-way ANOVA based on ranks for each parameter. Population pairs whose difference is not significant for a given parameter is shaded in blue. **Table 2.6b.** (Bottom) Number of samples for each parameter from each stream used for the Kruskal-Wallis test.

Stream Pair	NH_4^+	NO_3^-	TN	$\delta^{15}N_{nitrate}$	$\delta^{18}O_{nitrate}$
Waiāhole-Kahaluʻu	H= 5.91, P= 0.02	H= 21.76, P< 0.001	H=19.44, P< 0.001	H= 22.61, P< 0.001	H= 18.29, P< 0.001
Waiāhole-Waiheʻe	H= 1.78, P= 0.18	H= 12.86, P< 0.001	H= 5.18, P= 0.03	H= 6.37, P= 0.01	H= 2.18, P = 0.14
Kahaluʻu-Waiheʻe	H=01.78, P= 0.18	H= 31.69, P< 0.001	H= 18.83, P< 0.001	H= 24.78, P< 0.001	H= 24.78, P< 0.001
Kahaluʻu-Concrete	H= 13.4, P< 0.001	H= 19.32, P< 0.001	H= 0.17, P= 0.68	H= 12.62, P< 0.001	H= 11.15, P< 0.001

Watershed Pair	NH_4^+	NO_3^-	TN	$\delta^{15}N_{nitrate}$	$\delta^{18}O_{nitrate}$
Waiāhole	10	10	10	11	11
Kahaluʻu	29	29	28	31	31
Waiheʻe	23	23	22	25	25
Concrete	13	13	7	10	10

5.3. OSDS density effect on water quality

Spatial distribution of OSDS throughout the Kahaluʻu regional study area was incorporated into a Spearman's rank-order correlation to identify relationships between geographic OSDS distribution and stream DIN content. Stream water quality samples (n = 98) were input into this non-parametric test for data not normally distributed. The reported Spearman's rank correlation coefficient (ρ) were evaluated at a 99.9% confidence interval (P < 0.01, ρ > 0.3) and a 95% confidence interval in identifying a relationship between two variables (P < 0.05, ρ > 0.2) (**Table 2.7**). The variable "OSDS Sample" represents the number of OSDS with ~210 ft of a sample upstream, an arbitrary "buffer" distance chosen for this study, as HDOH highlights increased

health risks from OSDS within 200 ft of shoreline (HDOH, 2018). The variable "OSDS Stream" represents any OSDS upstream of a sample within the 210 ft "buffer" distance of the stream, regardless of distance to the sample. The variable "OSDS remaining" includes all OSDS upstream of a sample in a watershed regardless of distance to the stream or the sample.

A relationship is evident between increased OSDS density and increased N species concentrations and increased $\delta^{15}N_{nitrate}$ values under certain conditions (Table 2.7). At the 99% confidence interval, increasing NO_3^- concentration correlated strongly ($\rho = 0.36$) with increasing OSDS within a 210 ft upstream radius of the sample ("OSDS Sample"). Also at the 99% confidence interval, increasing $\delta^{15}N_{nitrate}$ values correlated strongly with increasing OSDS upstream within the 210 ft "buffer" distance of the stream ("OSDS Stream") at $\rho = 0.41$, as well as increasing OSDS upstream in the entire watershed area ("Remaining OSDS") at $\rho = 0.42$. At the 95% confidence interval, increasing TN correlates with increasing OSDS with a 210 ft upstream radius of the sample ($\rho = 0.25$), NO_3^- concentrations and $\delta^{18}O_{nitrate}$ values increase with increasing OSDS upstream in the 210 ft "buffer" distance of the stream ($\rho = 0.2$ for both variables), and NH_4^+ concentrations increase with increasing OSDS upstream in the entire watershed area ($\rho = 0.25$). Total area of agricultural land adjacent to the stream and upstream of a sample has a strong negative correlation with NO_3^- concentration ($\rho = -0.41$) and moderate negative correlation with TN concentration ($\rho = -0.24$), implying agricultural inputs may be more dilute compared to wastewater inputs in the study area. Increased OSDS density directly adjacent to the sample, the stream as a whole, and the entire watershed appears to correlate with increased NO_3^- concentrations and $\delta^{15}N_{nitrate}$ values.

Table 2.7. Spearman Rank correlation test results with ρ value and confidence interval.

Spatial Parameter	NH_4^+ concentration	NO_3^- concentration	TN concentration	$\delta^{15}N_{nitrate}$ value	$\delta^{18}O_{nitrate}$ values
OSDS Sample	$\rho = 0.11$	$\rho = 0.36$ ($P < 0.01$)	$\rho = 0.25$ ($P < 0.05$)	$\rho = 0.03$	$\rho = 0.11$
OSDS Stream	$\rho = 0.1$	$\rho = 0.2$ ($P < 0.05$)	$\rho = 0.16$	$\rho = 0.41$ ($P < 0.01$)	$\rho = 0.20$ ($P < 0.05$)
Remaining OSDS	$\rho = 0.25$ ($P < 0.05$)	$\rho = 0.13$	$\rho = 0.08$	$\rho = 0.42$ ($P < 0.01$)	$\rho = 0.17$
Agricultural Land	$\rho = -0.01$	$\rho = -0.41$ ($P < 0.01$)	$\rho = -0.24$ ($P < 0.05$)	$\rho = -0.14$	$\rho = 0.05$

5.3.1. Haiamoa and Kaalaea Streams: highest regional OSDS density

Stretches of stream with high OSDS density in close proximity to the channels of Kaalaea and Haiamoa Streams have the most evidence of wastewater presence. In these areas we

observed elevated NO_3^-concentrations, high $\delta^{15}N_{nitrate}$ values, and highest common ion concentrations (Appendix 1, Table A1.4). As schematically illustrated in Figure 2.10, a small depth to water table affords minimal opportunity for substantial nitrification of NH_4^+ to NO_3^-, providing high concentrations of relatively unaltered sewage effluent to be discharged to the groundwater and delivered to the nearby stream channel. Raw sewage has the highest TN and NH_4^+ concentrations of any endmember (Table 2.3, Table 2.4), and nearby groundwater receiving OSDS leachate can have high NH_4^+ concentrations as organic N mineralizes to NH_4^+. Secondary and tertiary treatments at the WWTP significantly reduce NH_4^+ by an order of magnitude while increasing NO_3^-, mimicking the expected evolution of N species in the natural environment when discharged from an OSDS. However, in septic systems, minimal active wastewater treatment occurs in the sampled septic system transfer from Septic Tank 1 to Septic Tank 2, leaving high NH_4^+ and low NO_3^- in both tanks. With short subsurface transit time in the natural environment, OSDS-borne NH_4^+ may not nitrify extensively to NO_3^-. Therefore, NH_4^+ concentrations are high in some surface waters where OSDS units are well-connected to the stream channel or coastal waters via shallow water table. As a consequence, high NO_3^- concentrations and high $\delta^{15}N_{nitrate}$ values in streams, or NH_4^+ concentration higher than naturally occurring concentrations caused by organic matter degradation is concluded to be indicative of the most directly concentrated wastewater presence.

One of 10 B field samples corroborated wastewater presence at the coast of Kaalaea watershed as previously identified through the 3rd-highest NO_3^- concentration (55.8±1.3 μM), 6th-highest TN concentration (96.5±4.9 μM), and 3rd-highest $\delta^{15}N_{nitrate}$ value (20.6±0.3‰). This coastal spring had a high B concentration of 141 ppb eliminating groundwater (31 ppb±0, 0.11 salinity) as a dominant source, and low salinity of 0.66 eliminating seawater (255±0 ppb, 34.65 salinity) as a dominant B source. Further, its $\delta^{11}B$ of 27.6±0.4‰ was lower than all field and endmember samples other than wastewater (8.6±0.4‰) (Table 2.5, Figure 2.6). While B is commonly attenuated during transport due to its high susceptibility for absorption onto clays, ferrihydroxides, and other solid surfaces (Widory et al., 2005) that would lower its concentration, this sample clearly retained a high B concentration at the point of coastal discharge. It is ^{10}B that sorbs more readily to surfaces than ^{11}B, thereby increasing $\delta^{11}B$ values as transport progresses (Vengosh et al., 1994) through equilibrium isotope fractionation (Zeebe, 2005). The other two B

composition field samples from Haiamoa and Kaalaea Streams had B concentrations (32 and 27 pbb±0, respectively) and $\delta^{11}B$ values (35.5 and 37.5±0.4‰, respectively) consistent with that of regional groundwater (31 ppb, 32.9±0.4‰). In these 2 field samples from Haiamoa and Kaalaea, NO_3^- concentrations (72.1 and 8.0±1.3 μM) and $\delta^{15}N_{nitrate}$ values (8.0 and 7.3±0.3‰, respectively) appeared to imply wastewater presence, but the $\delta^{15}N_{nitrate}$ values do not indicate as strong a wastewater signal as evidenced at the Kaalaea coastline. As a result, we conclude B concentration coupled with $\delta^{11}B$ values can provide wastewater source-tracking evidence in areas where wastewater signals are strong, such as the shallow groundwater adjacent to an OSDS grouping at the Kaalaea coast. However, natural B compositions can dominate in streams chronically fed by groundwater where uncontaminated base flow greatly outweighs contaminated wastewater discharge to the stream volumetrically, including Haiamoa and Kaalaea Streams.

5.3.2. Haiamoa and Kaalaea Coastline: highest up-gradient OSDS density

Kaalaea and Haiamoa watersheds have the highest number and highest density of OSDS within the study area. Dense vegetation cover limited pore water sampling access along much of Kaalaea and Haiamoa coastline, but, nearshore seawater samples in this region nonetheless reveal the presence of nutrient-rich freshwater SGD with $\delta^{15}N_{nitrate}$ values and NO_3^- concentrations greater than ambient seawater (Table 2.3). Multiple coastal samples north of Kaalaea Stream have low NO_3^- concentrations comparable to seawater despite close proximity to dense OSDS coverage along the coastline. One coastal sample north of Kaalaea had NO_3^- higher than ambient seawater and one of the highest coastal $\delta^{15}N_{nitrate}$ values in the entire region (6.6±0.3‰), implying wastewater-borne DIN.

All nearshore seawater samples south of Kaalaea Stream outlet and north of Haiamoa contained high NO_3^- concentrations and high $\delta^{15}N_{nitrate}$ values suggesting wastewater presence (Figure 2.4). We believe the same nutrient-rich groundwater influencing the SGD of the coastline south of Haiamoa Stream discharges to the western bank of Kahaluʻu estuary, with SGD flowing down-gradient to both to the coastline and estuary's shores, as discussed further in section 5.5.

5.4. Waiheʻe Stream: agricultural vs. wastewater influence on the DIN pool

On Waiheʻe Stream, agriculturally-sourced nutrients were determined to be the primary contributors to the stream DIN pool. In the stream, areas of lower OSDS density had high stream NO_3^- concentrations and high $\delta^{15}N_{nitrate}$ values (Figure 2.4) suggesting wastewater presence. However, N-cycling systematics alone cannot explain this trend in increased NO_3^- because other study area streams display decreases in NO_3^- concentration downstream while $\delta^{15}N_{nitrate}$ values increase, which is indicative of denitrification of NO_3^- during transport. B analysis explains this discrepancy, revealing agricultural discharge as the main source of high NO_3^- concentrations and high $\delta^{15}N_{nitrate}$ values in Waiheʻe Stream. B concentration is low along Waiheʻe Stream (18-29±0 ppb) and $\delta^{11}B$ is high (43.2-47.3±0.4‰), identical to the composition of taro paddy drainage (B concentration of 21 ppb±0, $\delta^{11}B$ of 42.8±0.4) (Table 2.5, Figure 2.7). Therefore, in light of the agricultural connection evidenced throughout downstream Waiheʻe, we conclude the coupled use of B concentration and $\delta^{11}B$ values has utility in identifying agricultural discharge to streams.

5.5. Kahaluʻu Stream and estuary

5.5.1. Natural vs. Concrete-lined stream channel of Kahaluʻu

Stretches along Kahaluʻu Stream with high OSDS density in close proximity to it's channel have strong evidence of wastewater presence in the form of high NO_3^- concentrations and high $\delta^{15}N_{nitrate}$ values, much like Kaalaea and Haiamoa Streams. This is evident in the upstream branching of Kahaluʻu Stream and in Ahuimanu Stream, just above its confluence with Kahaluʻu in the channelized concrete stretch (Table 2.4, Figure 2.4). Natural attenuation, most likely in the form of denitrification, takes place as DIN loads flow downstream through Kahaluʻu.

Concrete-lined stream channels permit rapidly delivery of wastewater-borne nutrient-rich groundwater to enter stream channels through discrete drainage pipes from adjacent properties and through structural fissures in the concrete. These are labelled as "springs" entering the concrete-lined stream channels (Figure 2.9). Such spring-leakages were identified as upwelling through joints in concrete slabs and other engineered conduits. This delivery allows lower densities of OSDS to contribute disproportionately high concentrations of wastewater-borne N species to concrete-lined stretches of streams, such as the lower stretches of Ahuimanu Stream above its confluence with Kahaluʻu Stream (Figure 2.4). Groundwater transport of NO_3^- and

NH_4^+ is directed to stream waters via drainage pipes and springs (Figure 2.9), conserving relatively high NO_3^- concentrations and $\delta^{15}N_{nitrate}$ values, as well as residual NH_4^+ that did not nitrify during transport.

The ability of B concentrations and $\delta^{11}B$ values to identify a discrete source of agriculturally-sourced nutrient inputs in Kahaluʻu Stream that was otherwise dominated by wastewater inputs further illustrates B composition's utility to serve as an agricultural discharge tracer in the Kahaluʻu region. In the natural streambed channel of Kahaluʻu Stream, two surface water samples and one streambed pore water sample have B concentrations (31, 32, 23±0 ppb) and $\delta^{11}B$ values (36.8, 36.8, and 37.4±0.4‰) comparable to pristine baseline local groundwater (31 ppb, 32.9‰). One location contains low B of 20±0 ppb and high $\delta^{11}B$ value of 45.2±0.4‰ comparable to local agriculture (B concentration 21±0 ppb, $\delta^{11}B$ value 42.8±0.4‰). The location of this stream sample is adjacent to a large pasture abutting the streambank previously unmapped in the region, and was originally proposed to evidence a wastewater presence based on high NO_3^- concentrations and $\delta^{15}N_{nitrate}$ values. Therefore, we conclude agricultural discharge must dominate the B composition of this particular sample and outweigh both the natural composition and any potential wastewater signal, indicating manure to be the source of high NO_3^- concentrations and $\delta^{15}N_{nitrate}$ values.

5.5.2. Kahaluʻu estuary: a type example of contaminated SGD

Surface water samples of Kahaluʻu estuary have high $\delta^{15}N_{nitrate}$ values and high NO_3^- concentrations, suggesting a wastewater presence (Figure 2.4). The eastern, seaward shore of Kahaluʻu estuary represents transport of wastewater-borne N species typical of nearshore SGD, with discharge flowing locally down-gradient into the estuary. Organic N and NH_4^+ leach from the local OSDS systems present in the shallow groundwater (Table 2.4). Due to the high modeled water table in this region surrounding Kahaluʻu estuary and the local groundwater interconnectivity with the estuary, the OSDS in this region are hypothesized to discharge immediately into the phreatic zone (Figure 2.11). Groundwater interconnectivity with estuary waters was identified through pump tests for two local wells, 25 and 40 m from the estuary, respectively. No drawdown was measured in the well 25 m from the estuary after 3 minutes of pumping at 0.75 L min^{-1}. The well 40 m from the coast evidenced 0.29 m of drawdown under the

same conditions. The well closer to the estuary evidencing strong hydraulic connection to the water table through 0 m of drawdown is roughly parallel with and 25 m from two local septic tanks. These tanks are 20 m from the shore and provided our septic wastewater endmembers. The natural local groundwater composition is inferred from the well 40 m from the estuary and 50 m from the septic tanks, and is naturally low in $\delta^{15}N_{nitrate}$ values but moderate in NO_3^- and NH_4^+ concentrations. With the introduction of OSDS leachate from nearby septic tanks, this NH_4^+ increases by an order of magnitude to 296.3±0.6 μM at the well 25 m from the septic tanks, over 17.5 times greater than any other shallow groundwater NH_4^+ concentration. Surface samples from the estuary shoreline show this groundwater is discharged to the estuary as evidenced by lower salinities immediately adjacent to the shoreline. The NH_4^+ content has been primarily nitrified to NO_3^- and has a high $\delta^{15}N_{nitrate}$ value due to denitrification in transit and its wastewater source. Once in the estuary's surface water and flowing seaward, NO_3^- concentrations lower but $\delta^{15}N_{nitrate}$ values remain high.

Moderate NO_3^- concentration in surface water and low NO_3^-, high NH_4^+ concentrations in pore water near Waiheʻe Stream's input to Kahaluʻu estuary suggests that organic matter degradation is the major source of nutrients at this confluence. Due to the influence of the mangrove forest at this confluence, the mineralization of organic N to NH_4^+ and the resulting nitrification to NO_3^- causes the moderate NO_3^- concentrations. Slightly higher $\delta^{15}N_{nitrate}$ values in this region of Kahaluʻu estuary as compared to Waiāhole Mangrove implies a higher $\delta^{15}N_{nitrate}$ value of the source N pool from the higher density of OSDS in Waiheʻe, or perhaps a further progression to denitrification at Kahaluʻu estuary than occurs at Waiāhole Stream.

5.6. Mangrove leaves as a potential indicator of wastewater presence

Waiāhole mangrove forest exits at the coastline of pristine Waiāhole control watershed, where Waiāhole stream discharges to Kāneʻohe Bay. Mean foliar $\delta^{15}N$ value of coastal mangrove samples from Waiāhole forest was 2.8±0.3‰ (n = 11), lowest of all three regions (Figure 2.8). Waiheʻe mangrove stand encompasses the outlet of Waiheʻe Stream into Kahaluʻu estuary. Waiheʻe Stream DIN species are concluded to be affected by agricultural drainage, and the mangroves trees at the Waiheʻe Stream inlet to Kahaluʻu estuary had a mean foliar $\delta^{15}N$ value 2.9±0.3‰ (n =13), similar to that of the coastal Waiāhole mangroves to the north (Figure

2.8). Mangroves cover the coastlines of Kaalaea and Haiamoa watersheds. Mean foliar $\delta^{15}N$ value for foliar mangrove samples across the Kaalaea and Haiamoa shoreline was 6±0.3‰ (n = 18), more than double all other locations. Fifteen of these samples came from Haiamoa watershed, and the remaining three were directly north of the proposed watershed divide in Kaalaea watershed.

There was not a strong quantitative relationship between NO_3^- concentrations and $\delta^{15}N_{nitrate}$ values in surrounding surface water or pore water vs. $\delta^{15}N$ values of mangrove leaves. Future work is required to properly define the connection of $\delta^{15}N_{nitrate}$ values in pore water as well as mangrove root, stem, and leaf extracts $\delta^{15}N$ values. However, despite these caveats, foliar mangrove $\delta^{15}N$ values in the coastal setting of the study area do appear to increase semi-quantitatively with increasing OSDS-density in the up-gradient watershed. Waiāhole mangrove forest average $\delta^{15}N$ value of 2.8±0.3‰ has a corresponding up-gradient OSDS-density of only 8.5 units per km^2. The comparable average $\delta^{15}N$ value of 2.9±0.3‰ in Waiheʻe mangrove has a corresponding up-gradient OSDS-density of 26.5 units per km^2. Haiamoa coastline mangroves had a mean $\delta^{15}N$ value of 6±0.3‰ and a corresponding up-gradient OSDS-density in Haiamoa watershed of 133.7 units per km^2.

5.7. Regional aqueous carbonate geochemistry

5.7.1. Relationships between DIC and DIN

$\delta^{15}N_{nitrate}$ values increase linearly with DIC concentration and TA throughout those samples analyzed for all 3 parameters (**Figure 2.12**). Based on the previous results, the 3 main sources of high $\delta^{15}N_{nitrate}$ values in the study area include: (1) wastewater leachate with high initial $\delta^{15}N_{nitrate}$ values as seen in Kaalaea, Haiamoa, and Kahaluʻu Streams, (2) agricultural discharge evidenced by Waiheʻe Stream, and (3) decomposition of naturally-sourced organic matter followed by nitrification and denitrification seen in both Waiāhole and Waiheʻe mangrove forests. Mean study area groundwater DIC is 652±19.7 μmol kg^{-1}, with average $\delta^{13}C_{DIC}$ value of -19.9±0.3‰ (n=2). In contrast, wastewater endmember DIC concentrations range from 2537±19.7 (final clarifier, partially treated effluent) to 5602±19.7 μmol kg^{-1} (raw influent) with TA from 2244±19.5 (final clarifier, partially treated effluent) to 5666±19.5 μmol kg^{-1} (raw influent) and an average $\delta^{13}C_{DIC}$ value of -13.1±0.3‰ (n = 3). Surface DIC concentrations and TA of seawater

for Kāneʻohe Bay are 1954 µmol kg^{-1} and 2226±3.1 µmol kg^{-1}, respectively (Terlouw, 2017). Such values are in agreement with open ocean data from SOEST Station ALOHA (2016) with average DIC concentrations of 1988 µmol kg^{-1} (n = 9), comparable to historic DIC concentrations at Station ALOHA from 1988-2007 (Dore et al., 2009), and average TA of 2305±19.5 µmol kg^{-1} (n = 9) to be endmembers. $\delta^{13}C_{DIC}$ seawater endmembers from Station ALOHA data over the same time period had an average value of 1.2‰ DIC (n = 9), slightly lower than average 1.55‰ $\delta^{13}C_{DIC}$ values of Pacific surface waters (Quay et al., 2003). All DIC-TA samples are from the subsurface as pore water, shallow groundwater, or deep groundwater.

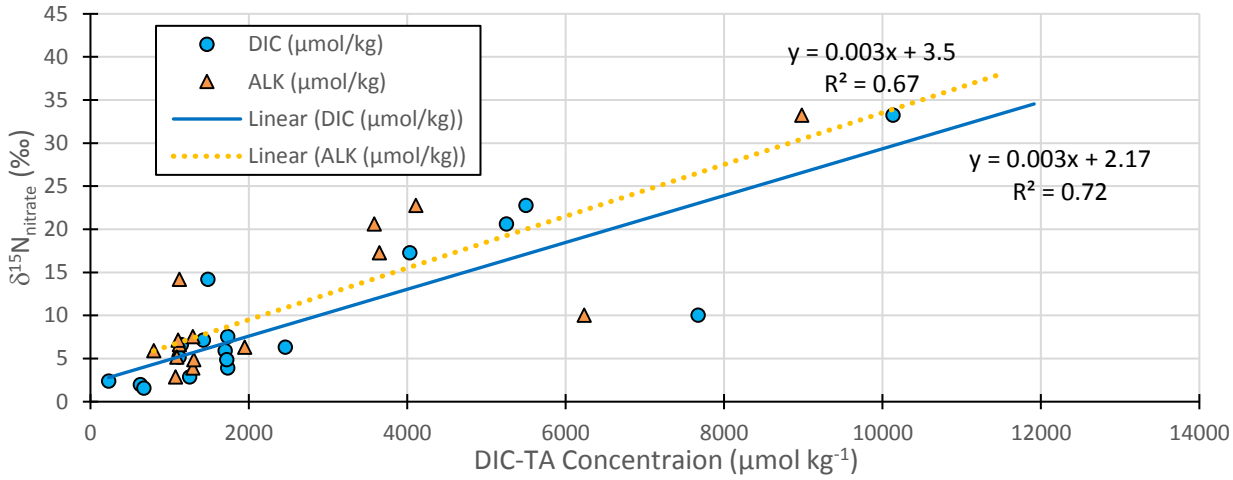

Figure 2.12. DIC and TA against $\delta^{15}N_{nitrate}$. Both concentrations increase linearly with increased $\delta^{15}N_{nitrate}$.

The linear correlation (R^2 = 0.72) for DIC concentration vs. $\delta^{15}N_{nitrate}$ values and TA vs. $\delta^{15}N_{nitrate}$ values (R^2 = 0.67) expressed by

$$\delta^{15}N_{nitrate} = 0.003*TA + 3.5 \quad \textbf{(Equation 2.4)}$$

$$\delta^{15}N_{nitrate} = 0.003*DIC + 2.17 \quad \textbf{(Equation 2.5)}$$

(Figure 2.12) allows us to approximate $\delta^{15}N_{nitrate}$ values for those samples with NO_3^- concentrations too low for isotope analysis through these equations. This is particularly useful for those pore and shallow groundwater samples well-connected to a wastewater source where NH_4^+ dominates the DIN pool. Such a sample exists for this study on the coast of Kaalaea

watershed, with 33.6±0.6 µM NH_4^+ concentration and 0.1±1.3 µM NO_3^- concentration, below the threshold to be analyzed for $\delta^{15}N_{nitrate}$. Using Equation 2.5 and the measured DIC of 11915±19.7 µmol kg^{-1} predicts a $\delta^{15}N_{nitrate}$ value of 37.9‰. Such a value is not far from the 33.3±0.3‰ $\delta^{15}N_{nitrate}$ value of a comparable coastal sample with 32.9±1.3 µM NO_3^- concentration and 0.1±0.6 µM NH_4^+ concentration. The same calculation used for raw untreated sewage to the WWTP with a DIC concentration of 5666±19.7 µmol kg^{-1}, yields a $\delta^{15}N_{nitrate}$ value of 19.2‰ as a reasonable estimate of untreated wastewater $\delta^{15}N_{nitrate}$ before denitrification in treatment before it progresses to the 24.1±0.3‰ measured in the final clarifier (2nd treatment stage) and 26.0±0.3‰ measured in the sand filter (3rd treatment stage).

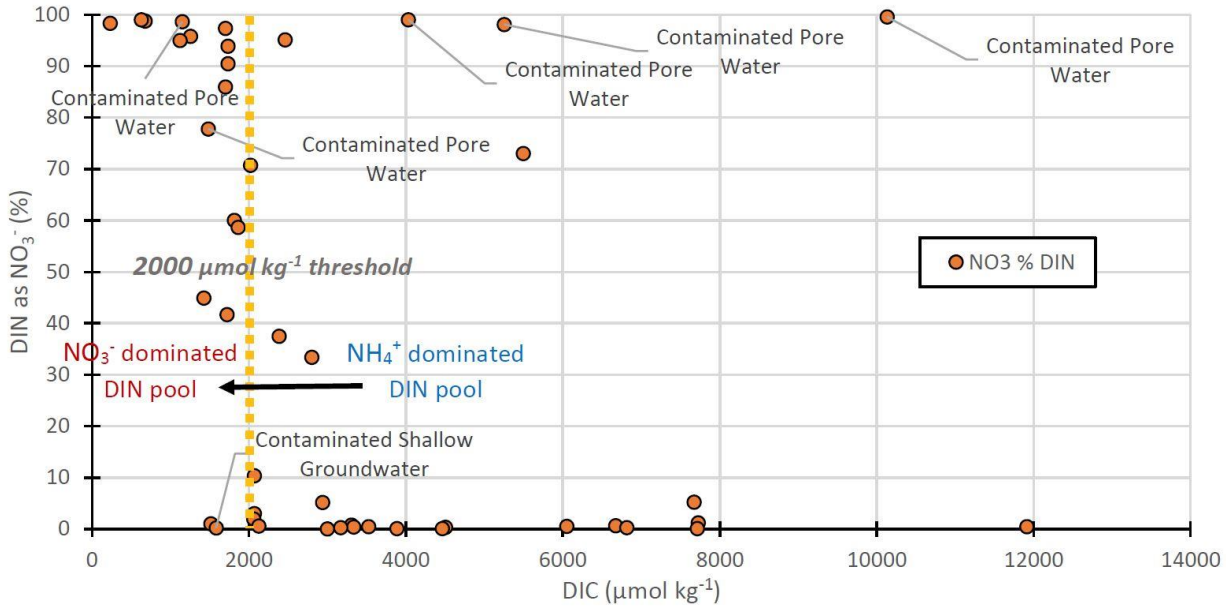

Figure 2.13. DIC against DIN % compositions. At ~2000 µmol kg^{-1}, systems switch from the DIN pool being dominated by NO_3^- to NH_4^+. Below this turning point, NO_3^- makes up the larger share of the DIN pool, and above this concentration, NH_4^+ becomes the dominant DIN species.

Two-thirds of all samples have DIC and TA concentrations < ~2000 µmol kg^{-1}, suggesting they lack a significant wastewater component. Most samples with high DIC also have NH_4^+ as the dominant DIN species. As shown in **Figure 2.13**, concentrations of DIC ~2000 µmol kg^{-1} appear to represent a transition in NO_3^-:NH_4^+. Below ~2000 µmol kg^{-1} DIC, the DIN pool is dominated by NO_3^-; above this concentration, the majority samples contain DIN is NH_4^+. The samples with highest DIC concentration and TA, representing the highest organic matter

concentration, typically have the lowest percentage of NO_3^- and thus the highest percentage of NH_4^+ (Figure 2.13). Such high NH_4^+ content indicates less nitrification and implies a closer proximity to organic N sources.

DIC concentrations and NO_3^-:NH_4^+ can be used as secondary indicators of wastewater presence supplementary to NO_3^- concentrations and $\delta^{15}N_{nitrate}$ and $\delta^{18}O_{nitrate}$ values. Typically, it was high DIC, high NO_3^-:NH_4^+, and high NO_3^- concentration that coupled with high $\delta^{15}N_{nitrate}$ values to identify samples with wastewater presence. Lower DIC concentrations and TA have high percent NO_3^- speciation in the DIN pool, but such samples had NO_3^- concentrations or $\delta^{15}N_{nitrate}$ values too low to be considered for wastewater presence. However, of the 4 samples with NO_3^- DIN percentage > 70% and high DIC (> 2000 μmol kg^{-1}), 3 were identified for sewage presence via high NO_3^- concentration and high $\delta^{15}N_{nitrate}$ and $\delta^{18}O_{nitrate}$ values. Most samples with high DIC concentration have low NO_3^-:NH_4^+, but not necessarily high concentrations of either NO_3^- or NH_4^+. When NH_4^+ concentration was high, implying a strong connection to an organic matter source such as OSDS or heavy degradation of vegetation such as mangroves, DIC concentration was used to predict the $\delta^{15}N_{nitrate}$ value to help estimate a potential wastewater signal. To be sure the high NH_4^+ concentration was from an OSDS source rather than decaying naturally occurring organic material, we used the methods described in section 5.7.2.

5.7.2. Potential calcite dissolution vs. organic matter degradation contributions to DIC

Understanding the origin of the high DIC concentrations helps to differentiate sources of organic matter as being either wastewater or naturally occurring. To begin, we must first delineate sources of organic matter degradation against other possible contributors to the DIC pool. Although to our knowledge limestone has not been reported within this area, given the extensive and unknown nature of valley fill in the area through which the groundwater flows, the potential for contributions to the DIC of these water via calcite ($CaCO_3$) dissolution cannot be excluded. We therefore utilize DIC, TA, and $\delta^{13}C_{DIC}$ measurements to isolate the effects of organic matter degradation and its balance with potential $CaCO_3$ dissolution in contributing to the DIC pool. By comparing measured DIC and $\delta^{13}C_{DIC}$ values in Kahaluʻu to the expected DIC and $\delta^{13}C_{DIC}$ values based on a simple salinity mixing model (e.g. Bhavya et al., 2018), samples can be separated into sites where organic matter degradation dominates the DIC pool, or where

$CaCO_3$ dissolution has the greatest contribution (data available in Appendix 1). Such delineations are based off regional characteristic values of $\Delta\delta^{13}C_{DIC}$ and Δ[DIC] where

$$\Delta\delta^{13}C_{DIC} = \delta^{13}C_{sample} - \delta^{13}C_{mix} \quad \textbf{(Equation 2.6)}$$

$$\Delta[DIC] = ([DIC]_{sample} - [DIC]_{mix})/[DIC]_{mix} \quad \textbf{(Equation 2.7)}$$

represent the differences between the expected values of $\delta^{13}C_{DIC}$ and DIC based on a simple salinity mixing model labeled with the "mix" subscript, and the measured values labeled with the "sample" subscript. A full introduction to this method regarding salinity mixing models and determination of freshwater fractions is described by Bhavya et al. (2018). The mixed values for DIC and $\delta^{13}C_{DIC}$ are calculated based on a simple mixing model between freshwater and saline endmembers (data available in Appendix 1, Table A1.5.). Any deviations from the theoretical mixed values, represented by Δ[DIC] and $\Delta\delta^{13}C_{DIC}$, imply introduction or removal of DIC species through $CaCO_3$ dissolution or precipitation or organic matter degradation. The expected mixing between freshwater and saltwater endmembers for both variables is defined by

$$[DIC]_{mix} = [DIC]_{fw}F_{fw} + [DIC]_{sw}(1 - F_{fw}) \quad \textbf{(Equation 2.8)}$$

$$\delta^{13}C_{mix} = \frac{[DIC]_{fw}\delta^{13}C_{fw}F_{fw} + [DIC]_{sw}\delta^{13}C_{sw}(1-F_{fw})}{[DIC]_{fw}F_{fw} + [DIC]_{sw}(1-F_{fw})} \quad \textbf{(Equation 2.9)}$$

where the subscript "fw" represents freshwater and "sw" is saltwater. When S is salinity, the freshwater fraction as F_{fw} is calculated using

$$S_{mix} = S_{fw}F_{fw} + S_{sw}(1 - F_{fw}). \quad \textbf{(Equation 2.10)}$$

A linear regression was developed from all 42 samples for which DIC concentrations and TA data exist to define a relationship between DIC concentrations and TA, resulting in the equation

$$[\text{Total Alkalinity}] = 0.8984*[\text{Dissolved Inorganic Carbon}] - 236.77 \quad \textbf{(Equation 2.11)}$$

with an R^2 = 0.95 (**Figure 2.14**). This allows us to calculate TA for the freshwater endmember for which only DIC concentration data are available. Using this calculated TA as an endmember in a mixing analysis of TA vs. Ca^{2+} concentration, our TA and Ca^{2+} data could then be used to verify trends between DIC concentrations vs. Ca^{2+} concentrations.

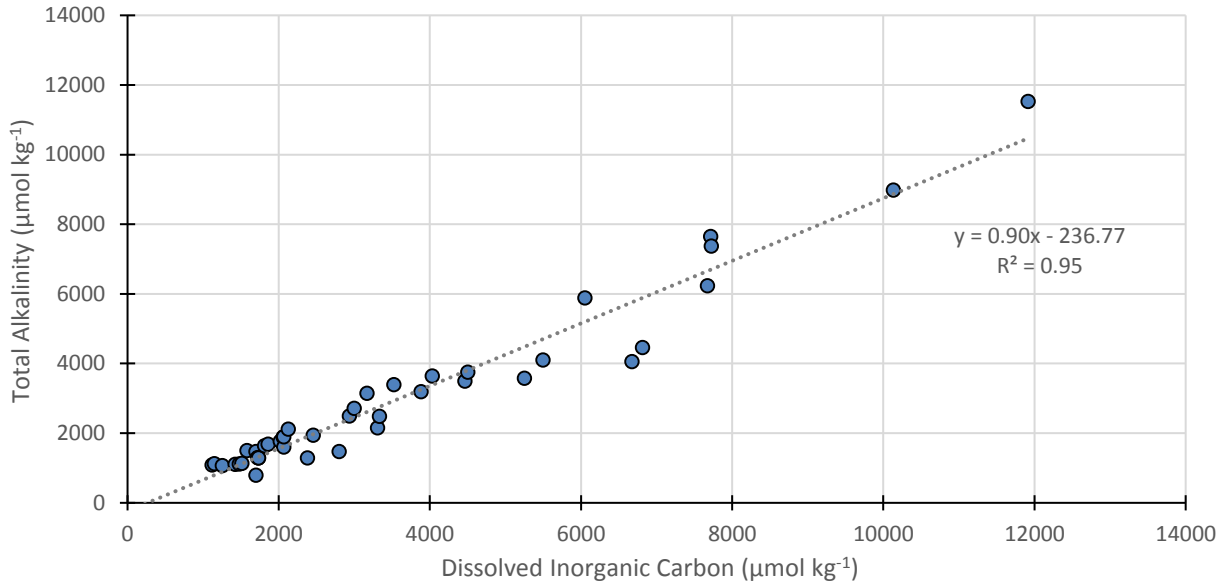

Figure 2.14. DIC vs. TA concentrations throughout the study area and the linear relationship the two possess.

The results of this TA calculation, along with measured TA, are plotted vs. Ca^{2+} in **Figure 2.15d**. The plot also contains the expected salinity mixing line of TA vs. Ca^{2+} and shows two distinct relationships between Ca^{2+} and TA (Figure 2.15d). The same relationships are seen in Ca^{2+} vs. DIC (**Figure 2.15c**). The first relationship is a simple continuation of the trend between expected concentrations based on salinity mixing, encircled by a dashed line on both Figure 2.15c and Figure 2.15d. Thus, the deviations from the expected mixing triggered by $CaCO_3$ dissolution, described as

$$CaCO_3(s) + CO_2(aq) + H_2O \rightarrow Ca^{2+} + 2HCO_3^- \qquad \textbf{(Equation 2.12)}$$

which increases the total DIC and TA pool through the introduction of HCO_3^- and Ca^{2+}. While slight increases to the trend of the relationship between calculated concentrations are expected, there is a complete second linear trend derived specifically from $CaCO_3$ dissolution. Under this

trend, DIC and TA increase at a ~2:1 ratio to Ca^{2+}, encircled by a solid line on both Figure 2.15c and Figure 2.15d. The 14 samples identified as undergoing significant organic matter decomposition via $\Delta\delta^{13}C_{DIC}$ vs. Δ[DIC] (**Figure 2.15a**, quadrant IV) and $\Delta\delta^{13}C_{DIC}$ vs. salinity plots (**Figure 2.15b**, below the curve) are the same samples that follow the anticipated relationship for organic matter degradation based on both DIC vs. Ca^{2+} (Figure 2.15c, dashed circle) and TA vs. Ca^{2+} plots (Figure 2.15d, dashed circle). Those samples with sharp increases in DIC (Figure 2.15c, solid circle) and TA relative to Ca^{2+} (Figure 2.15d, solid circle) are the same samples hypothesized to be sourced from $CaCO_3$ dissolution (Figure 2.15a, quadrant I).

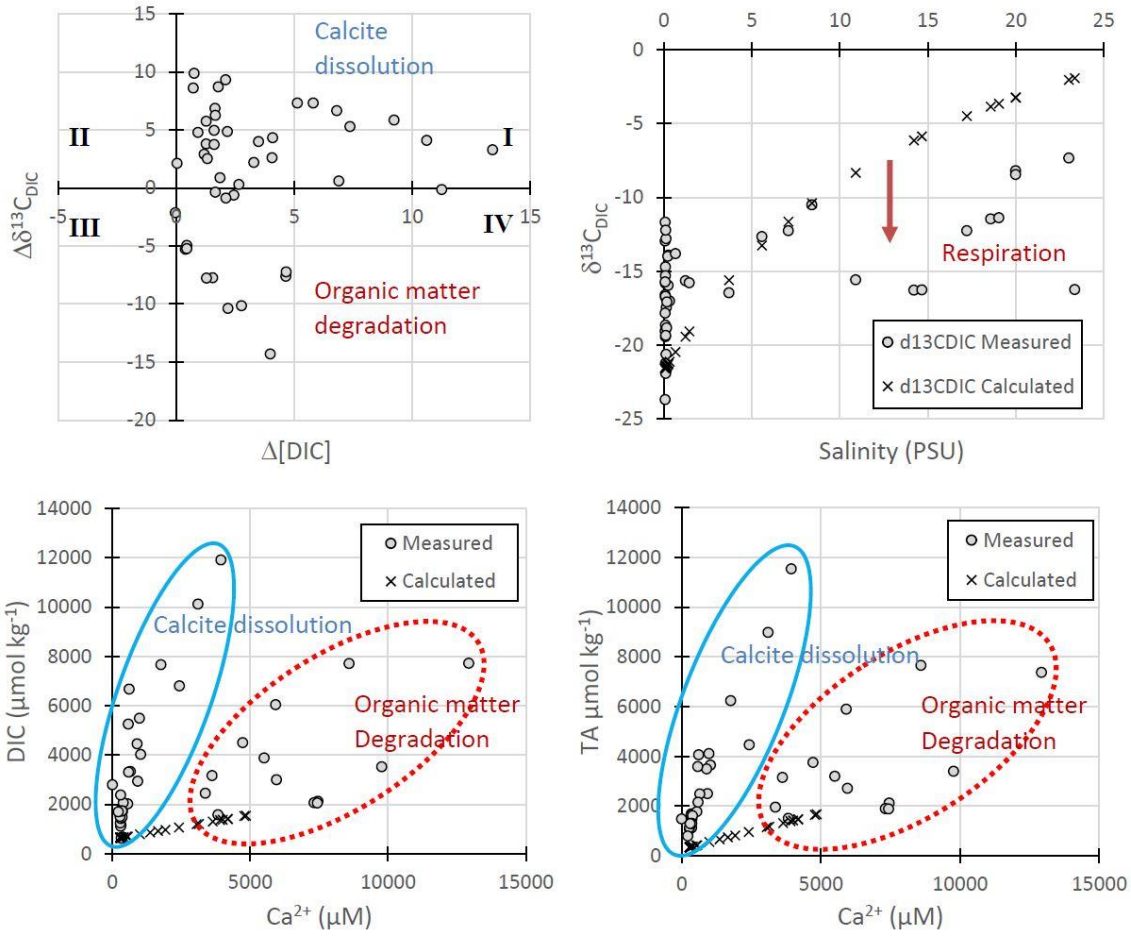

Figure 2.15a. (Top Left) $\Delta\delta^{13}C_{DIC}$ vs. Δ[DIC] (e.g. Bhavya et al., 2018) to determine the dominant mechanism controlling local aqueous carbonate geochemistry throughout the Kahalu'u study region. A collection of samples from estuarine environments show preference to the degradation of organic matter, while the rest of the system is controlled by $CaCO_3$ dissolution. **Figure 2.15b.** (Top Right) The measured $\delta^{13}C_{DIC}$ values against the anticipated $\delta^{13}C_{mix}$ values as interpreted through salinity mixing models and the determination of each samples freshwater fraction. **Figure 2.15c.** (Bottom Left) DIC vs. Ca^{2+} representing showing to distinct mixing ratios for the dissolved species. The mixing model with the steeper slope represents carbonate dissolution, while the lower ratio is representative of a system controlled by the degradation of organic matter and only partly influenced by $CaCO_3$ dissolution. **Figure 2.15d.** (Bottom Right) TA vs. Ca^{2+} representing the same phenomenon in the area.

As such, we designated environments where degradation of organic matter is the primary driver of the DIC pool. No sample with $\Delta\delta^{13}C_{DIC}$ values (Figure 2.15a quadrant IV, Figure 2.15b below the curve) and Δ[DIC] (Figure 2.15a) indicative of organic matter decomposition was indicated in the previous sections to have wastewater presence based on its NO_3^- concentrations, NH_4^+ concentrations, DIC concentrations, and $\delta^{15}N_{nitrate}$ values. Organic matter decomposition is the dominant process contributing to the DIC pool of the groundwater and pore waters of the study area's coastal environments, including Kahaluʻu estuary, Waiāhole mangrove, and portions of the Kaalaea and Haiamoa coastline. This is expected due to their high vegetation cover by *R. mangle* and other supported species. By this method, the remaining samples have DIC pools controlled by $CaCO_3$ dissolution (Figure 2.15a**,** quadrant I). Only areas dominated by $CaCO_3$ dissolution are proposed to have a potential wastewater presence.

If samples are shown to have a DIC-TA pool dominated by naturally occurring organic matter, we exclude them from consideration as having a potential wastewater presence. Only a select group of samples with a DIC-TA pool dominated by $CaCO_3$ dissolution were suggested to have a wastewater presence based on DIN parameters: five pore water samples and one shallow groundwater sample for which DIC-TA data were available were determined to have wastewater presence via high NO_3^- concentration, high $\delta^{15}N_{nitrate}$ values, and in certain cases, high NH_4^+ as annotated in Figure 2.14. We therefore suggest only samples with $CaCO_3$ dissolution as the dominant DIC-TA systematic to undergo our predictive estimates of $\delta^{15}N_{nitrate}$ values based on DIC concentration.

6. Conclusion

We documented wastewater-borne nutrients from OSDS leachate, including effluent from cesspools and malfunctioning septic tanks, are transported through groundwater to streams and nearshore coastal waters of the Kahaluʻu region of Oʻahu, Hawaiʻi. This was determined with a multi-tracer approach to distinguish nutrient sources using NH_4^+ concentrations, NO_3^- concentrations, $\delta^{15}N_{nitrate}$ values, B concentrations, and $\delta^{11}B$ values. High NO_3^- concentration and $\delta^{15}N_{nitrate}$ values revealed wastewater presence in streams and pore water of sites down-gradient of highest OSDS density. High NH_4^+ concentrations were found in shallow groundwater adjacent to OSDS, interpreted as raw sewage in local wastewater leachate that is primarily organic N

mineralized to NH_4^+. Such groundwater samples where NH_4^+ was the dominant DIN species showed systemically higher DIC concentrations and TA above ~2000 μmol kg^{-1}. Where $\delta^{15}N_{nitrate}$ values increased with DIC and TA, DIC values were used to estimate $\delta^{15}N_{nitrate}$ values in those samples not dominated by naturally occurring organic matter degradation, as determined through a comparison of expected and measured DIC concentrations and $\delta^{13}C_{DIC}$ values. *R. mangle*'s $\delta^{15}N$ values in foliage did not have a quantitative relationship with adjacent pore or surface water NO_3^- concentration or $\delta^{15}N_{nitrate}$ values, and more work is needed to properly establish a connection between $\delta^{15}N_{nitrate}$ values in pore water and $\delta^{15}N$ values in mangrove root, stem, and leaf extracts. This study did, however, note a semi-quantitative relationship in $\delta^{15}N$ values in leaves of mangroves at the coastline of watersheds with high up-gradient OSDS densities vs. the pristine control watershed and the watershed identified to experience agricultural nutrient influx. Such agricultural nutrient discharge was assessed with high $\delta^{11}B$ values and low B concentrations indicating nutrient-rich agricultural drainage to the stream. This solidifies agricultural discharge as an important nutrient source in the Kahaluʻu region, but spatially second to and paling in comparison with OSDS-sourced wastewater. OSDS-sourced nutrient delivery through the groundwater aquifer to fresh and saline surface waters of the study area has been found to vary as a function of OSDS density, distance from OSDS to the stream or shoreline, and depth to the water table. Our results prove the utility of the paired N-B-C approach to identifying and source-tracking wastewater presence through groundwater in tropical coastal environments.

CHAPTER 3. SEASONAL DISTRIBUTION OF THE STABLE ISOTOPIC COMPOSITION OF PRECIPITATION TO INFER GROUNDWATER RECHARGE IN TROPICAL VOLCANIC SETTINGS: O‘AHU

Abstract

The first local meteoric water line (LMWL) for O‘ahu was established in this study to develop a hydrologic connection between precipitation and aquifer recharge for the island. Over one year, a network of 20 precipitation collectors was deployed across O‘ahu. Our LWML shows δ^2H values correlate linearly with $\delta^{18}O$ values island-wide, with a slope of 7.3 and y-intercept of 10.4 (compared to the global meteoric water line values of 8 and 10, respectively), with altitude exercising much less control on precipitation δ^2H and $\delta^{18}O$ values than other Hawaiian Islands. Lowest island wide precipitation occurs during the dry season (2017 May-2017 September) along with the highest δ^2H and $\delta^{18}O$ precipitation values. Highest island-wide cumulative precipitation occurred throughout the wet season (2017 October-2018 March) with the highest collected volume from the 2018 January-2018 March 3-month sampling window. Precipitation during both wet season sampling windows has the lowest δ^2H and $\delta^{18}O$ values for the year. For all 9 collector locations where groundwater isotopic data exists, annual volume-weighted average (VWA) δ^2H values in local precipitation differ from mean δ^2H values of surrounding groundwater by absolute values by 0.6‰ to 3.3‰, suggesting localized aquifer recharge. The wet season VWA from 2017 October-2018 March minimizes this absolute difference for all stations except the southeastern Honolulu region of the Southern Pearl Harbor Aquifer. During the weak La Niña conditions of the 2017-2018 wet season, O‘ahu experienced one of its wettest winters in 30 years. Based on the volumetric share of annual precipitation comprised by wet season (2017 October-2018 March) rainfall, similarities in δ^2H values between wet season precipitation and regional groundwater, and increase in rainfall intensity under winter rainfall regimes, O‘ahu’s wet season is considered to have the greatest contribution to local aquifer recharge island-wide.

1. Introduction

Maximizing the potential of fresh groundwater resources under threats of climate change and sea level rise is a priority for an island system like Hawai‘i, which obtains 99% of its domestic water supply from groundwater (Gingerich and Oki, 2000). Understanding hydrologic connections between precipitation-based recharge and subsurface flow to aquifer storage is paramount to this end. The goal of this research is to understand the seasonal and spatial distribution of aquifer recharge on the tropical volcanic island of O‘ahu, Hawai‘i to enhance water resource management. Particularly on O‘ahu, precipitation in the form of rainfall occurs in areas of high elevation, while the majority of the island’s 1 million residents live in low-lying coastal regions (U.S. Census Bureau, 2017). This uneven distribution of precipitation and population has already caused legal disputes surrounding water rights and usage (Earth Justice, 2006). The future of socioeconomic development on O‘ahu remains intrinsically tied to fresh water availability. Establishing a hydrologic link between the origins of aquifer recharge on O‘ahu will dictate sustainable usage and serve as a model for other tropical volcanic islands.

Variations in the isotopic composition of water serve as naturally occurring tracers in precipitation, groundwater, and surface water, allowing us to connect groundwater in aquifers to its origins as rainfall. The relationship between δ^2H (deuterium abundance relative to Vienna Standard Mean Ocean Water, or VSMOW) and $\delta^{18}O$ (oxygen-18 abundance relative to VSMOW) values in global precipitation forms the basis of the global meteoric water line (GMWL) (Craig, 1961). δ^2H and $\delta^{18}O$ values and their ensuing relationship are defined by kinetic and equilibrium isotope fractionation during evaporation from the oceans and eventual condensation (Dansgaard, 1964). Such fractionation is controlled by relative humidity at the time of evaporation and temperature of the air at the time of condensation (Clark and Fritz, 1997). Therefore, a local meteoric water line (LMWL) represents a subgroup of the GMWL as the relationship between δ^2H and $\delta^{18}O$ values in regional precipitation where these conditions may vary locally (Dansgaard, 1964). This is particularly necessary for coastal volcanic settings where regional microclimates experience distinct, localized weather, including O‘ahu, Costa Rica (Rhodes et al., 2006), Hawai‘i (Scholl et al., 1996), Maui (Scholl et al., 2002; Scholl et al., 2007), and Puerto Rico (Scholl and Murphy, 2014). The project undertook a yearlong, island-wide precipitation collection for O‘ahu at 20 locations to establish a record of characteristic δ^2H

and $\delta^{18}O$ values in rainwater for distinct regions and elevations at a seasonal resolution of 3 months. The results are the first LMWLs on O‘ahu, tracking patterns in changes to the isotopic composition of precipitation across the island.

This study combines new $\delta^{2}H$ and $\delta^{18}O$ values for O‘ahu’s groundwater with a comprehensive record of existing stable isotope measurements in aquifers across the island to create projected areas of groundwater recharge. From the LMWL, hypothetical flow vectors link rainwater from a collector in a discrete region of precipitation to well water from an aquifer with the same isotopic composition, relating the origin of recharge and subsequent subsurface flow (Scholl et al., 1996; Scholl et al., 2002). Stable isotopic compositions and major ion concentrations were determined at every location for all 4 intervals throughout the year, and volume-weighted average (VWA) calculations produced an annual synthesis of results. These rainfall compositions, coupled with $\delta^{2}H$ and $\delta^{18}O$ values of groundwater, yield the first isotopically derived recharge maps for O‘ahu.

2. Background

2.1. Hydrogeology of O‘ahu

The island of O‘ahu, formed from two ancient overlapping shield volcanoes, is primarily basaltic in composition (Stearns and Vaksvik, 1935). Pleistocene and Pliocene aged Ko‘olau Basalt comprise the compositionally homogeneous eastern Ko‘olau volcano, the younger of the two shield volcanos (Hunt, 1996; Nichols et al., 1996). Ko‘olau collapsed and lost approximately 40% of its mass to a catastrophic landslide east into the Pacific, leaving behind the Ko‘olau Range (Moore and Clague, 2002). The Ko‘olau rift zone has nearly vertical dikes striking north-northwest and extending away from the caldera axis (Takasaki and Mink, 1982), with a few dikes present in the caldera itself (Walker 1986, 1987). Lava flows from the Ko‘olau volcano partially overlay the older Waianae Volcanics in the “saddle” of O‘ahu (Hunt, 1996; Nichols et al., 1996). The Waianae Range on the leeward side of O‘ahu is comprised of the remnants of the older of the two volcanoes. The Waianae Volcano consists of a variety of igneous material from two major formations, the Pliocene Waianae Volcanics and Pleistocene Kolekole Volcanics (Stearns and Vaksvik, 1935; Zbinden and Sinton, 1988). This Waianae shield volcano eventually collapsed and suffered a massive slumping event to the west of O‘ahu (Presley et al., 1997).

Within the northwest Waianae volcano rift zone, dikes dip vertically and sub-vertically, although, unlike the Koʻolau volcano, many more dikes exist in the caldera itself with gentler dip angles (Zbinden and Sinton, 1988).

The dike complex of both the Waianae and Koʻolau rift zones are important for the storage of high-level groundwater. There are four major igneous rock types on Oʻahu including lava flows (ʻaʻā and pāhoehoe), dikes, pyroclastic deposits, and weathered basalt, or saprolite. Fractures, voids between horizontal layers, and porosity derived from their vesicular texture make lava flows the most hydrologically conductive igneous material on the island. The increased density of dikes and their vertical orientation in crosscutting lava flows make them effective horizontal flow barriers (Takasaki, 1969; Takasaki and Mink, 1981). As a result, the majority of Oʻahu's groundwater is stored in porous basaltic lava flows and compartmentalized between dikes of low permeability in its two main mountain ranges (Hunt, 1996; Nichols et al., 1996).

Sedimentary "caprock" covers the southern and western coastal plains. This lithified calcareous and volcanogenic sediment is Holocene and Pleistocene in age. Deposited atop basaltic lava flows and other igneous aquifer materials, the caprock's low permeability acts as a confining layer to the saturated zone and prevents submarine groundwater discharge (SGD) from the volcanic aquifer (Hunt, 1996; Nichols et al., 1996).

2.2. Aquifers of Oʻahu

Groundwater is impounded and compartmentalized at both a minor scale within aquifers and at a major, island-wide scale delineating principal aquifers through lithographic (i.e. dikes and ponded lavas) or surficial (alluvial fills of deep valley cuts) flow barriers (Hunt, 1996). There are seven major aquifers on Oʻahu: Waianae rift zone of Waianae Range, North-Central, Schofield in the saddle of Oʻahu, Koʻolau rift zone of the Koʻolau Range, Kahuku in the northeast, Southern Pearl Harbor aquifer, and Southeastern Oʻahu near Honolulu (**Figure 3.1**). The dikes of Waianae and Koʻolau rift zone aquifers provide no-flow barriers that trap and compartmentalize groundwater as elevated dike-impounded water and low permeability volcanic deposits create smaller perched aquifers, developing the highest hydraulic head values on island (Takasaki et al., 1969; Takasaki and Mink, 1981). Schofield aquifer is also impounded to high hydraulic head values, although it lacks the significant compartmentalization of dike-impounded waters in the

Waianaes and Koʻolaus. The North-Central, Kahuku, Southern, and Southeastern aquifers are basal freshwater lens systems subdivided regionally into minor aquifers based on valley-fill flow barriers. These basal freshwater lenses float above denser saturated saltwater zone and the majority are unconfined, barring the presence of sedimentary caprock (Hunt, 1996; Nichols et al., 1996).

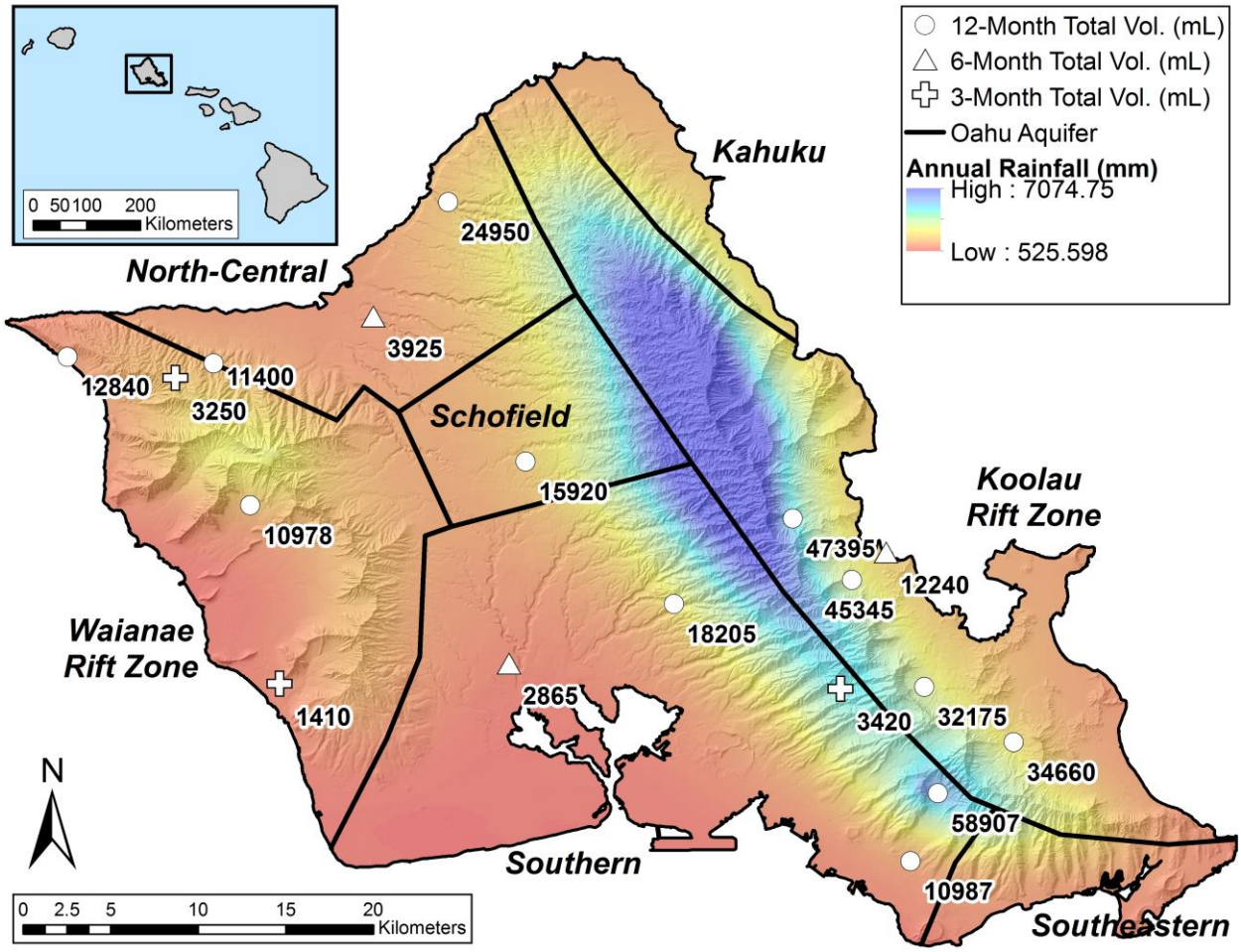

Figure 3.1. Map of the precipitation collector network deployed in this study. The total volume of precipitation collected as rainfall across Oʻahu throughout the duration of the study is marked adjacent to each site in mL, and symbolized with the duration of deployment. Names of major aquifers are in bold. Aquifer delineations are adapted from Hunt (1996), Nichols et al. (1996), and Shade and Nichols (1996). Precipitation coverage from Giambelluca et al., 2013.

Daily recharge estimates for Oʻahu increased or stabilized for each aquifer under urban development conditions. Based on mid-1980s recharge budgets from Shade and Nichols (1996), almost half Oʻahu's island-wide recharge total occurs in the Southern Pearl Harbor Oʻahu aquifer, followed by North-Central and Windward aquifers which each make up roughly a

quarter of the total recharge budget. Waianae and Southeastern O‘ahu aquifer receive an order of magnitude less in daily recharge than these 3 aquifers. The dominant share of trade-wind-driven precipitation falls on Ko‘olau Range, contributing substantially to O‘ahu’s three most-recharged aquifers.

2.3. Freshwater flow through O‘ahu

Deep, dense saltwater flow underlying shallow, fresh groundwater flow are the two overarching groundwater flow regimes on O‘ahu. Gravity-driven freshwater flow predominantly moves down gradient from higher elevations of inland recharge to lower coastal altitudes. This general freshwater flow can be subdivided into five major flow systems: (1) eastern, (2) north-central, (3) south-central, (4) western, and (5) southeastern. The freshwater flow is faster than saltwater flow, leading to a lower residence time. Studies estimate most groundwater ages to be 20-60 years old (Hunt, 2004), although some estimate the basal aquifers of southern O‘ahu in the Pearl Harbor and Honolulu regions to be hundreds of years old (Hufen et al., 1980). All flow systems originate with the dike-impounded waters of high hydraulic head of either the Waianae or Ko‘olau rift zone aquifers, with groundwater ultimately flowing seaward as interpreted by Hunt (1996) and Nichols et al. (1996). These current projections of freshwater flow systems rely heavily on topographic divides and geohydrologic barriers for expected groundwater flow.

2.4. Precipitation on O‘ahu

Trade winds dominate the climate of O‘ahu; blowing east-to-west, the winds vary seasonally, and are strongest from May to September (Blumenstock, 1961, Lyons, 1982; Schroeder, 1993; Giambelluca and Sanderson, 1993). In this period, trade winds blow 80 to 95% of the time. Trade winds continue to control weather patterns through the winter months of October to April, but decrease to 65 to 80% of the monthly average (Blumenstock, 1961). As a result, O‘ahu experiences two dominant seasons: a 5-month warm, “dry” summer of May to September and a 7-month cool, “wet” winter from October to April (Giambelluca and Sanderson, 1993). Rainfall varies greatly both seasonally and spatially across O‘ahu dictated by the trade winds (Nichols et al., 1996).

The majority of rain on O‘ahu falls on the windward (eastern) side of the island over the Ko‘olau Range (Giambelluca et al., 2013) (Figure 3.1). This precipitation is orographic, as

northeasterly trade winds push moist air up and over the peaks of the Koʻolau Mountains, with average daily orographic precipitation increasing under stronger trade wind cycles (Hartley and Chen, 2010). Local maximum rainfall occurs just leeward of the Koʻolau ridgeline (Giambelluca and Sanderson, 1993) (Figure 3.1) at Kahana in the north and Tantalus in the south. The Waianae Range on the leeward side of Oʻahu receives significantly less rain in the trade wind shadow of the Koʻolaus (Hunt, 1996). The local maximum precipitation on the leeward side of the island occurs in the northwestern region of the Waianae range at Kaʻala (Giambelluca and Sanderson, 1993), while the island-wide minimum rainfall occurs in the southwestern lowlands (Hunt, 1996; Nichols et al., 1996). Diurnal land-sea breezes help further diversify microclimates caused by trade winds (Leopold, 1949), especially on leeward Oʻahu (Hartley and Chen, 2010).

Mid-latitude frontal rain band storms, extratropical cyclones, and tropical cyclones comprise Oʻahu's other precipitation sources (Blumenstock, 1961; Schroeder, 1993). In winter, mid-latitude frontal rain bands, or cold fronts, bring storms that vary in number annually from 1-8 across the entire state (Blumenstock, 1961). However, many frontal patterns pass north of the Hawaiian Islands affecting only Kauai and can miss Oʻahu entirely (Chu et al. 1993). Extratropical cyclones, known colloquially as Kona Lows, are non-frontal low-pressure systems with deep convection, bringing with them precipitation lasting days or weeks during the winter months (Chu et al., 1993). Intermittent periods of intensified precipitation can interrupt the pattern of prolonged, moderate rainfall characteristic of Kona storms (Blumentsock, 1961). A result of Kona Lows is an increase in rainfall in many regions that do not see steady precipitation under the orographic trade wind regime (Norton et al., 2011). Tropical cyclones become tropical storms when winds surpass 64 km hr^{-1} (38 mph) or hurricanes if winds top 105 km hr^{-1} (63 mph) (Schroeder, 1993). These storms form off the west coast of Central America, arriving in the Hawaiian Islands from July to December, although they rarely reach the archipelago (Blumenstock, 1961; Schroeder, 1993).

Trade wind rainfall accounts for the majority of summer rainfall variability in precipitation patterns on Oʻahu. However, contributions of winter cold front and Kona storms produce additional rainfall variability in the wet season (Lyons, 1982). Trade wind rainfall increases in intensity with increased elevation/decreased distance from the summit is proportional to ridgeline proximity (Stidd and Leopold, 1951; Mink, 1960), and thus leaves a large portion of

O‘ahu with low-intensity rainfall patterns for most of the year. Even on windward slopes, numerous light, scattered showers occur throughout the day, producing 0.25 mm of rain each (Blumenstock, 1961). Precipitation caused by cold fronts, Kona storms, and tropical cyclones is much more intense, if not more irregular (Hunt, 1996). In areas of O‘ahu not experiencing precipitation from orographic uplift of trade wind precipitation, approximately two-thirds of annual rainfall comes from several winter storms (Reihl, 1949; Simpson, 1951).

On O‘ahu, recharge is predicted to increase with both intensity and duration of rainfall events (Nichols et al., 1996). Recent studies conclude increased rainfall intensity (10 mm day^{-1}) in the tropics lead to higher groundwater recharge (Owor et al., 2009). While models predict rainfall too intense will limit groundwater recharge at extreme intensities of 75 mm h^{-1}, they show substantial aquifer recharge at 45 mm h^{-1} (Wang et al., 2015). As such, the authors predict greatest infiltration will occur during periods of intense rainfall, anticipated to occur in the wet season in the presence of winter storms, primarily subject to the influence of Kona Lows.

The 2017-2018 wet season for the Hawaiian Islands was considered to be erratic, yet generally very wet statewide. According to the National Oceanic and Atmospheric Administration’s (NOAA) wet season rainfall summaries for Hawai‘i from 2017-2018, O‘ahu’s 2017 dry season was El Niño Southern Oscillation System-normal (ENSO-normal), beginning at the end of a wet April 2017. O‘ahu’s 2017-2018 wet season had weak La Niña conditions in October 2017 lasting until April 2018, leading to a prediction that the upcoming 2018 dry season would be ENSO-normal. Under these weak La Niña conditions, leeward O‘ahu is typically wetter than its historical average. From 1956-1982, the Hawaiian Islands typically receive more wet season rainfall under La Niña conditions. From 1983-2010, however, the Hawaiian Islands are receiving less wet season rainfall under La Niña conditions (O’Connor et al., 2015). Nonetheless, NOAA considers the 2017-2018 winter to be the 5th wettest seasons in the last 30 years for the Hawaiian Islands.

3. Materials and Methods

3.1. Precipitation collector network

A network of 20 precipitation collectors was deployed across the island over a period of 12 months to collect rainwater samples (**Table 3.1**, Figure 3.1). This network includes four transects

of four collectors each running in a westerly direction across O‘ahu at Northern, Central, Southern, and Southeastern intervals. However, due to permitting constraints, vandalism, and land use availability, the number of collectors deployed and their locations varied from season to season. The east-to-west linear position of collectors tracked changes in the composition of rainfall as weather moves in a westward direction across the island under the influence of the northeasterly trade winds.

Table 3.1. Deployment dates and locations for all rainfall collectors, as well as dates removed due to vandalism where applicable. Elevation and distance from the coast are also displayed in reference to known GPS coordinates for each location in UTM Zone 4.

Location	Deployment	Removal	UTM Easting	UTM Northing	Elev. (m)	Dist. East (m)
Kahalu‘u Ridge	27-Feb-2017		619516	2371546	100	2323
Waiāhole F.R.	27-Feb-2017		616351	2375013	160	3744
Ewa Waimano	20-Mar-2017	21-Mar-2017	610052	2370111	291	10671
HIG UH Mānoa	20-Mar-2017		622760	2355609	22	14456
Honolulu F.R.	20-Mar-2017	7-Jul-2017	618954	2365377	188	6882
Wahiawa B.G.	20-Mar-2017		602113	2378146	309	16025
Ewa Poamoho	21-Mar-2017		605044	2378810	375	12,629
Hau‘ula F.R.	21-Mar-2017	15-Apr-2017	612189	2389867	25	683
Hawai‘i Ag. Center	21-Mar-2017		628197	2362396	111	5542
Ho‘omaluhia B.G.	21-Mar-2017		623417	2365502	65	3737
Lyon Arboretum	21-Mar-2017		624183	2359481	152	10329
Waimea Valley	21-Mar-2017		597896	2392848	4	12234
Ka‘ena Point	22-Mar-2017		577713	2383945	11	34176
Mokuleia F.R.	22-Mar-2017		585481	2383615	167	27766
Nanakuli F.R.	22-Mar-2017	16-Oct-2017	589090	2365463	51	32235
Waianae Kai F.R.	22-Mar-2017	20-Mar-2018	587481	2375570	262	30438
Kamehameha Hwy.	11-Sep-2017		621325	2373115	6	29
Haleiwa Wells	23-Oct-2017		593961	2386342	64	18999
Kunia III Wells	23-Oct-2017		601295	2366681	98	20019
Mokuleia F.R. 2	16-Jan-2018		583448	2382783	610	29826

3.2. Collector construction

A precipitation collector is approximately 1 m tall and 0.5 m in diameter, consisting of a 20 L HDPE bucket with lid and attached 110 mm diameter plastic Buchner funnel, deployed on a small wooden platform with three metal legs (e.g. Scholl et al., 1996). The footprint of each collector is less than 0.3 m^2. At the bucket’s base is a spigot to drain the collector of the sample. A 1 cm thick layer of mineral oil prevents evaporation of the sample.

3.3. Sampling procedure

Sample collection occurred every 3 months from the date of deployment over 1 year beginning at the start of the dry season in March 2017 through March 2018. Sixteen collectors were originally deployed in March 2017. Throughout this study, 4 collectors were lost to vandalism, and an additional 4 collectors were installed at new locations. Table 3.1 lists deployment dates, sampling schedules, and volumes of rainfall captured at each location.

The 3 month sampling intervals captured variation in isotopic composition of rainfall between wet and dry seasons. Seasonal and annual VWA $\delta^{18}O$ and $\delta^{2}H$ values for each sample site were calculated using Equation 3.1 after Jaeschke et al. (2011):

$$Volume\ Weighted\ Average = \frac{\sum_{i=1}^{n}(P_i * \delta_i)}{\sum_{i=1}^{n} P_i} \qquad \textbf{(Equation 3.1)}$$

where δ_i represents the $\delta^{18}O$ or $\delta^{2}H$ value (‰) of the sample, P is the sample volume (mL), and n is the total number of samples utilized in the summation.

Rainwater from the collector was drained into a graduated cylinder to measure total collected volume in that window. A subsample (60 mL) was poured through a standard bleached paper filter from that graduated cylinder, and refrigerated (4ºC) in a HDPE bottle prior to laboratory analysis. To prepare the collector for redeployment on site for the next 3 month interval, the collector was fully drained and the remaining oil skimmed for the removal of organics.

Total collected volume was measured with a 2000 mL graduated cylinder to a precision of 20 mL per filling of the graduated cylinder. Total cylinder fills including partial fills ranged from 1 to 10 per sample site per 3 month sample, and a propagated error was calculated for each 3 month sampling period, ranging from 20.0 to 63.2 mL. This error was then propagated for each sample site for the total annual volume, and ranged from 20.0 to 114.9 mL (**Appendix 2**).

3.4. Analytical Procedure

Stable isotopic compositions of rainwater were measured in triplicate at the University of Hawai‘i School of Ocean and Earth Science and Technology (UH SOEST) Biogeochemical Stable Isotope Facility using a fully automated Picarro L2130-*i* WS-CRDS. Laboratory results of $\delta^{2}H$ and $\delta^{18}O$ values are expressed in per mil notation (‰) against VSMOW. Sample precision

calculated from duplicate pairs (n = 19) at 1 standard deviation was 0.39‰ for δ^2H values and 0.12‰ for $\delta^{18}O$ values. The propagated error for the VWA calculated from 4 samples over 12 months is 0.79‰ δ^2H and 0.24‰ $\delta^{18}O$; for the location with 7 samples over 12 months, this increases to 1.03‰ δ^2H and 0.32‰ $\delta^{18}O$. Concentrations of major common ions species were determined at the Water Resources Research Center Analytical Chemistry Laboratory at the University of Hawai‘i at Mānoa using a Dionex ICS-1100s(IC). Sample precision calculated from duplicate pairs (n = 20) at 1 standard deviation was as follows: 25.5 μM Cl^-, 1.9 μM SO_4^-, 32.4 μM Na^+, 9.9 μM K^+, 4.6 μM Mg^{2+}, 9.3 μM Ca^{2+}.

4. Results

All precipitation collected was rainfall. δ^2H values (**Table 3.2, Figure 3.2**) were most variable throughout the study and thus used as a proxy for variation in isotopic composition. Twelve sites provided complete annual coverage; two sites were vandalized and recorded no data; two were vandalized and recorded the first 3 months of precipitation; three sites were added 6 months into the study; one site was added with 3 months remaining. The study's full collected data is provided in Appendix 2.

δ^2H and $\delta^{18}O$ values for O‘ahu's precipitation do not have a strong relationship with a precipitation collector's distance from O‘ahu's windward shore as measured via topographic transects aligned to a 67.5° angle to the east-northeast (with north being 0°), as this is the daily average wind direction measured at Kāne‘ohe Bay from 2000-2018 and representative for trade wind direction. However, total annual rainfall volume at a collection station did correlate with distance from the eastern shore of O‘ahu ($R^2 = 0.51$) for 12 annual sites; each individual 3 month sampling window displayed a range of linear correlation coefficients close to 0.40. Such a relationship supports a decrease in precipitation as trade winds carry moisture across the island from east to west.

Cumulatively, the Lyon Arboretum location in Mānoa Valley received the highest annual precipitation volume at 58.9 L. Waianae Kai had the lowest at 11 L. The location with the lowest values for both δ^2H and $\delta^{18}O$ was Mokuleia Forest Reserve at -14.1‰ δ^2H and -3.4‰ $\delta^{18}O$. Full descriptions of all collected volumes and isotopic compositions are presented in Table 3.2, with mapped total volumes in Figure 3.1, and volume-weighted average of δ^2H mapped in Figure 3.2.

Table 3.2. Isotopic composition of each sample collected once every 3 months for the yearlong study. The volume-weighted average (VWA) calculation determined the isotopic composition of precipitation at that location.

Location	March, 2017			Apr-Jun, 2017			Jul-Sep, 2017			Oct-Dec, 2017			Jan-Mar, 2018			Total	Annual Vol. Wt. Avg.	
	Vol. (mL)	$\delta^{18}O$ (‰)	$\delta^{2}H$ (‰)	Vol. (mL)	$\delta^{18}O$ (‰)	$\delta^{2}H$ (‰)	Vol. (mL)	$\delta^{18}O$ (‰)	$\delta^{2}H$ (‰)	Vol. (mL)	$\delta^{18}O$ (‰)	$\delta^{2}H$ (‰)	Vol. (mL)	$\delta^{18}O$ (‰)	$\delta^{2}H$ (‰)	Vol. (mL)	$\delta^{18}O$ (‰)	$\delta^{2}H$ (‰)
Ewa Waimano				2320	-1.5	-1.5	4445	-2.3	-7	5650	-3.6	-13.9	5790	-2.7	-9.2	18205	-2.73	-9.14
Hawai‘i Ag. Center				7060	-2.1	-1.1	5050	-2	-4.5	12780	-2.8	-7.7	9770	-2.7	-8.7	34660	-2.51	-6.17
HIG UH Mānoa				2240	-1.5	-2.4	912	-1.6	-4	4940	-3.1	-15.5	2895	-3.4	-14.2	10987	-2.73	-11.53
Ho‘omaluhia B.G.				12380	-1.7	-0.2	5400	-2.2	-5.1	4995	-3.3	-11	9400	-3	-10.1	32175	-2.41	-5.59
Kahalu‘u Ridge	2840	-4.4	-22.4	8010	-2.0	-0.5	7200	-2.3	-6.7	15890	-2.9	-8.5	11405	-3.4	-13.6	45345	-2.87	-8.95
Ka‘ena Point				2820	-1.3	-0.2	1270	-3.1	-15.7	2280	-2.2	-5.3	6470	-3	-11.3	12840	-2.49	-8.23
Mokuleia F.R.				2980	-2.7	-9.9	2090	-4.1	-19.8	4380	-3.5	-13.9	1950	-3.5	-15	11400	-3.40	-14.12
Waiāhole F.R.	2495	-3.4	-13.9	9940	-2.2	-1.1	10500	-2.6	-7.4	7695	-2.5	-4.2	16765	-3.2	-11.5	47395	-2.75	-7.35
Waianae Kai F.R.				2490	-1.7	-4	3998	-2.9	-11	3300	-2.7	-11.4	1190	1.8†	7.6†	10978	-2.06	-7.52
Wahiawa B.G.				4820	-2.1	-5.6	3345	-1.9	-3.1	4240	-3.3	-13	3515	-3.1	-11.5	15920	-2.60	-8.35
Waimea Valley				12755	-1.5	-0.6	2580	-2.3	-9.8	3340	-2.7	-8.1	6275	-2.6	-9.1	24950	-2.02	-4.69
Lyon Arboretum				18357	-1.2	0.7	8730	-2	-5.0	16150	-2.5	-6.2	15670	-2.0	-5.7	58907	-1.9	-3.7
Nanakuli F.R.				1410	-2.1	-5.9										1410	-2.10	-5.90
Honolulu F.R.				3420	-1.8†	-2.7†										3420	-1.80	-2.70
Kamehameha Hwy.										4850	-2.8	-9.4	7390	-3.8	-17.8	12240	-3.40	-14.47
Kunia III Wells										1175	-3.9	-20.9	1690	-3.3	-14.2	2865	-3.55	-16.95
Haleiwa Wells										845	-4	-22.8	3080	-3.8	-17.7	3925	-3.84	-18.80
Mokuleia F.R. 2													3250	-3.9	-16.6	3250	-3.90	-16.60

*Samples were collected at 6 week intervals during these three periods due to increased rainfall at the station, putting the collector at risk of overflowing and losing sample. The isotopic compositions reported for these intervals are VWA of the two 6 week intervals comprising the 3 month sample window.

†Due to the vandalism noted at the time of collection, sample could be contaminated or altered via evaporation. The sample from the collector at Honolulu Forest Reserve is not thought to have been greatly altered via evaporation from the Apr-Jun 2017 interval. The sample from the collector at Waianae Kai Forest Reserve from Jan-Mar 2018 is thought to have vastly altered data due to evaporation, and is therefore not included in the VWA calculation.

Ion concentrations at coastal sampling stations were used to evaluate saltwater contamination to the sample in the collector throughout the duration of deployment. Highest concentrations of Cl^- and Na^+ ions amongst all collectors were found at Kaʻena Point on the western side of the island during each collection period, and were seasonally highest from October-December 2017. Using salinity and ion concentrations from 131 groundwater, stream, coastal, and pore water samples from windward Oʻahu (where Waiāhole, Kahaluʻu Ridge, and Kamehameha Hwy. Stations were deployed), linear relationships were developed between salinity and ion concentrations to predict salinity for the Kaʻena Point precipitation samples lacking salinity measurements (**Table 3.3**). The mean of five salinity predictions for Kaʻena Point from October to December, 2017 estimates the salinity of the sample to be 6.61.

Table 3.3. Five linear relationships between salinity and common ion concentrations, including the linear regression equation and R^2 value, used to predict the salinity of rainfall samples for which no salinity data was observed. Also included is the average of these results for salinity.

Ion	Salinity Equation	Ion Concentration (µM)	Predicted Salinity	R^2
Chloride	Salinity = $0.0018(Cl^-) + 0.2341$	2970.4	5.58	0.99
Sodium	Salinity = $0.0032(Na^+) + 0.2409$	2609.8	8.59	0.99
Potassium	Salinity = $0.0937(K^+) + 0.1426$	110.0	10.45	0.98
Magnesium	Salinity = $0.0221(Mg^{2+}) – 0.0016$	279.8	6.18	0.98
Sulfate	Salinity = $0.0126(SO_4^-) + 0.2386$	158.2	2.23	0.99
Average	--	--	6.61	--

Five samples were taken from the UH Mānoa location to represent even-based precipitation in periods of high rainfall. Two of these storms presented isotopic compositions significantly depleted in ^2H compared to any 3 month sample, with values of -29.7‰ and -40‰ for δ^2H and -5.2‰ and -6.3‰ for $\delta^{18}O$.

5. Discussion

To the best of the authors' knowledge, this study created the first catalogue of $\delta^{18}O$ and δ^2H values in Oʻahu's precipitation and established a LMWL for the island. These data allow significant insight into how the isotopic composition of rainwater on the island varies spatially and seasonally over the course of 1 year. Our results suggest that wet season precipitation δ^2H values predict that the increased volume and intensity of rainfall during the wet season dictates Oʻahu's aquifer recharge.

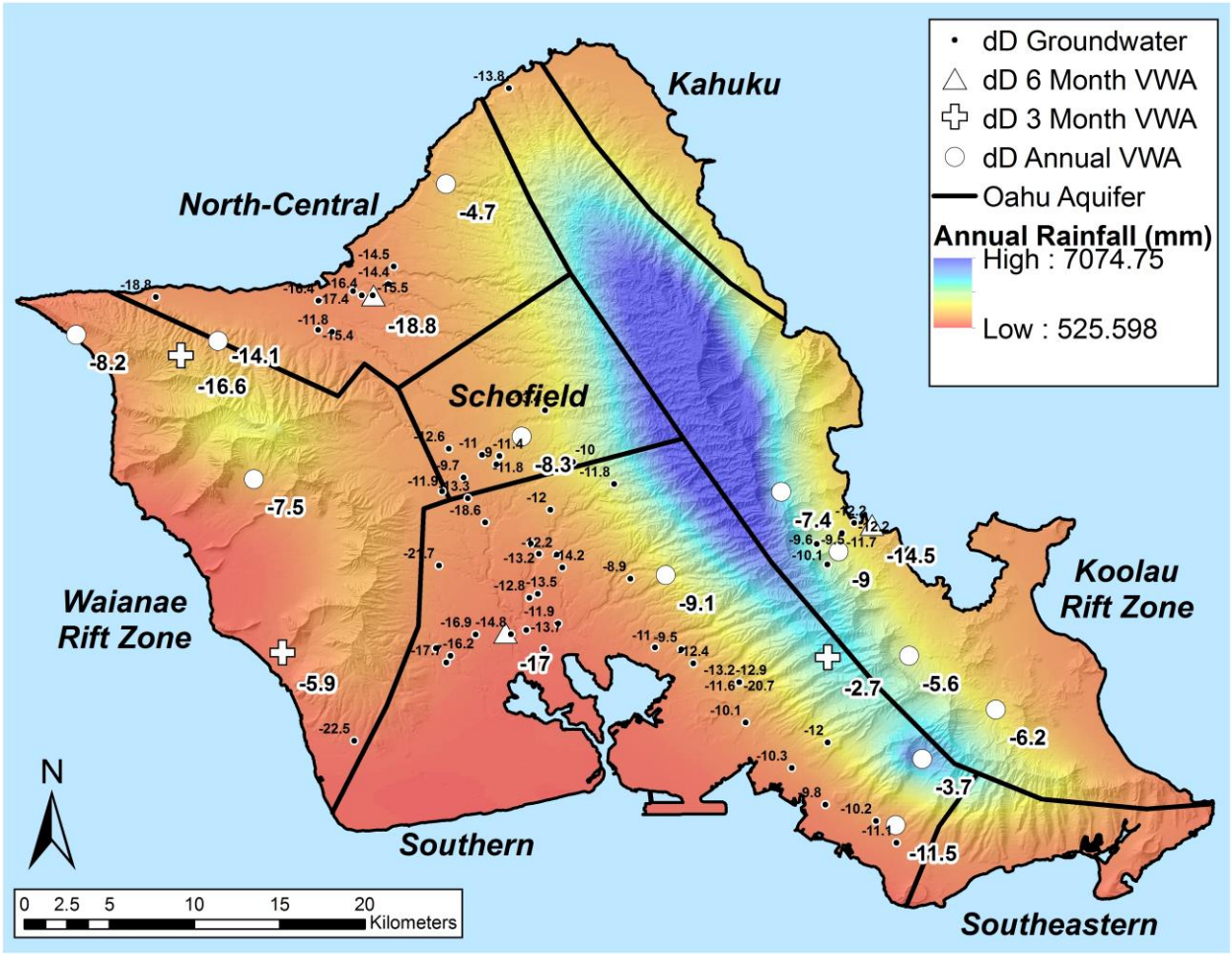

Figure 3.2. Map of deployed precipitation collector network. Annual VWA δ^2H values expressed in ‰ are listed next to each collector location, symbolized by the duration of its deployment and thus the time encompassed by the annual VWA. Names of major aquifers are in bold. δ^2H of groundwater in ‰ is listed from the USGS NAQWA data point or a sample taken during this study. Precipitation coverage from Giambelluca et al., 2013.

5.1. O'ahu's Local Meteoric Water Line

From the values recorded, we create the first LMWL for the island of O'ahu (Equation 3.2, **Figure 3.3**). This relationship is defined from the isotopic composition of precipitation from 18 locations across the island (Figure 3.2). All sites are incorporated, including 12 annual samples, three 6 month samples, and one 3 month samples.

$$\delta\,^2H = 7.28 * \delta^{18}O + 10.45 \qquad R^2 = 0.92 \qquad \textbf{(Equation 3.2)}$$

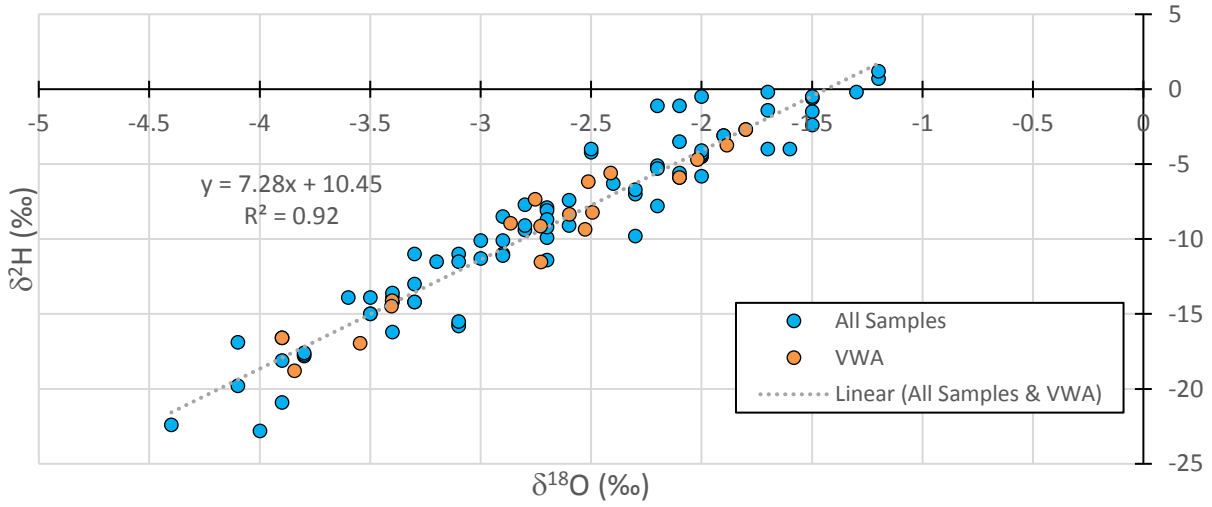

Figure 3.3. Local meteoric water line (LMWL) of O‘ahu. The slope is 7.28 and y-intercept is 10.45, compared to the global meteoric water line (GMWL) with a slope of 8 and y-intercept of 10. This is calculated with a linear regression for the plot of VWA $\delta^{18}O$ and $\delta^{2}H$ values (‰) for each location.

5.2. Seasonal trends

5.2.1. Volume of precipitation as seasonal trend

From our dataset, we interpret the wet season to be most important for aquifer recharge on O‘ahu. Of the 12 annual collectors, five show they receive 60-71% of annual precipitation from 2017 October-2018 March, and another three show 52-56% accumulation during this time. Of the remaining four locations, the individual window with greatest volume of rain is 2017 April-2017 June, implying residual wet season weather lasting through April, the last month of O‘ahu’s winter, most likely contributes significantly to rainfall in these regions.

Cumulatively the average volume of rainfall collected across all 12 annual sites increased in total precipitation collected throughout the climatic year. The sampling window covering the peak dry season months, July-September 2017, collected the lowest total volume of precipitation across the 12 annual collectors at 46.8 L. The 75.4 L collected from January-March 2018, the end of the wet season, was by far the highest total volume of precipitation for those annual 12 collectors. The beginning of the wet season window of October-December 2017 had the second highest island-wide total volume at 69.5 L, closely followed by the beginning of the dry season in April-June 2017 with 67.8 L.

There is no defining island-wide pattern for the seasonal fluctuations in precipitation volume applicable to all sites across O‘ahu. Many locations varied in the seasonal distribution of local

minimum and maximum volumes of rainfall collected. Of the general patterns existing in the changes of precipitation volume collected at each location, one can be applied to five of the 12 precipitation locations with 12-months of coverage. The dominant pattern is a decrease in precipitation from April-June (early dry season) to July-September (late dry season), a dramatic increase in precipitation for October-December (early wet season) well above the April-June threshold for certain locations, and then a slight decrease for January-February (late wet season). This pattern exists for five of 12 annual precipitation locations, all on either side of the Koʻolau ridgeline. Waiāhole station displays the inverse pattern despite its close spatial proximity to the other five stations.

Table 3.4. Annual, dry season, and wet season VWAs for $\delta^{18}O$ and $\delta^{2}H$ values in precipitation on Oʻahu.

	Geography		**Year VWA**		**Dry VWA**		**Wet VWA**	
Sample Name	Elevation (m)	Distance East (m)	$\delta^{18}O$ (‰)	$\delta^{2}H$ (‰)	$\delta^{18}O$ (‰)	$\delta^{2}H$ (‰)	$\delta^{18}O$ (‰)	$\delta^{2}H$ (‰)
Ewa Waimano	291	10,671	-2.7	-9.1	-2.0	-5.1	-3.1	-11.5
Hawaiʻi Ag. Center	111	5,542	-2.5	-6.2	-2.1	-2.5	-2.8	-8.1
HIG UH Mānoa	22	14,456	-2.7	-11.5	-1.5	-2.9	-3.2	-15.0
Honolulu F.R.	188	6,882	-1.8	-2.7	-1.8	-2.7		
Hoʻomaluhia B.G.	65	3,737	-2.4	-5.6	-1.9	-1.7	-3.1	-10.4
Kahaluʻu Ridge	100	2,323	-2.9	-9.0	-2.1	-3.4	-3.1	-10.6
Kaʻena Point	11	34,176	-2.5	-8.2	-1.9	-5.0	-2.8	-9.7
Lyon Arboretum	152	10,329	-1.9	-3.7	-1.5	-1.1	-2.3	-5.9
Mokuleia F.R.	167	27,766	-3.4	-14.1	-3.3	-14.0	-3.5	-14.2
Nanakuli F.R.	51	32,235	-2.1	-5.9	-2.1	-5.9		
Waiāhole F.R.	155	3,744	-2.8	-7.4	-2.4	-4.3	-3.0	-9.2
Waianae Kai	262	30,438	-2.5	-9.4	-2.4	-8.3	-2.7	-11.4
Wahiawa B.G.	309	16,025	-2.6	-8.3	-2.0	-4.6	-3.2	-12.3
Waimea Valley	4	12,234	-2.0	-4.7	-1.6	-2.1	-2.6	-8.8
Kamehameha Hwy.	6	29	-3.4	-14.5			-3.4	-14.5
Kunia III Wells	98	20,019	-3.5	-16.9			-3.5	-16.9
Haleiwa Wells	64	18,999	-3.8	-18.8			-3.8	-18.8
Mokuleia F.R. 2	610	29,826	-3.9	-16.6			-3.9	-16.6

Three collectors show a similar decrease from the April-June 2017 early dry season sample to the July-September 2017 late dry season sample, but there is no dramatic increase in the October-December 2017 early wet season. Precipitation volume does not return to its elevated status until January-March 2018, the end of the wet season. That increase in precipitation volume from early wet season to late wet season is also seen in the three 6 month stations. The two

annual stations exists on the Koʻolaus, but the other four samples supporting this trend are from some of Oʻahu's driest areas.

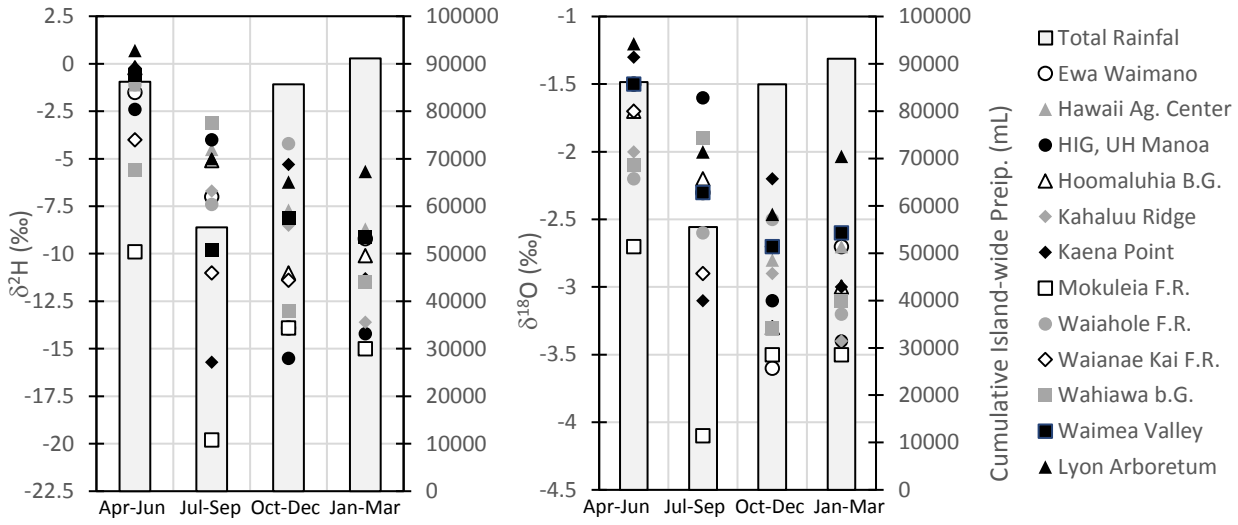

Figure 3.4a. (Left), Seasonality of precipitation volume and δ^2H values for each sampling interval in ‰ notation across the 4 sampling windows. The volume is Oʻahu's island-wide cumulative expressed in mL. **Figure 3.4b.** (Right) Seasonality of precipitation volume with $\delta^{18}O$ values for each sampling location over all sampling windows. Total volume of island-wide precipitation is included.

5.2.2. Isotopic composition as seasonal trend

For the network of 12 annual collectors, each rainfall station generally becomes more depleted in both ^2H and ^{18}O as the climatic year continued from dry to wet season (**Figure 3.4a, 3.4b, Table 3.4**). These samples have the lowest δ^2H and $\delta^{18}O$ values in rainfall from the end of the wet season, from January-March 2018. The sample window corresponds to the highest total volume of precipitation across the 12 annual collector locations. This demonstrates wet season rainfall on Oʻahu causes progressive lowering of δ^2H and $\delta^{18}O$ values in precipitation over the course of the 7-month wet winter. Samples, on average, had higher δ^2H and $\delta^{18}O$ values at the start of the dry season from 2017 April to 2017 June. Thus, there is a shift in the isotopic composition of Oʻahu's precipitation from the annual maximum isotopic depletion occurring at the end of the wet season, immediately preceding the annual minimum occurring at the beginning of the dry season. April-June 2017 has the second-lowest total precipitation volume for the climatic year. With the transition to the dry season comes the end of winter storm patterns

(i.e. Kona Lows), and samples have substantially lower δ^2H and $\delta^{18}O$ values in April-June 2017 precipitation than the previous wet season precipitation.

Table 3.5. Five storm event samples across 2 wet seasons, both 2017 and 2018, at the UH Mānoa sampling site. Samples show both extreme variations in each isotopic ratio.

Location	Date	Vol (mL)	$\delta^{18}O$ (‰)	δ^2H (‰)
HIG, UH Mānoa	2.6.17	3700	-0.7	2.7
HIG, UH Mānoa	2.25.18	8395	-1.9	-5.7
HIG, UH Mānoa	3.22.18	1500	-5.2	-29.7
HIG, UH Mānoa	3.24.18	1000	-6.3	-40.0
HIG, UH Mānoa	4.2.18	200	-1.5	0.6

5.2.3. Event-based precipitation

Event-based precipitation was collected at Station HIG UH Mānoa to track changes in the isotopic composition of storm event rainfall during the wet season on O'ahu (**Table 3.5**). Five winter storms events were characterized over 14-months coinciding with the 2017-2018 La Niña influenced climatic year observed in this study. These storm events occurred in 2017 February and 2018 March. Two samples fall outside the climatic year captured by the 12 annual precipitation collectors: a sample from 2017 February in the wet season days before the study began in 2017 March, and a sample from 2018 April, in the end of the wet season days after the winter 2018 wet season sampling. The remaining three samples occurred in the end of the 2018 wet season during January-March.

The isotopic composition of rainfall at Station HIG UH Mānoa had -3.4‰ $\delta^{18}O$ and -14.2‰ δ^2H for the 3 month period of January-March 2018. The isotopic composition of storm events during this time was significantly variable. The February storm event was at -1.9‰ $\delta^{18}O$ and -5.7‰ δ^2H, thus more enriched in ^{18}O and ^2H than the 3 month cumulative. Storm events in the end of March were depleted in both ^{18}O and ^2H with -5.2‰ $\delta^{18}O$ and -29.7‰ δ^2H for the March 22 event and -6.3‰ $\delta^{18}O$ and -40.0‰ δ^2H for the March 24 event. The 2018 February 25, 2018 March 22, and 2018 March 24 intense rainfall events are suspected to be part of the same Kona storm system over the island.

The low $\delta^{18}O$ and δ^2H values of the two 2018 March storm samples shows the nature of precipitation in major storm events during O'ahu's wet winter. Kona Low storm systems are characterized by moderate precipitation lasting days to weeks interrupted by periods of intense

rainfall. The storm events captured at the end of March represent these periods of intense rainfall. Occurring in the midst of a Kona Low event at the end of the wet season explains their low $\delta^{18}O$ and $\delta^{2}H$ values compared to the rest of O‘ahu’s climatic year. Such regionally extreme depletion in ^{18}O and ^{2}H is expected after heavy seasonal and event-based rainout containing a much lighter isotopic signature, as evidenced by the February sample more enriched in ^{2}H.

The remaining event-based samples from just outside the yearlong study duration were the most anomalous samples of this research. The 2017 February sample from the month before the annual study began had higher $\delta^{18}O$ and $\delta^{2}H$ values compared to all other samples at 2.7‰ $\delta^{18}O$ and -0.7‰ $\delta^{2}H$. This relative enrichment in ^{18}O and ^{2}H for the region could be caused by preferential rainout of the heavier isotope during the onset of a winter new storm event. The 2018 April event sample collected immediately after the study concluded also had higher $\delta^{18}O$ and $\delta^{2}H$ values compared to all other samples at 0.6‰ $\delta^{18}O$ and -1.5‰ $\delta^{2}H$. This isotopic composition looks remarkably like that of the April-June 2017 sample from Lyon Arboretum, a location only 4000 m deeper in a valley of the Ko‘olau Mountains at -1.2‰ $\delta^{2}H$ and 0.7‰ $\delta^{18}O$. Year-to-year climatic variation could bring precipitation typical of higher elevations farther out of the valley and was captured in our storm sample.

5.3. Effect of elevation on isotopic composition and volume

Neither $\delta^{2}H$, $\delta^{18}O$, nor volume in O‘ahu’s precipitation showed a significant relationship with elevation in the island-wide dataset. Other areas on the Hawaiian Islands, including East Maui (Scholl et al., 2002), windward Hawai‘i (Scholl et al., 1996), and leeward Hawai‘i (Fackrell, 2016) have shown elevation trends in $\delta^{2}H$ and $\delta^{18}O$ values. In these larger islands of Maui and Hawai‘i with higher altitudes, precipitation patterns are defined more strongly by elevation gradients than on O‘ahu, creating systematic depletions in ^{2}H and ^{18}O with increased altitude. Haleakalā Mountain in eastern Maui is 3055 m; Mauna Kea and Mauna Loa on Hawai‘i which affect both windward and leeward weather are 4207 and 4169 m, respectively. O‘ahu’s tallest windward peak of Kōnāhuanui is 960 m, and its tallest leeward peak of Ka‘ala is 1237 m. Therefore, O‘ahu appears to lack the consistent elevation gradients necessary to control stepwise relationships of $\delta^{2}H$ and $\delta^{18}O$ in precipitation as a function of altitude.

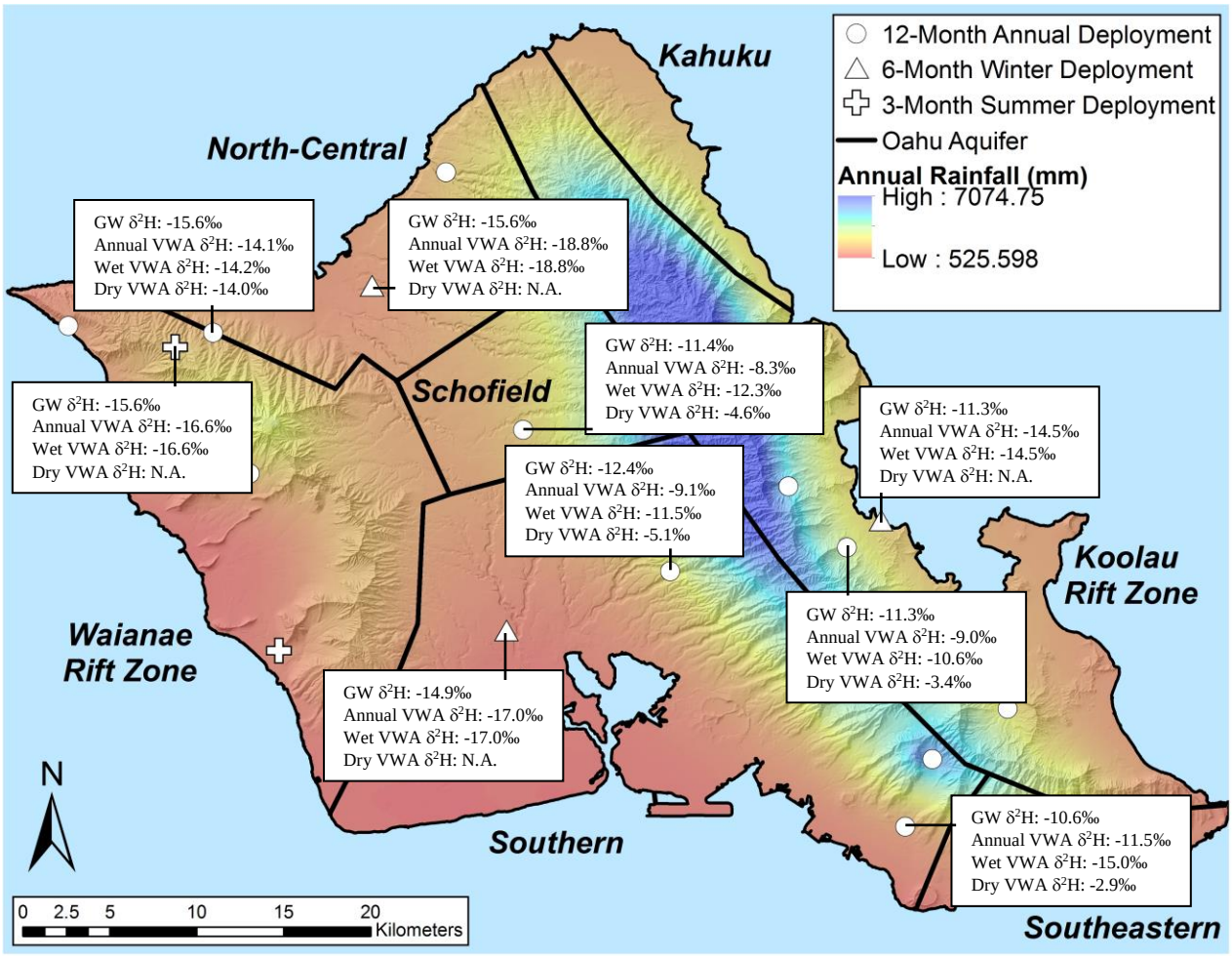

Figure 3.5. Map of O‘ahu’s groundwater recharge areas interpreted from the isotopic composition of rainfall and groundwater. Annual, wet winter, and dry summer VWA δ^2H values of precipitation as ‰ labeled next to the collector location. Collectors are symbolized based off their deployment schedules. Average δ^2H values of groundwater in ‰ is listed from the USGS NAQWA for a regional groundwater. Precipitation coverage from Giambelluca et al., 2013.

5.4. Regional groundwater recharge

The average isotopic composition of groundwater was interpreted using data from the U.S. Geological Survey National Water Quality Assessment Program (USGS NAWQA, 1991-present) for the northern, central, and southern portions of O‘ahu and supplemented by regionally collected data for the eastern portion of the island (**Table 3.6**). The δ^2H and $\delta^{18}O$ values are considered representative of local isotopic composition in O‘ahu’s seven major aquifers for the purposes of this study. Groundwater samples from the NAWQA dataset range in depth from 27 to 545 m. Eastern O‘ahu samples were collected for the purpose of this study from

dike-impounded groundwater in the Koʻolau Mountains with a depth range from 36 to 137 m, except one location where the dike-impounded groundwater table intersects local topography.

Table 3.6. Average δ^2H values in groundwater, corresponding annual VWA local precipitation, and the difference between the two.

Groundwater Location	Mean δ^2H Groundwater (‰)	Annual VWA δ^2H (‰)	Collector Location	Dif. (‰)	Number of Groundwater Samples
Pearl Harbor West	-14.9	-17.0*	Kunia III Wells	2.1	17
Pearl Harbor East	-12.4	-9.1	Ewa Waimano	-3.3	10
Pearl Harbor Southeast	-10.6	-11.5	HIG UH Mānoa	0.9	6
Schofield	-11.4	-8.3	Wahiawa B.G.	-3.1	9
Koʻolau	-11.3	-9.0	Kahaluʻu Ridge	-2.3	7
Koʻolau	-11.3	-14.5*	Kamehameha Hwy.	3.2	7
North-central	-15.6	-18.8*	Haleiwa Wells	3.2	9
North-central	-15.6	-14.1	Mokuleia F.R.	-1.5	9
North-central	-15.6	-16.6*	Mokuleia F.R. 2	1.0	9

*Sampling location was only deployed for 6 wet season months (Oct 2017 – Dec 2018).

Aquifers recharged by local precipitation include North-Central aquifer, eastern "Pearl Harbor" or Southern aquifer, Honolulu region of Southern Pearl Harbor aquifer, and Kāneʻohe watersheds of Koʻolau Rift Zone aquifer. Using the 12-month annual VWA to corroborate areas of regional recharge on the island, we find δ^2H and $\delta^{18}O$ values correspond to local groundwater in all paired regions and developed zones of recharge using δ^2H values of precipitation compared to the average δ^2H values in the local groundwater (Table 3.6, **Figure 3.5, Figure 3.6**). The absolute difference between δ^2H values of precipitation from the annual VWA and the average δ^2H values of groundwater in the local groundwater was ≤ 3.3‰ (x = mean groundwater – VWA), being as low as 0.9‰ for one groundwater-precipitation pairing.

Wet season VWA δ^2H values (2017 October to 2018 March) are consistently lower than annual VWA values in all 12 month stations around Oʻahu, being anywhere from 0.1 to 4.8‰ lower in the wet season VWA than the annual VWA. Absolute differences between wet season VWA δ^2H precipitation values and surrounding regional groundwater average δ^2H values are minimized at all paired groundwater-precipitation locations except in the Honolulu region of southeast Oʻahu in comparison to these same calculations using annual VWA (Figure 3.5, **Table 3.7**). This same absolute difference between δ^2H values then greatly increases to 6.8-7.9‰ for all

locations when the dry season VWA is used in the calculation, more than double the maximum absolute differences seen with the annual VWA (**Table 3.8**). This builds upon on evidence of seasonal volumetric trends that O‘ahu’s wet season dominates aquifer recharge on the island as proposed in section 5.2.

Table 3.7. Average δ^2H values in groundwater, corresponding wet season VWA in local precipitation, and the difference between the two.

Groundwater Location	Mean δ^2H Groundwater (‰)	Winter Wet VWA δ^2H (‰)	Collector Location	Dif. (‰)	Number of Groundwater Samples
Pearl Harbor West	-14.9	-17.0	Kunia III Wells	2.1	17
Pearl Harbor East	-12.4	-11.5	Ewa Waimano	-0.9	10
Pearl Harbor Southeast	-10.6	-15.0	HIG UH Mānoa	4.4	6
Schofield	-11.4	-12.3	Wahiawa B.G.	0.9	9
Koʻolau	-11.3	-10.6	Kahaluʻu Ridge	-0.7	7
Koʻolau	-11.3	-14.5	Kamehameha Hwy.	3.2	7
North-central	-15.6	-18.8	Haleiwa Wells	3.2	9
North-central	-15.6	-14.2	Mokuleia F.R.	-1.4	9
North-central	-15.6	-16.6	Mokuleia F.R. 2	1.0	9

To understand what may cause the higher absolute difference in δ^2H values between the Pearl Harbor Southeast groundwater in the Honolulu region and the VWA δ^2H value of wet season local precipitation, a simple volumetric mixing equation was applied to account for the upslope precipitation occurring at Lyon Arboretum precipitation station. The VWA of wet season δ^2H values of Lyon Arboretum station combined with the local HIG UH Mānoa station used in previous applications provides a δ^2H value of 7.7‰, narrowing the absolute difference to 2.9‰. This is a gross oversimplification of the groundwater mixing that will occur throughout the aquifer from the two precipitation sources, but it lends insight into the seasonal mixing potential of such valley-fill sub-aquifers in the southeastern groundwater region of the Pearl Harbor/Southern aquifer in contributing to down-gradient groundwater volumes and isotopic compositions.

Table 3.8. Average δ^2H values in groundwater, corresponding dry season VWA in local precipitation, and the between the two.

Groundwater Location	Mean δ^2H Groundwater (‰)	Summer Dry VWA δ^2H (‰)	Collector Location	Dif. (‰)	Number of Groundwater Samples
Pearl Harbor East	-12.4	-5.1	Ewa Waimano	-7.29	10
Pearl Harbor Southeast	-10.6	-2.9	HIG UH Mānoa	-7.7	6
Schofield	-11.4	-4.6	Wahiawa B.G.	-6.8	9
Koʻolau	-11.3	-3.4	Kahaluʻu Ridge	-7.9	7
North-central	-15.6	-14.0	Mokuleia F.R.	-1.6	9

The 6 month VWA for those stations only deployed during the wet season contribute additional points of prospective regional recharge areas (Figure 3.5). Verified with precipitation predictions via Giambelluca et al., 2013 and NOAA National Climate Data Center (NCDC) rainfall records for Oʻahu's 2017-2018 climatic year, minimum precipitation occurs during the dry season in these three regions where only 6 months of data are available, including Mokuleia F.R. 2, Haleiwa Wells, Kunia III Wells, and Kamehameha Hwy. Stations. As such, and in light of our results interpreted to show a wet season dominance in aquifer recharge island-wide, it is assumed that wet season δ^2H and $\delta^{18}O$ values measured in precipitation for these locations represent the bulk of significant aquifer recharge.

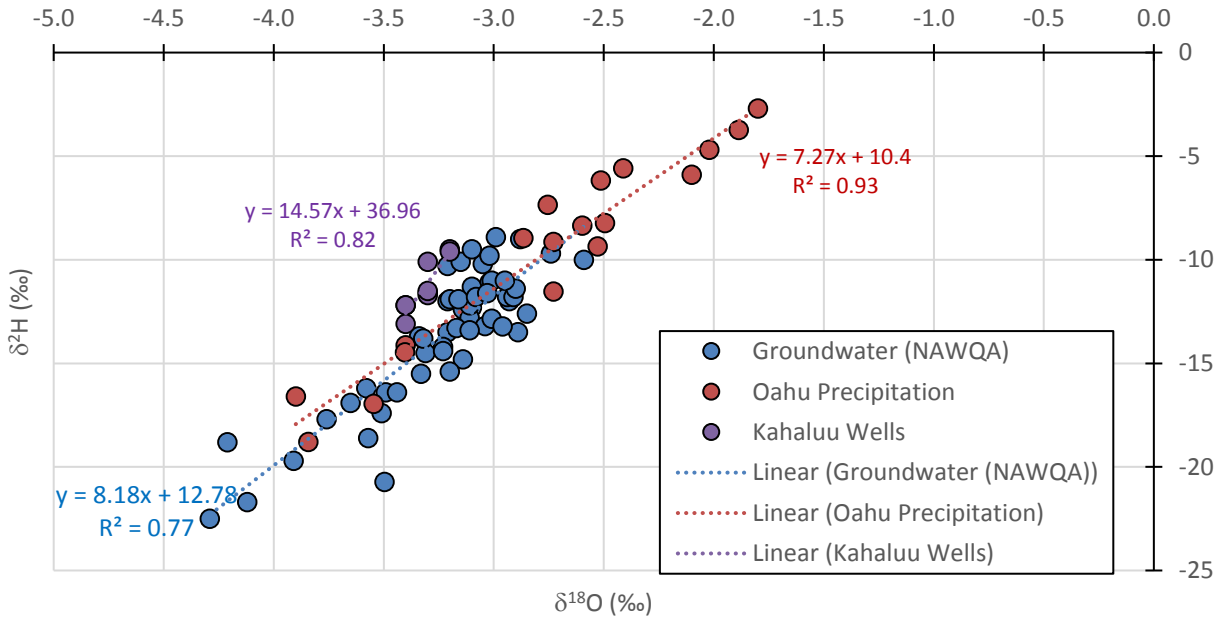

Figure 3.6. Oahu's LMWL, the isotopic composition of USGS NAWQA groundwater data, and groundwater samples taken throughout the study. The isotopic composition of all 3 and resulting linear regression trends show variation in y-intercept and slope for each dataset.

We consider the 3 month sample station at Mokuleia F.R. 2 Station from 2018 January to 2018 March representative of the isotopic composition of recharge in the region (Figure 3.5). This is supported by the yearlong collector only 2000 m west and 440 m lower at Mokuleia F.R. Station, where annual VWA δ^2H value for the collector is only 0.88‰ higher than the collector's 2018 January to 2018 March sample. This suggests Mokuleia F.R. 2 Station will behave similarly, and the recorded isotopic composition from 2018 January to 2018 March will have a similar composition to its annual VWA. Additionally, precipitation models from Giambelluca et al., 2013 predict the greatest precipitation at Mokuleia F.R. 2 Station occurring in winter months from October to March, leaving less influence for dry season precipitation volumes on the annual VWA.

5.5. Salinity corrections

Elevated ion concentrations in the coastal collector at Ka'ena Point implies a significant source of dissolved ion species not found at other locations. The three most probable additions include volumetric contributions of sea spray where some of the sample collected has an addition of seawater, salt precipitates of evaporated sea spray in which no seawater is incorporated into the sample but only its salt residues, and elevated ion concentrations in the rainfall itself. We conclude the measured elevated ion concentrations are a result of precipitates from sea spray with no volumetric ocean water contributions. This is based on the consistent depletion in ^2H in precipitation at the Ka'ena Point station from all sampling windows, including one sample from October-December 2017 (δ^2H -5.3‰ and $\delta^{18}O$ -2.2‰) when collected precipitation was most saline (estimated salinity 6.61) relative to seawater (δ^2H 3.6‰ and $\delta^{18}O$ 0.4‰). Comparisons of volume of rainfall collected at the Ka'ena Point station from all four sampling windows, in which the most saline sample had the lowest total volume, also supports this claim. As sea spray precipitates are relatively constant throughout the year, they have a greater influence on dissolved ion concentration for volumetrically low sampling windows.

6. Conclusions

Rainfall volume, intensity, and isotopic composition evidence wet season precipitation on O'ahu as dominant to localized groundwater recharge in all areas of the island. Highest cumulative island-wide precipitation occurs during the wet season from 2017 October to 2018

March, and is substantially highest from January-March at the end of Oʻahu's wet season. Not only is cumulative precipitation highest in the wet season, but rainfall events have increased intensity in this season (i.e., Kona Lows). With increased rainfall duration and intensity predicted to increase Oʻahu's aquifer recharge, these two lines of evidence suggest cumulative wet season precipitation has the greatest control on Oʻahu's groundwater recharge. This high volume occurs at the time of greatest depletion in ^{2}H and ^{18}O in precipitation for island-wide $\delta^{2}H$ and $\delta^{18}O$ values. The annual VWA $\delta^{2}H$ value of rainfall corresponds to the local groundwater $\delta^{2}H$ value as reported by USGS NAWQA data by an absolute difference of 3.3‰ or less implying localized groundwater recharge on Oʻahu. When calculated with wet season VWA $\delta^{2}H$ value, this absolute difference lowered for all but one paired precipitation-groundwater region in our study, evidencing that this localized aquifer recharge is in fact dominated by winter wet season precipitation in comparison to the dry season rainfall patterns on Oʻahu.

There is also some correlation with distance from Oʻahu's eastern shore and total volumetric rainfall at a site ($R^2 = 0.51$), both in individual seasons and in the annual accumulation. This reinforces the effect of trade wind rainfall that carries precipitation in a westerly direction across the island, dominating Oʻahu's climate and precipitation patterns. Oʻahu is shown to lack the same altitude-controlled effects on precipitation's isotopic composition that has been established on the islands of Maui and Hawaiʻi.

CHAPTER 4. CONCLUSIONS

Oʻahu and the Hawaiian Islands are one subset to a much larger group of Pacific Island communities struggling to maintain proper wastewater management infrastructure, jeopardizing their limited freshwater resources and unique coastal ecosystems. Eutrophication, coral reef death, and public health hazards are just some of the results of wastewater-borne nutrient pollution to groundwater and surface water in coastal environments. This research presented investigations into the hydrologic flow on the island of Oʻahu, both with a regional case study and island-wide, to enhance aquifer management and land use, as well as highlighted the natural environment's response when exposed to excessive nutrient loads in OSDS leachate.

Chapter 2 provided a comprehensive analysis of nutrient cycling throughout a tropical volcanic aquifer in a coastal environment. Through a multi-tracer geochemical and isotopic approach, this study elucidates the transport and chemical evolution of OSDS-sourced nutrient loads throughout the subsurface and identifies the locations and geochemistry of ultimate discharge into streams and nearshore waters. It also observes the ability of the natural environment to attenuate wastewater signals along transport paths in response to nutrient loading above baseline conditions in the presence of OSDS leachate. We showed the Kahaluʻu-Kāneʻohe Bay region as a "type example" for coastal Pacific island environments at risk of sewage contamination minimally treated OSDS wastewater, by design or malfunction.

Chapter 3 establishes the first recorded values for the isotopic composition of precipitation on Oʻahu, contributing to the global body of work. It presents an easily-cited data set for future studies of groundwater flow on Oʻahu, offering a key piece of scientific data notably previously lacking for the island's hydrology. Through the identification of regional recharge utilizing the USGS NAWQA data set, the study shows the utility of the precipitation data in aquifer recharge studies.

This thesis as a whole combines these two studies to improve water management practices on Oʻahu. Chapter 2 provides a case study for Oʻahu as to how these groundwater resources can be contaminated in regions with OSDS density via wastewater leachate. Chapter 3 expands the scope to the overall groundwater flow regimes that contribute to the island's irreplaceable freshwater reservoirs. Ideally, the research presented herein will be used to improve the water resource management on Oʻahu and further the science for other Pacific Island communities.

APPENDIX 1. Chapter 2 Data

Table A1.1. Sampling times and locations for Chapter 2.

SAMPLE	SITE/WELL NAME	DATE	TIME	TYPE	WATERSHED	STREAMBED MATERIAL	LONG. (°)	LAT. (°)
Kahaluu Special 3	HDOH Site 3	7-Oct-16	9:01	Estuary	Kahaluu Lagoon	--	-157.8385	21.4570
Kahaluu Special 1	HDOH Site 1	7-Oct-16	9:37	Estuary	Kahaluu Lagoon	--	-157.8396	21.4601
Kahaluu Special 2	HDOH Site 2	7-Oct-16	9:57	Estuary	Kahaluu Lagoon	--	-157.8401	21.4590
Kahaluu Special 7	HDOH Site 7	7-Oct-16	10:33	Estuary	Kahaluu Lagoon	--	-157.8393	21.4562
Kahaluu Special 6	HDOH Site 6	7-Oct-16	10:52	Estuary	Kahaluu Lagoon	--	-157.8404	21.4577
Kahaluu Special 4	HDOH Site 4	7-Oct-16	11:48	Stream	Waihee	Natural	-157.8452	21.4551
Kahaluu Special 8	HDOH Site 8	7-Oct-16	12:18	Estuary	Kahaluu Lagoon	Natural	-157.8380	21.4553
Kahaluu Special 5	HDOH Site 5	7-Oct-16	12:45	Stream	Kahaluu Lagoon	Channelized	-157.8365	21.4545
Kahaluu Special 10	HDOH Site 10	7-Oct-16	13:03	Stream	Ahuimanu	Channelized	-157.8345	21.4481
Kahaluu Special 9A	HDOH Site 9A	14-Oct-16	9:18	Stream	Waihee	Natural	-157.8593	21.4459
Kahaluu Special 17	HDOH Site 17	14-Oct-16	10:00	Stream	Ahuimanu	Natural	-157.8323	21.4453
Kahaluu Special 18	HDOH Site 18	14-Oct-16	10:16	Stream	Ahuimanu	Natural	-157.8330	21.4462
Kahaluu Special 11	HDOH Site 11	14-Oct-16	10:55	Stream	Ahuimanu	Channelized	-157.8375	21.4396
Kahaluu Special 15	HDOH Site 15	14-Oct-16	11:28	Stream	Kahaluu	Natural	-157.8418	21.4435
Kahaluu Special 12	HDOH Site 12	14-Oct-16	11:58	Stream	Kahaluu	Natural	-157.8436	21.4371
Kahaluu Special 13	HDOH Site 13 / Kahaluu SR-01	14-Oct-16	12:17	Stream	Kahaluu	Natural	-157.8444	21.4386
Waihee Tunnel	3-2651-002	23-Jan-17	9:40	Groundwater	Waihee	--	-157.8583	21.4464
Waihee Inclined Wells	3-2652-001	23-Jan-17	10:20	Groundwater	Waihee	--	-157.8675	21.4419
Kahaluu Headwaters	Kahaluu Headwaters	25-Jan-17	14:00	Stream	Kahaluu	Natural	-157.8521	21.4353
Kahaluu Well	3-2651-003	25-Jan-17	14:30	Groundwater	Kahaluu	--	-157.8526	21.4356
Kahaluu Nuts	Kahaluu SR-01	1-Mar-17	9:45	Stream	Kahaluu	Mix	-157.8418	21.4436
Waihee Nuts	Waihee SR-01	1-Mar-17	12:30	Stream	Waihee	Natural	-157.8482	21.4551
Kahaluu SR-01	Kahaluu SR-01	6-Mar-17	10:25	Stream	Kahaluu	Mix	-157.8418	21.4436
Kahaluu SR-02	Kahaluu SR-02	6-Mar-17	11:20	Stream	Kahaluu	Natural	-157.8421	21.4428

SAMPLE	SITE/WELL NAME	DATE	TIME	TYPE	WATERSHED	STREAMBED MATERIAL	LONG. (°)	LAT. (°)
Kahaluu SR-03	Kahaluu SR-03	6-Mar-17	12:00	Stream	Kahaluu	Natural	-157.8422	21.4423
Kahaluu SR-04	Kahaluu SR-04	6-Mar-17	13:00	Stream	Kahaluu	Natural	-157.8431	21.4422
Kahaluu SR-05	Kahaluu SR-05	6-Mar-17	13:45	Stream	Kahaluu	Natural	-157.8426	21.4406
Kahaluu SR-06	Kahaluu SR-06	6-Mar-17	14:30	Stream	Kahaluu	Natural	-157.8437	21.4394
Kahaluu SR-07	Kahaluu SR-07	6-Mar-17	15:00	Stream	Kahaluu	Natural	-157.8438	21.4387
Waihee SW 170320	Waihee SR-01	20-Mar-17	14:30	Stream	Waihee	Natural	-157.8482	21.4551
Waihee GW 170320	Waihee SR-01 (GW)	20-Mar-17	14:35	Groundwater	Waihee	--	-157.8482	21.4551
Kahaluu SW 170320	Kahaluu SR-01	20-Mar-17	15:30	Stream	Kahaluu	Mix	-157.8419	21.4434
Kahaluu GW 170320	Kahaluu SR-01 (GW)	20-Mar-17	15:45	Groundwater	Kahaluu	--	-157.8419	21.4434
Waihee SR-01	Waihee SR-01	22-Mar-17	9:40	Stream	Waihee	Natural	-157.8482	21.4551
Waihee SR-02	Waihee SR-02	22-Mar-17	10:50	Stream	Waihee	Natural	-157.8490	21.4551
Waihee SR-03	Waihee SR-03	22-Mar-17	11:47	Stream	Waihee	Natural	-157.8515	21.4531
Waihee SR-04	Waihee SR-04	22-Mar-17	12:36	Stream	Waihee	Natural	-157.8515	21.4532
Waihee (DUP)	Waihee DUP	22-Mar-17	12:36	Stream	Waihee	Natural	-157.8515	21.4532
Waihee SR-05	Waihee SR-05	22-Mar-17	13:38	Stream	Waihee	Natural	-157.8527	21.4516
DPKAH01	DPKAH01	10-Jul-17	9:00	Pore water	Kahaluu	--	-157.8419	21.4434
DSKAH01 (DUP)	DSKAH01 Dup	10-Jul-17	9:00	Stream	Kahaluu	Mix	-157.8419	21.4434
DSKAH01	DSKAH01	10-Jul-17	9:00	Stream	Kahaluu	Mix	-157.8419	21.4434
DWKAH01	DWKAH01	10-Jul-17	10:00	Groundwater	Kahaluu	--	-157.8419	21.4434
DSKAH02	DSKAH02	10-Jul-17	10:45	Stream	Kahaluu	Natural	-157.8421	21.4428
DSKAH03	DSKAH03	10-Jul-17	11:20	Stream	Kahaluu	Natural	-157.8422	21.4423
DSKAH04	DSKAH04	10-Jul-17	11:45	Stream	Kahaluu	Natural	-157.8431	21.4422
DSKAH05	DSKAH05	10-Jul-17	12:20	Stream	Kahaluu	Natural	-157.8431	21.4419
DPKAH05	DPKAH05	10-Jul-17	12:20	Pore water	Kahaluu	--	-157.8431	21.4419
DSKAH06	DSKAH06	10-Jul-17	12:55	Stream	Kahaluu	Natural	-157.8426	21.4406
DSKAH07	DSKAH07	10-Jul-17	13:20	Stream	Kahaluu	Natural	-157.8437	21.4394
DSKAH08	DSKAH08	10-Jul-17	14:00	Stream	Kahaluu	Natural	-157.8437	21.4393
DPKAH09	DPKAH09	10-Jul-17	14:30	Pore water	Kahaluu	--	-157.8437	21.4392
DSKAH10	DSKAH10	10-Jul-17	15:00	Stream	Kahaluu	Natural	-157.8437	21.4394

SAMPLE	SITE/WELL NAME	DATE	TIME	TYPE	WATERSHED	STREAMBED MATERIAL	LONG. (°)	LAT. (°)
DPKAH11	DPKAH11	10-Jul-17	15:30	Pore water	Kahaluu	--	-157.8437	21.4385
DSKAH11	DSKAH11	10-Jul-17	15:35	Stream	Kahaluu	Natural	-157.8437	21.4385
DSKAH12	DSKAH12	10-Jul-17	16:05	Stream	Kahaluu	Natural	-157.8443	21.4385
DPKAH12	DPKAH12	10-Jul-17	16:10	Pore water	Kahaluu	--	-157.8443	21.4385
DPWEE01	DPWEE01	11-Jul-17	9:00	Pore water	Waihee	--	-157.8482	21.4551
DSWEE01 (DUP)	DSWEE01 Dup	11-Jul-17	9:35	Stream	Waihee	Natural	-157.8482	21.4551
DSWEE01	DSWEE01	11-Jul-17	9:35	Stream	Waihee	Natural	-157.8482	21.4551
DWWEE01	DWWEE01	11-Jul-17	9:55	Groundwater	Waihee	--	-157.8482	21.4551
DSWEE02	DSWEE02	11-Jul-17	10:20	Stream	Waihee	Natural	-157.8475	21.4548
DPWEE02	DPWEE02	11-Jul-17	10:25	Pore water	Waihee	--	-157.8475	21.4548
DSWEE03	DSWEE03	11-Jul-17	10:55	Stream	Waihee	Natural	-157.8460	21.4550
DSWEE04	DSWEE04	11-Jul-17	11:30	Stream	Waihee	Natural	-157.8443	21.4547
DSWEE05	DSWEE05	11-Jul-17	12:10	Stream	Waihee	Natural	-157.8432	21.4554
DPWEE05	DPWEE05	11-Jul-17	12:50	Pore water	Waihee	--	-157.8430	21.4552
DSWEE08	DSWEE08	11-Jul-17	13:00	Stream	Waihee	Natural	-157.8423	21.4553
DSWEE09	DSWEE09	11-Jul-17	13:15	Stream	Waihee	Natural	-157.8419	21.4553
DSWEE10	DSWEE10	11-Jul-17	13:55	Agriculture	Waihee	Natural	-157.8479	21.4549
DSWEE11	DSWEE11	11-Jul-17	14:25	Stream	Waihee	Natural	-157.8491	21.4541
DSWEE12	DSWEE12	11-Jul-17	15:45	Stream	Waihee	Natural	-157.8521	21.4533
DPWEE12	DPWEE12	11-Jul-17	15:50	Pore water	Waihee	--	-157.8521	21.4533
DSWEE13	DSWEE13	11-Jul-17	16:35	Stream	Waihee	Natural	-157.8519	21.4523
DSWEE14	DSWEE14	11-Jul-17	16:55	Stream	Waihee	Natural	-157.8513	21.4531
DSWOL01	DSWOL01	12-Jul-17	9:25	Stream	Waiahole	Natural	-157.8440	21.4814
DSWOL01 (DUP)	DSWOL01 Dup	12-Jul-17	9:25	Stream	Waiahole	Natural	-157.8440	21.4814
DPWOL01	DPWOL01	12-Jul-17	9:55	Pore water	Waiahole	--	-157.8440	21.4814
DSWOL02	DSWOL02	12-Jul-17	10:20	Stream	Waiahole	Natural	-157.8451	21.4815
DSWOL03	DSWOL03	12-Jul-17	11:00	Stream	Waiahole	Natural	-157.8480	21.4816
DSWOL04	DSWOL04	12-Jul-17	11:35	Stream	Waiahole	Natural	-157.8489	21.4815
DPWOL04	DPWOL04	12-Jul-17	11:40	Pore water	Waiahole	--	-157.8489	21.4815

SAMPLE	SITE/WELL NAME	DATE	TIME	TYPE	WATERSHED	STREAMBED MATERIAL	LONG. (°)	LAT. (°)
DSWOL06	DSWOL06	12-Jul-17	12:05	Stream	Waiahole	Natural	-157.8507	21.4814
DSWOL07	DSWOL07	12-Jul-17	12:30	Stream	Waiahole	Natural	-157.8527	21.4812
DPWOL07	DPWOL07	12-Jul-17	13:00	Pore water	Waiahole	--	-157.8527	21.4812
DSWOL08	DSWOL08	12-Jul-17	13:15	Stream	Waiahole	Natural	-157.8536	21.4803
DSWOL09	DSWOL09	12-Jul-17	13:50	Stream	Waiahole	Natural	-157.8451	21.4815
DSLAG01	DSLAG01	13-Jul-17	9:40	Estuary	Kahaluu Lagoon	Natural	-157.8387	21.4559
DPLAG01 (DUP)	DPLAG01 Dup	13-Jul-17	9:50	Pore water	Kahaluu Lagoon	--	-157.8387	21.4559
DPLAG01	DPLAG01	13-Jul-17	9:50	Pore water	Kahaluu Lagoon	--	-157.8387	21.4559
DSLAG02	DSLAG02	13-Jul-17	10:20	Estuary	Kahaluu Lagoon	Natural	-157.8384	21.4555
DPLAG02	DPLAG02	13-Jul-17	10:30	Pore water	Kahaluu Lagoon	--	-157.8384	21.4555
DSLAG03	DSLAG03	13-Jul-17	10:35	Estuary	Kahaluu Lagoon	Natural	-157.8387	21.4554
DPLAG04	DPLAG04	13-Jul-17	11:00	Pore water	Kahaluu Lagoon	--	-157.8381	21.4555
DSLAG04	DSLAG04	13-Jul-17	11:10	Estuary	Kahaluu Lagoon	Natural	-157.8380	21.4554
DPLAG05	DPLAG05	13-Jul-17	11:40	Pore water	Kahaluu Lagoon	--	-157.8381	21.4553
DPLAG06	DPLAG06	13-Jul-17	12:00	Pore water	Kahaluu Lagoon	--	-157.8382	21.4558
DPLAG07	DPLAG07	13-Jul-17	12:30	Pore water	Kahaluu Lagoon	--	-157.8388	21.4559
DPMAN01	DPMAN01	14-Jul-17	10:05	Pore water	Waiahole	--	-157.8420	21.4813
DSMAN02	DSMAN02	14-Jul-17	10:25	Stream	Waiahole	Natural	-157.8420	21.4824
DPMAN03	DPMAN03	14-Jul-17	10:45	Pore water	Waiahole	--	-157.8420	21.4832
DSMAN04	DSMAN04	14-Jul-17	11:20	Stream	Waiahole	Natural	-157.8425	21.4845
DSMAN05	DSMAN05	14-Jul-17	11:35	Stream	Waiahole	Natural	-157.8430	21.4849
DPMAN04	DPMAN04	14-Jul-17	11:45	Pore water	Waiahole	--	-157.8427	21.4847
DPMAN06	DPMAN06	14-Jul-17	12:15	Pore water	Waiahole	--	-157.8437	21.4847
DPMAN07	DPMAN07	14-Jul-17	13:00	Pore water	Waiahole	--	-157.8448	21.4840
DPMAN08	DPMAN08	14-Jul-17	13:30	Pore water	Waiahole	--	-157.8436	21.4834
DSMAN09	DSMAN09	14-Jul-17	14:50	Marsh	Waiahole	--	-157.8436	21.4832
DSCON01	DSCON01	21-Aug-17	9:26	Stream	Kahaluu	Channelized	-157.8414	21.4447
DPCON02	DPCON02	21-Aug-17	9:48	Pore water	Kahaluu	Channelized	-157.8412	21.4447

SAMPLE	SITE/WELL NAME	DATE	TIME	TYPE	WATERSHED	STREAMBED MATERIAL	LONG. (°)	LAT. (°)
DSCON03	DSCON03	21-Aug-17	10:23	Stream	Kahaluu	Channelized	-157.8377	21.4477
DPCON03	DPCON03	21-Aug-17	10:32	Pore water	Kahaluu	Channelized	-157.8377	21.4477
DSCON04	DSCON04	21-Aug-17	10:54	Stream	Kahaluu	Channelized	-157.8360	21.4507
DPCON05	DPCON05	21-Aug-17	11:11	Pore water	Kahaluu	Channelized	-157.8371	21.4484
DSCON06	DSCON06	21-Aug-17	11:39	Stream	Kahaluu Lagoon	Channelized	-157.8351	21.4526
DSCON07	DSCON07	21-Aug-17	11:45	Stream	Kahaluu Lagoon	Channelized	-157.8352	21.4528
DSCON08	DSCON08	21-Aug-17	11:55	Stream	Kahaluu Lagoon	Channelized	-157.8355	21.4533
DSCON09	DSCON09	21-Aug-17	12:02	Stream	Kahaluu Lagoon	Channelized	-157.8361	21.4540
COAST-01	COAST-01	22-Aug-17	7:50	Ocean	Hakipuu	--	-157.8369	21.5089
COAST-02	COAST-02	22-Aug-17	8:15	Ocean	Kaalaea	--	-157.8443	21.4718
COAST-03	COAST-03	22-Aug-17	8:26	Ocean	Kaalaea	--	-157.8438	21.4700
COAST-04	COAST-04	22-Aug-17	8:40	Ocean	Kahaluu Segment	--	-157.8398	21.4608
COAST-04 (DUP)	COAST-04 (DUP)	22-Aug-17	8:40	Ocean	Kahaluu Segment	--	-157.8398	21.4608
COAST-05	COAST-05	22-Aug-17	9:02	Ocean	Kahaluu Segment	--	-157.8317	21.4590
COAST-06	COAST-06	22-Aug-17	9:13	Ocean	Kahaluu Segment	--	-157.8256	21.4541
COAST-07	COAST-07	22-Aug-17	9:25	Ocean	Heeia	--	-157.8144	21.4500
COAST-08	COAST-08	22-Aug-17	9:34	Ocean	Kahaluu Segment	--	-157.8201	21.4529
WWWTPSF	WWWTP Sand Filter	25-Sep-17	10:00	Wastewater	Kahawai	--	-157.7054	21.3388
WWWTPFC	WWWTP Final Clarifier	25-Sep-17	10:30	Wastewater	Kahawai	--	-157.7054	21.3388
WWWTPIN	WWWTP Influent	25-Sep-17	10:45	Wastewater	Kahawai	--	-157.7054	21.3388
Kahaluu Fishpond Stream	Kahaluu Fishpond Stream	30-Oct-17	12:05	Ocean	Kahaluu Segment	--	-157.8340	21.4593
USWOL01	USWOL01	31-Oct-17	8:45	Stream	Waiahole	Natural	-157.8459	21.4819
USKAL01	USKAL01	31-Oct-17	9:15	Stream	Kaalaea	Natural	-157.8435	21.4665
USHAI01	USHAI01	31-Oct-17	9:57	Stream	Haiamoa	Natural	-157.8430	21.4623
USLAG01 (DUP)	USLAG01	31-Oct-17	10:25	Estuary	Kahaluu Lagoon	--	-157.8404	21.4577
USLAG01	USLAG01	31-Oct-17	10:25	Estuary	Kahaluu Lagoon	--	-157.8404	21.4577
USWEE01	USWEE01	31-Oct-17	11:12	Stream	Waihee	Natural	-157.8489	21.4545
USKAH01	USKAH01	31-Oct-17	11:55	Stream	Kahaluu	Natural	-157.8419	21.4435

SAMPLE	SITE/WELL NAME	DATE	TIME	TYPE	WATERSHED	STREAMBED MATERIAL	LONG. (°)	LAT. (°)
USCON03	USCON03	3-Nov-17	7:45	Stream	Kahaluu	Channelized	-157.8381	21.4475
USCON01	USCON01	3-Nov-17	8:05	Stream	Kahaluu Lagoon	Channelized	-157.8381	21.4528
USCON02	USCON02	3-Nov-17	8:25	Stream	Ahuimanu	Channelized	-157.8333	21.4475
USKAH02	USKAH02	3-Nov-17	9:00	Stream	Kahaluu	Natural	-157.8433	21.4375
WSKAL01	WSKAL01	4-Dec-17	11:20	Stream	Kaalaea	Natural	-157.8431	21.4667
WPKAL01	WPKAL01	4-Dec-17	11:40	Pore water	Kaalaea	Natural	-157.8431	21.4667
WSKAL02	WSKAL02	4-Dec-17	12:40	Stream	Kaalaea	Natural	-157.8549	21.4664
WSHAI01	WSHAI01	4-Dec-17	13:35	Stream	Haiamoa	Natural	-157.8474	21.4596
NCOAST-01	NCOAST-01	5-Dec-17	9:45	Ocean	Kaalaea	--	-157.8428	21.4683
WPKAL03	WPKAL03	5-Dec-17	10:16	Pore water	Kaalaea	--	-157.8431	21.4679
WPKAL04	WPKAL04	5-Dec-17	10:35	Pore water	Kaalaea	--	-157.8443	21.4698
NCOAST-02	NCOAST-02	5-Dec-17	10:48	Ocean	Kaalaea	--	-157.8442	21.4712
WPKAL05	WPKAL05	5-Dec-17	11:13	Pore water	Kaalaea	--	-157.8445	21.4721
NCOAST-03	NCOAST-03	5-Dec-17	11:46	Ocean	Kaalaea	--	-157.8424	21.4732
NCOAST-04	NCOAST-04	5-Dec-17	11:57	Ocean	Kaalaea	--	-157.8430	21.4733
WOLAE01	WOLAE01	11-Dec-17	12:08	Ocean	Kahaluu Segment	--	-157.8283	21.4610
WOLAE02	WOLAE02	11-Dec-17	12:48	Ocean	Kahaluu Segment	--	-157.8292	21.4666
WPKAS01	WPKAS01	11-Dec-17	14:00	Pore water	Kahaluu Segment	--	-157.8260	21.4541
WSKAS01	WSKAS01	11-Dec-17	14:00	Ocean	Kahaluu Segment	--	-157.8260	21.4541
WSKAS02	WSKAS02	11-Dec-17	15:02	Ocean	Kahaluu Segment	--	-157.8308	21.4577
WPKAS02	WPKAS02	11-Dec-17	15:04	Pore water	Kahaluu Segment	--	-157.8307	21.4576
WPKAS03	WPKAS03	11-Dec-17	15:40	Pore water	Kahaluu Segment	--	-157.8317	21.4582
WSKAS03	WSKAS03	11-Dec-17	15:43	Ocean	Kahaluu Segment	--	-157.8316	21.4583
WSKAS04	WSKAS04	11-Dec-17	16:04	Ocean	Kahaluu Segment	--	-157.8319	21.4591
WSHAI03	WSHAI03	11-Dec-17	17:24	Ocean	Kaalaea	--	-157.8427	21.4647
WSMAN01	WSMAN01	11-Dec-17	17:54	Stream	Waiahole	Natural	-157.8420	21.4832
WSMAN02	WSMAN02	11-Dec-17	18:12	Ocean	Waiahole	--	-157.8416	21.4792
WWKAH01	WWKAH01	20-Dec-17	10:50	Groundwater	Kahaluu	--	-157.8419	21.4434
WWKAH01 (DUP)	WWKAH01 (DUP)	20-Dec-17	10:50	Groundwater	Kahaluu	--	-157.8419	21.4434

SAMPLE	SITE/WELL NAME	DATE	TIME	TYPE	WATERSHED	STREAMBED MATERIAL	LONG. (°)	LAT. (°)
KBRS01	KBRS01	20-Dec-17	12:17	Ocean	Kahaluu Lagoon	--	-157.8408	21.4608
WSHAI02 (DUP)	WSHAI02 (DUP)	20-Dec-17	12:37	Stream	Haiamoa	Natural	-156.8433	22.4643
WSHAI02	WSHAI02	20-Dec-17	12:37	Stream	Haiamoa	Natural	-157.8433	21.4643
KS171226	KS171226	26-Dec-17	17:20	Stream	Kahaluu	Natural	-157.8431	21.4419
WWJPR01	3-2751-005	1-Feb-18	10:20	Groundwater	Haiamoa	--	-157.8573	21.4558
WWHYG01	Hygienic Store MW01	1-Feb-18	11:40	Groundwater	Kahaluu Segment	--	-157.8385	21.4575
WWHYG01 (DUP)	Hygienic Store MW01	1-Feb-18	12:20	Groundwater	Kahaluu Segment	--	-157.8385	21.4575
WWHYG02	Hygienic Store MW02	1-Feb-18	13:15	Groundwater	Kahaluu Segment	--	-157.8388	21.4575
WWVOT01	3-2550-001	1-Feb-18	14:00	Groundwater	Ahuimanu	--	-157.8315	21.4292
WWFLD01	3-2750-003	2-Feb-18	10:30	Groundwater	Waihee	--	-157.8450	21.4522
WWFLD01 (DUP)	3-2750-003	2-Feb-18	10:30	Groundwater	Waihee	--	-157.8450	21.4522
TANK 1	Church Septic Main entrance	28-Feb-18	10:00	Septic	Kahaluu	--	-157.8390	21.4576
TANK 1 DUP	Church Septic Main entrance	28-Feb-18	10:00	Septic	Kahaluu	--	-157.8390	21.4576
TANK 2	Church Septic side	28-Feb-18	10:00	Septic	Kahaluu	--	-157.8390	21.4576
Ahuimanu Head 1	Ahuimanu Head 1	28-Feb-18	11:34	Stream	Ahuimanu		-157.8418	21.4291
Ahuimanu Head 1 (DUP)	Ahuimanu Head 1	28-Feb-18	11:34	Stream	Ahuimanu		-157.8418	21.4291
Ahuimanu Head 2	Ahuimanu Head 2	28-Feb-18	11:52	Stream	Ahuimanu		-157.8407	21.4298
Ahuimanu Head 3	Ahuimanu Head 3	28-Feb-18	12:05	Stream	Ahuimanu		-157.8390	21.4307
DSLAG20	DSLAG20	27-Apr-18	9:00	Estuary	Kahaluu Lagoon	Natural	-157.8390	21.4572
DSLAG21	DSLAG21	27-Apr-18	9:10	Estuary	Kahaluu Lagoon	Natural	-157.8390	21.4573
DSLAG22	DSLAG22	27-Apr-18	9:30	Estuary	Kahaluu Lagoon	Natural	-157.8390	21.4574
DSLAG23	DSLAG23	27-Apr-18	9:40	Estuary	Kahaluu Lagoon	Natural	-157.8390	21.4577
DSKFS02	DSKFS02	27-Apr-18	10:30	Estuary	Kahaluu Lagoon	Natural	-157.8339	21.4585
DSKAH01DIC	DSKAH01DIC	27-Apr-18	11:00	Stream	Kahaluu	Natural	-157.8418	21.4433

TableA1.2. Basic water quality parameters for Chapter 2.

SAMPLE	Temperature (°C)	Sp. Cond. (µS/cm)	Salinity (PSU)	pH	TDS	ODO (% saturation)	ODO (mg/L)
Kahaluu Special 3	23.93	3890.00	2.04	7.37	--	89.10	--
Kahaluu Special 1	24.26	8920.00	5.04	7.35	--	100.20	--
Kahaluu Special 2	24.25	7850.00	4.39	7.46	--	93.20	--
Kahaluu Special 7	24.77	2550.00	1.29	7.82	--	112.30	--
Kahaluu Special 6	25.47	5110.00	2.75	7.57	--	111.20	--
Kahaluu Special 4	23.21	340.00	0.14	8.02	--	106.20	--
Kahaluu Special 8	24.98	3420.00	1.78	7.31	--	97.50	--
Kahaluu Special 5	29.32	4100.00	2.16	7.16	--	94.90	--
Kahaluu Special 10	29.87	340.00	0.14	8.49	--	120.00	--
Kahaluu Special 9A	23.71	130.00	0.05	8.59	--	101.20	--
Kahaluu Special 17	27.50	360.00	0.15	7.61	--	125.00	--
Kahaluu Special 18	26.05	310.00	0.13	8.01	--	115.20	--
Kahaluu Special 11	25.04	270.00	0.11	7.85	--	104.80	--
Kahaluu Special 15	22.96	250.00	0.10	7.77	--	102.90	--
Kahaluu Special 12	23.10	240.00	0.10	7.53	--	90.50	--
Kahaluu Special 13	20.87	240.00	0.10	7.08	--	89.10	--
Waihee Tunnel	19.82	138.00	0.07	--	100.00	100.90	9.21
Waihee Inclined Wells	19.33	86.00	0.04	--	63.00	97.60	8.99
Kahaluu Headwaters	19.34	131.00	0.06	--	85.00	97.60	8.99
Kahaluu Well	20.34	191.00	0.09	--	124.00	100.00	9.03
Kahaluu SR-01	20.82	175.00	0.08	7.85	114.00	98.10	8.77
Kahaluu SR-02	21.36	174.00	0.08	7.87	113.00	99.40	8.79
Kahaluu SR-03	21.56	174.00	0.08	7.88	113.00	99.30	8.75
Kahaluu SR-04	21.52	178.00	0.08	7.86	115.00	98.70	8.71
Kahaluu SR-05	21.35	200.00	0.09	7.86	129.00	99.10	8.77
Kahaluu SR-06	21.16	171.00	0.08	7.77	111.00	97.20	8.64
Kahaluu SR-07	21.06	167.00	0.08	7.77	108.00	98.30	8.75

SAMPLE	Temperature (°C)	Sp. Cond. (µS/cm)	Salinity (PSU)	pH	TDS	ODO (% saturation)	ODO (mg/L)
Waihee GW 170320	24.87	532.00	0.26	7.29	345.00	25.20	2.09
Kahaluu SW 170320	21.67	171.00	0.08	7.82	111.00	96.30	8.48
Kahaluu GW 170320	23.19	208.00	0.10	7.32	135.00	88.30	7.55
Waihee SR-01	21.01	157.00	0.07	7.36	102.00	99.00	8.82
Waihee SR-02	21.63	154.00	0.07	7.83	100.00	101.70	8.95
Waihee SR-03	21.29	151.00	0.07	7.81	98.00	99.40	8.81
Waihee SR-04	21.18	151.00	0.07	7.94	98.00	97.50	8.66
Waihee (DUP)	21.18	151.00	0.07	7.94	98.00	97.50	8.66
DPKAH01	22.50	175.00	0.08	7.96	114.00	93.50	8.10
DSKAH01 (DUP)	21.74	172.00	0.08	8.02	112.00	95.40	8.38
DSKAH01	21.74	172.00	0.08	8.02	112.00	95.40	8.38
DWKAH01	23.39	194.00	0.09	7.52	126.00	50.40	4.27
DSKAH02	21.97	176.00	0.08	7.99	111.00	96.10	8.41
DSKAH03	22.03	171.00	0.08	8.01	111.00	97.40	8.51
DSKAH04	22.17	171.00	0.08	8.03	111.00	96.70	8.43
DSKAH05	22.36	170.00	0.08	8.02	111.00	97.10	8.42
DPKAH05	24.18	652.00	0.32	7.23	423.00	31.10	2.60
DSKAH06	22.67	169.00	0.08	8.06	110.00	97.10	8.38
DSKAH07	22.65	276.00	0.13	8.06	179.00	98.70	8.51
DSKAH08	22.27	170.00	0.08	7.99	111.00	97.90	8.51
DPKAH09	25.02	243.00	0.11	6.77	158.00	48.70	4.02
DSKAH10	22.17	168.00	0.08	7.97	109.00	98.70	8.60
DPKAH11	24.36	189.00	0.09	7.25	123.00	34.30	2.86
DSKAH11	24.87	192.00	0.09	7.46	125.00	79.70	6.59
DSKAH12	21.80	165.00	0.08	7.87	107.00	95.60	8.38
DPKAH12	22.48	166.00	0.08	7.87	108.00	91.80	7.95
DPWEE01	23.19	228.00	0.11	7.39	148.00	43.30	3.70
DSWEE01 (DUP)	21.61	154.00	0.07	7.79	100.00	94.40	8.31
DSWEE01	21.61	154.00	0.07	7.79	100.00	94.40	8.31
DWWEE01	24.34	312.00	0.15	7.39	203.00	23.80	1.96

SAMPLE	Temperature (°C)	Sp. Cond. (µS/cm)	Salinity (PSU)	pH	TDS	ODO (% saturation)	ODO (mg/L)
DSWEE02	21.90	154.00	0.07	7.90	100.00	96.00	8.41
DPWEE02	23.29	161.00	0.08	7.90	105.00	75.80	6.46
DSWEE03	22.32	155.00	0.07	7.92	101.00	93.90	8.16
DSWEE04	22.74	157.00	0.07	7.94	102.00	95.00	8.19
DSWEE05	22.96	160.00	0.07	7.95	104.00	95.70	8.21
DPWEE05	25.52	515.00	0.25	7.07	335.00	29.20	3.38
DSWEE09	23.72	162.00	0.08	8.02	105.00	97.80	8.27
DSWEE11	22.94	151.00	0.07	7.93	98.00	99.10	8.51
DSWEE12	21.34	148.00	0.07	8.01	96.00	95.20	8.42
DPWEE12	22.67	195.00	0.09	6.69	127.00	19.00	1.63
DSWEE13	21.52	148.00	0.07	8.02	96.00	95.30	8.41
DSWEE14	21.70	149.00	0.07	7.86	97.00	93.30	8.20
DSWOL01	21.83	129.00	0.06	7.93	84.00	97.80	8.57
DSWOL01 (DUP)	21.83	129.00	0.06	7.93	84.00	97.80	8.57
DPWOL01	23.05	179.00	0.08	7.49	117.00	32.20	2.74
DSWOL02	23.89	126.00	0.06	7.66	82.00	84.50	7.13
DSWOL03	22.00	128.00	0.06	8.03	83.00	101.40	8.87
DSWOL04	22.34	127.00	0.06	8.23	83.00	107.30	9.32
DPWOL04	23.58	168.00	0.08	7.26	109.00	23.20	1.95
DSWOL06	22.26	126.00	0.06	8.24	82.00	104.50	9.10
DSWOL07	22.39	125.00	0.06	8.16	81.00	102.00	8.85
DPWOL07	24.77	223.00	0.10	7.22	145.00	46.60	3.86
DSWOL08	22.27	125.00	0.06	8.12	81.00	98.70	8.59
DSWOL09	22.97	128.00	0.06	8.19	83.00	103.70	8.90
DSLAG01	29.11	19691.00	11.62	7.79	12769.00	78.00	5.64
DPLAG01 (DUP)	29.01	32188.00	19.99	7.20	20922.00	13.80	0.95
DPLAG01	29.01	32188.00	19.99	7.20	20922.00	13.80	0.95
DSLAG02	26.64	13504.00	7.77	7.34	8777.00	52.10	3.99
DPLAG02	27.19	24236.00	14.66	7.26	15754.00	28.30	2.06

SAMPLE	Temperature (°C)	Sp. Cond. (µS/cm)	Salinity (PSU)	pH	TDS	ODO (% saturation)	ODO (mg/L)
DSLAG03	23.35	602.00	0.29	8.05	392.00	86.50	7.35
DPLAG04	28.11	6784.00	3.70	6.72	4410.00	71.40	5.47
DSLAG04	27.52	6174.00	3.65	7.50	4286.00	90.10	6.88
DPLAG05	27.78	9955.00	5.58	6.84	6470.00	33.80	2.59
DPLAG06	27.91	23558.00	14.21	6.99	15322.00	24.70	1.78
DPLAG07	29.43	28138.00	17.23	7.43	18290.00	33.30	2.31
DPMAN01	27.37	30758.00	19.04	7.48	19992.00	33.00	2.33
DSMAN02	22.19	150.00	0.07	7.94	97.00	79.80	6.95
DPMAN03	25.13	12382.00	7.08	7.89	848.00	25.00	1.97
DSMAN04	22.13	270.00	0.13	7.97	175.00	84.20	7.33
DSMAN05	26.66	4181.00	2.22	7.81	2729.00	82.10	6.45
DPMAN04	29.36	30113.00	18.58	7.70	19578.00	51.70	3.55
DPMAN06	31.09	36667.00	23.03	7.72	23833.00	35.80	2.33
DPMAN07	28.33	1344.00	0.07	7.03	874.00	41.90	3.24
DPMAN08	27.04	457.00	0.22	7.17	297.00	31.10	2.52
DSMAN09	27.82	685.00	0.33	7.59	445.00	50.20	3.92
DSCON01	23.23	184.00	0.09	8.25	120.00	107.80	9.20
DPCON02	23.58	212.00	0.10	7.06	138.00	70.80	6.00
DSCON03	25.11	142.00	0.07	8.06	92.00	111.80	9.22
DPCON03	24.56	342.00	0.16	7.03	222.00	32.40	2.69
DSCON04	25.15	173.00	0.08	7.72	112.00	109.90	9.07
DPCON05	25.16	371.00	0.18	7.14	241.00	34.70	2.85
DSCON06	26.28	177.00	0.08	8.88	115.00	131.30	10.60
DSCON07	28.40	172.00	0.08	9.10	111.00	127.10	9.87
DSCON08	26.75	177.00	0.08	9.14	115.00	128.00	10.25
DSCON09	27.48	645.00	0.31	9.14	423.00	134.80	10.64
COAST-01	27.62	52828.00	34.76	8.25	34345.00	85.50	5.54
COAST-02	27.02	37988.00	24.06	8.20	24692.00	80.50	5.60
COAST-03	27.18	37209.00	23.51	8.17	24186.00	85.20	5.94

SAMPLE	Temperature (°C)	Sp. Cond. (µS/cm)	Salinity (PSU)	pH	TDS	ODO (% saturation)	ODO (mg/L)
COAST-04	27.52	25489.00	15.48	8.14	16559.00	90.70	6.57
COAST-04 (DUP)	27.52	25489.00	15.48	8.14	16559.00	90.70	6.57
COAST-05	28.11	49875.00	32.57	8.27	32423.00	98.40	6.41
COAST-06	28.21	52406.00	34.42	8.26	34065.00	94.70	6.10
COAST-07	28.36	52767.00	34.69	8.32	34298.00	116.00	7.43
COAST-08	28.40	52971.00	34.84	8.24	34431.00	94.60	6.06
WWWTPSF	29.35	720.00	0.35	7.61	468.00	35.80	2.72
WWWTPFC	29.31	685.00	0.33	7.48	445.00	43.60	3.27
WWWTPIN	29.32	1011.00	0.49	7.72	657.00	36.30	2.74
Kahaluu Fishpond Stream	26.03	27203.00	18.93	--	--	--	--
USWOL01	20.61	128.00	0.06	8.21	83.00	93.30	8.38
USKAL01	24.79	281.00	0.13	7.87	183.00	76.20	6.31
USHAI01	23.24	350.00	0.17	7.67	227.00	33.80	2.89
USLAG01 (DUP)	27.06	19396.00	10.99	8.17	12420.00	94.20	7.11
USLAG01	27.06	19396.00	10.99	8.17	12420.00	94.20	7.11
USWEE01	21.75	153.00	0.07	8.12	100.00	99.20	8.71
USKAH01	22.77	180.00	0.08	8.20	117.00	96.00	8.31
USCON03	23.07	187.00	0.09	7.89	122.00	99.00	8.48
USCON01	23.75	246.00	0.12	8.27	160.00	113.60	9.60
USCON02	24.63	221.00	0.10	8.74	144.00	124.00	10.31
USKAH02	22.75	158.00	0.07	7.63	103.00	63.20	5.44
WSKAL01	22.96	267.00	0.13	7.80	174.00	84.90	7.24
WPKAL01	24.26	532.00	0.26	7.69	346.00	39.90	3.34
WSKAL02	21.81	173.00	0.08	7.92	112.00	92.60	8.12
WSHAI01	23.22	271.00	0.13	8.16	176.00	84.60	7.21
NCOAST-01	21.04	43830.00	28.30	8.44	28477.00	97.90	7.40
WPKAL03	23.64	14443.00	8.41	7.96	9416.00	51.50	4.15
WPKAL04	22.71	36916.00	23.36	7.76	23976.00	51.00	3.84
NCOAST-02	21.60	45645.00	29.62	8.46	29670.00	96.30	7.13
WPKAL05	23.01	1318.00	0.66	7.35	857.00	69.10	5.90

SAMPLE	Temperature (°C)	Sp. Cond. (µS/cm)	Salinity (PSU)	pH	TDS	ODO (% saturation)	ODO (mg/L)
NCOAST-03	21.79	46516.00	30.25	8.50	30235.00	103.90	7.65
NCOAST-04	21.80	41135.00	26.38	8.49	26738.00	101.20	7.62
WOLAE01	24.85	52420.00	34.69	8.53	34074.00	132.40	8.95
WOLAE02	25.28	52611.00	34.65	8.56	34194.00	125.40	8.48
WPKAS01	25.49	18765.00	10.91	7.97	12199.00	38.10	2.92
WSKAS01	26.59	51348.00	33.61	8.32	33370.00	84.30	5.64
WSKAS02	26.39	51654.00	33.90	8.30	33579.00	83.20	5.52
WPKAS02	24.45	48277.00	31.51	7.89	31391.00	54.70	3.80
WPKAS03	25.31	2810.00	1.44	7.72	1817.00	41.30	3.35
WSKAS03	26.18	51131.00	33.33	8.38	33244.00	94.00	6.31
WSKAS04	26.12	51680.00	33.92	8.46	33600.00	106.50	7.11
WSHAI03	26.97	46193.00	29.23	8.40	28910.00	105.00	7.09
WSMAN01	20.85	143.00	0.07	8.64	93.00	86.90	7.77
WSMAN02	24.26	35928.00	22.72	8.42	23397.00	91.50	6.73
WWKAH01	21.24	205.00	0.10	7.64	133.00	73.60	6.52
WWKAH01 (DUP)	21.24	205.00	0.10	7.64	133.00		6.52
KBRS01	22.83	43375.00	27.97	8.29	28193.00	80.80	5.92
WSHAI02 (DUP)	23.67	369.00	1.18	10.18	240.00	70.80	7.02
WSHAI02	22.67	368.00	0.18	9.18	239.00	69.80	6.02
KS171226	20.68	--	0.14	--	--	--	--
WWJPR01	23.60	230.00	0.11	7.98	149.00	58.10	4.92
WWHYG01	25.72	261.00	0.12	8.01	169.00	42.70	3.39
WWHYG01 (DUP)	25.72	261.00	0.12	8.01	169.00	42.70	3.39
WWHYG02	27.88	2419.00	1.23	7.33	1570.00	30.90	2.35
WWVOT01	23.49	171.00	0.08	7.90	111.00	68.10	5.77
WWFLD01	23.66	200.00	0.09	7.39	130.00	82.80	7.01
WWFLD01 (DUP)	23.66	200.00	0.09	7.39	130.00	82.80	7.01
DSLAG20	23.02	12809.00	7.36	8.17	8326.00	84.90	7.00
DSLAG21	22.97	9263.00	5.19	8.51	6021.00	94.00	7.83

SAMPLE	Temperature (°C)	Sp. Cond. (µS/cm)	Salinity (PSU)	pH	TDS	ODO (% saturation)	ODO (mg/L)
DSLAG22	23.46	19356.00	15.56	8.38	12977.00	76.00	5.89
DSLAG23	23.47	15769.00	9.04	8.42	9676.00	88.10	7.15
DSKAH01DIC	21.47	167.00	0.08	8.45	108.00	93.70	8.28

Table A1.3. Nutrient concentrations for Chapter 2.

SAMPLE	PO_4^{3-} (µM)	TP (µM)	NH_3 (µM)	$NO_3^- + NO_2^-$ (µM)	NO_2^- (µM)	TN (µM)	SiO_2 (µM)
Kahaluu Special 3	0.775	0.775	2.213	11.566	0.143	12.851	429.00
Kahaluu Special 1	0.743	0.839	2.285	6.854	0.286	14.993	374.00
Kahaluu Special 2	0.807	0.775	2.57	15.207	0.214	18.277	403.00
Kahaluu Special 7	0.549	0.807	0.143	4.498	0.214	15.778	433.00
Kahaluu Special 6	0.646	0.743	2.356	5.426	0.214	15.778	413.00
Kahaluu Special 4	1.065	0.807	0.143	6.854	0.071	9.495	499.00
Kahaluu Special 8	0.936	0.775	2.142	6.354	0.214	15.707	451.00
Kahaluu Special 5	0.743	1.291	0.714	5.283	0.143	16.849	428.00
Kahaluu Special 10	0.613	0.452	1	6.64	0.143	18.277	413.00
Kahaluu Special 9A	1.356	1.291	1.214	7.996	0.071	14.636	431.00
Kahaluu Special 17	0.355	0.323	0.286	0.357	0.071	7.068	428.00
Kahaluu Special 18	0.452	0.387	0.214	12.994	0.071	17.849	434.00
Kahaluu Special 11	0.678	0.484	0.143	7.354	0.071	16.492	479.00
Kahaluu Special 15	1.065	0.904	0.214	12.208	0.071	12.423	499.00
Kahaluu Special 12	0.42	0.355	0.357	33.627	0.071	34.412	343.00
Kahaluu Special 13	1.162	1.001	0.214	11.423	0.071	12.565	501.00
Waihee Tunnel	1.453	1.324	0.143	14.065	0.071	17.277	543.00
Waihee Inclined Wells	1.388	1.291	0.143	8.567	0.071	16.064	458.00
Kahaluu Headwaters	1.195	1.13	0.214	11.637	0.071	17.42	444.00
Kahaluu Well	1.517	1.421	0.143	11.566	0.071	17.563	579.00
Kahaluu Nuts	0.936	1.259	1.428	12.423	0.214	28.772	240.00

SAMPLE	PO_4^{3-} (µM)	TP (µM)	NH_3 (µM)	$NO_3^- + NO_2^-$ (µM)	NO_2^- (µM)	TN (µM)	SiO_2 (µM)
Waihee Nuts	1.162	0.969	0.857	5.355	0.071	21.561	356.00
Kahaluu SR-01	1.098	1.001	0.214	16.492	0.071	22.346	483.00
Kahaluu SR-02	1.033	0.872	0.286	15.921	0.071	21.204	484.00
Kahaluu SR-03	1.13	1.195	0.214	14.207	0.071	21.418	488.00
Kahaluu SR-04	1.098	0.936	0.214	15.207	0.071	19.705	484.00
Kahaluu SR-05	1.098	0.969	0.143	15.136	0.071	21.704	496.00
Kahaluu SR-06	1.098	0.904	1.071	14.707	0.071	19.633	489.00
Kahaluu SR-07	1.098	1.001	0.286	12.423	0.071	17.706	494.00
Waihee SW 170320	1.065	0.872	0.357	6.997	0.071	9.281	488.00
Waihee GW 170320	0.42	0.42	16.778	1.214	0.071	19.776	558.00
Kahaluu SW 170320	1.001	0.839	0.143	14.065	0.071	17.991	484.00
Kahaluu GW 170320	0.839	4.585	2.356	11.352	2.642	16.349	528.00
Waihee SR-01	1.033	0.839	0.5	3.498	0.071	9.71	491.00
Waihee SR-02	1.065	1.098	0.286	6.283	0.071	8.639	486.00
Waihee SR-03	1.13	0.969	0.143	10.138	0.071	22.989	488.00
Waihee SR-04	1.227	1.195	0.214	8.068	0.071	13.851	489.00
Waihee (DUP)	1.227	1.033	0.143	11.78	0.071	23.06	484.00
Waihee SR-05	1.195	1.098	0.357	6.568	0.071	10.995	486.00
DPKAH01	1.098	0.936	0.143	10.495	0.071	28.058	549.00
DSKAH01 (DUP)	1.098	1.001	0.214	11.709	0.071	29.7	548.00
DSKAH01	1.13	0.807	0.143	11.423	0.071	32.699	546.00
DWKAH01	0.71	0.387	1	0.714	0.071	5.497	596.00
DSKAH02	0.68	0.72	0.18	9.18		11.7	567.00
DSKAH03	0.84	1.05	1.09	10.27		13.53	566.00
DSKAH04	0.9	0.94	0.61	10.03		12.22	569.00
DSKAH05	1.13	0.839	0.286	10.067	0.071	24.917	551.00
DPKAH05	0.517	0.613	34.983	1.928	0.214	35.126	408.00
DSKAH06	0.92	0.97	1.12	9.94		12.78	570.00
DSKAH07	0.94	0.95	1.29	11.86		15.03	573.00
DSKAH08	0.88	0.93	0.15	10.48		12.48	570.00

SAMPLE	PO_4^{3-} (µM)	TP (µM)	NH_3 (µM)	$NO_3^- + NO_2^-$ (µM)	NO_2^- (µM)	TN (µM)	SiO_2 (µM)
DPKAH09	0.775	0.323	0.571	0.286	0.071	3.284	807.00
DSKAH10	1.227	0.936	0.214	9.781	0.071	23.703	551.00
DPKAH11	0.678	0.549	3.57	12.494	0.357	52.118	443.00
DSKAH11	0.775	0.936	2.427	41.623	0.286	50.119	458.00
DSKAH12	1.098	0.904	0.643	9.924	0.071		549.00
DPKAH12	1.227	0.969	0.571	10.852	0.071		551.00
DPWEE01	1.291	1.001	0.857	2.07	0.071	5.497	597.00
DSWEE01 (DUP)	1.098	0.872	1.285	6.211	0.071	9.995	538.00
DSWEE01	1.13	0.904	0.571	5.854	0.071	10.281	538.00
DWWEE01	0.807	2.26	13.208	0.714	0.357		627.00
DSWEE02	1.485	1.227	1.285	10.495	0.143	12.994	523.00
DPWEE02	1.227	1.098	0.928	6.283	0.071	9.353	538.00
DSWEE03	1.421	1.614	0.857	6.782	0.214	9.067	536.00
DSWEE04	1.356	1.776	0.928	5.64	0.214	7.211	536.00
DSWEE05	0.678	4.843	205.616	0.357	0.357		699.00
DPWEE05	1.324	1.421	1.928	5.212	0.214	12.78	536.00
DSWEE08	0.678	2.454	14.993	0.071	0.071	13.065	712.00
DSWEE09	1.324	1.647	0.643	4.426	0.214	4.855	533.00
DSWEE10	21.147	19.533	7.139	23.203	1.785	38.839	536.00
DSWEE11	1.195	1.033	0.714	5.497	0.071	9.924	528.00
DSWEE12	1.291	1.065	0.143	7.639	0.071	4.212	527.00
DPWEE12	0.646	0.839	0.357	0.214	0.071	1.785	760.00
DSWEE13	1.259	1.195	0.357	6.997	0.071	7.068	530.00
DSWEE14	1.195	1.098	0.214	6.997	0.071	13.208	525.00
DSWOL01	1.033		1.785	3.57	0.143	4.498	498.00
DSWOL01 (DUP)	1.485		1.214	0.071	0.143	11.423	529.00
DPWOL01	1.033		0.571	3.498	0.143		498.00
DSWOL02	1.388		3.998	4.069	0.143	13.993	486.00
DSWOL03	1.065		0.714	2.927	0.428	5.497	494.00

SAMPLE	PO_4^{3-} (µM)	TP (µM)	NH_3 (µM)	$NO_3^- + NO_2^-$ (µM)	NO_2^- (µM)	TN (µM)	SiO_2 (µM)
DSWOL04	1.098		0.214	2.713	0.071	4.712	503.00
DPWOL04	0.581		6.782	0.071	0.071		544.00
DSWOL06	1.13		0.286	2.713	0.071	3.713	503.00
DSWOL07	1.195		0.428	3.284	0.071	5.14	503.00
DPWOL07	0.678		3.713	0.428	0.071	3.427	596.00
DSWOL08	1.195		1.071	3.713	0.071	5.64	508.00
DSWOL09	1.13		0.643	2.57	0.143	4.712	511.00
DSLAG01	1.065	3.681	3.284	3.498	0.357	15.921	303.00
DPLAG01 (DUP)	0.517	1.582	14.636	0.286	0.071		268.00
DPLAG01	0.517	1.582	13.922	0.428	0.143		273.00
DSLAG02	0.743	3.39	18.92	2.927	0.286	28.915	398.00
DPLAG02	0.581	3.519	69.967	0.071	0.071		341.00
DSLAG03	1.76	1.99	3.25	8.4		17.82	526.00
DPLAG04	0.969	0.678	0.357	6.925	0.071	12.994	568.00
DSLAG04	1	1.41	3.39	5.4		13.33	476.00
DPLAG05	0.743	3.164	26.416	0.071	0.071		541.00
DPLAG06	0.646	0.775	22.846	0.071	0.071		361.00
DPLAG07	0.646	7.103	159.923	0.071	0.071		320.00
DPMAN01	0.613	0.807	16.421	0.071	0.071		293.00
DSMAN02	0.904	0.904	1.713	4.641	0.071	9.138	503.00
DPMAN03	2.26	1.517	24.988	0.071	0.071		281.00
DSMAN04	0.969	0.839	1.142	3.284	0.143		506.00
DSMAN05	1.033	1.969	4.284	4.498	0.286	8.21	463.00
DPMAN04	0.839	1.388	72.822	0.071	0.214		223.00
DPMAN06	0.775	2.066	23.917	0.143	0.214		205.00
DPMAN07	0.936	6.715	10.709	0.071	0.071		1015.00
DPMAN08	0.775	2.647	69.967	0.071	0.071		579.00
DSMAN09	0.581	0.581	348.405	0.071	0.071		503.00
DSCON01	0.839		1.856	5.426	0.143		511.00

SAMPLE	PO_4^{3-} (µM)	TP (µM)	NH_3 (µM)	$NO_3^- + NO_2^-$ (µM)	NO_2^- (µM)	TN (µM)	SiO_2 (µM)
DPCON02	0.161		2.713	2.213	0.071		511.00
DSCON03	0.936		5.926	0.857	0.214		373.00
DPCON03	0.161		8.924	0.071	0.071		484.00
DSCON04	0.743		4.141	1.428	0.143		471.00
DPCON05	0.161		19.276	0.071	0.071		539.00
DSCON06	0.743		9.281	0.143	0.143		478.00
DSCON07	0.226		1.428	0.357	0.143		374.00
DSCON08	0.42		1.071	0.5	0.143		463.00
DSCON09	0.452		2.499	0.357	0.071		421.00
COAST-01	0.161	0.549	0.143	0.143	0.071		8.00
COAST-02	0.387	1.13	1.785	0.071	0.071		73.00
COAST-03	0.291	1.033	1	0.071	0.071		68.00
COAST-04	0.613	0.969	3.141	2.356	0.214		251.00
COAST-04 (DUP)	0.581	1.001	3.713	2.999	0.214		262.00
COAST-05	0.194	0.775	1	0.071	0.071		26.00
COAST-06	0.161	0.646	1.356	0.143	0.071		14.00
COAST-07	0.161	0.387	0.571	0.071	0.071		10.00
COAST-08	0.161	0.613	1.071	0.071	0.071		9.00
WWWTPSF	48.93	50.25	315.23	188.89		558.61	1078.00
WWWTPFC	31.33	35.36	202.12	271		474.89	1070.00
WWWTPIN	134.25	151.15	3534.7	0.38		3855.44	1023.00
Kahaluu Fishpond Stream	0.484	0.904	12.494	6.211	1.285	25.631	21.00
USWOL01	0.678	0.613	1.499	4.712	0.071	10.424	491.00
USKAL01	0.613	1.033	4.355	12.565	0.071	34.198	297.00
USHAI01	0.484	1.388	2.427	13.351	0.071	35.412	246.00
USLAG01 (DUP)	0.387	0.549	4.426	3.855	0.214	10.495	272.00
USLAG01	0.839	0.839	5.64	2.142	0.214	13.208	180.00
USWEE01	0.71	0.775	0.5	6.14	0.071	10.138	306.00
USKAH01	0.646	0.839	0.286	11.423	0.071	15.921	388.00
USCON03	0.258	0.387	1.999	3.498	0.143	17.563	336.00

SAMPLE	PO_4^{3-} (µM)	TP (µM)	NH_3 (µM)	$NO_3^- + NO_2^-$ (µM)	NO_2^- (µM)	TN (µM)	SiO_2 (µM)
USCON01	0.355	0.42	2.427	2.57	0.571	13.851	395.00
USCON02	0.323	0.484	2.213	39.695	0.143	100.88	388.00
USKAH02	0.904	0.936	1.999	40.838	0.071	60.328	421.00
WSKAL01	0.646	0.807	3.927	7.996	0.143	31.842	369.00
WPKAL01	0.613	0.387	1.356	137.791	0.357	204.902	460.00
WSKAL02	0.452	0.42	0.428	9.638	0.5	25.345	450.00
WSHAI01	0.323	0.872	4.855	72.108	0.714	220.18	350.00
NCOAST-01	0.581	1.033	6.497	5.854	0.143	21.133	58.00
WPKAL03	0.387	0.743	33.555	0.143	0.071	32.627	220.00
WPKAL04	0.323	2.292	5.854	0.071	0.071	6.425	193.00
NCOAST-02	0.355	0.969	1.785	0.571	0.5	9.067	51.00
WPKAL05	0.194	0.581	1.071	55.759	0.571	96.454	391.00
NCOAST-03	0.226	0.678	0.214	1	0.143	4.498	46.00
NCOAST-04	0.42	0.775	0.5	0.571	0.071	5.212	56.00
WOLAE01	0.161	0.194	1.285	0.714	0.071	4.212	8.00
WOLAE02	0.161	0.258	1.571	0.357	0.071	4.998	8.00
WPKAS01	1.227	1.324	13.922	0.071	0.071	13.279	334.00
WSKAS02	0.323	0.355	1.428	0.643	0.071	7.568	13.00
WPKAS03	3.293	3.035	0.143	32.913	0.071	46.692	739.00
WSKAS04	0.291	0.42	0.785	1.071	0.071	4.569	16.00
WSHAI03	0.904	1.743	3.713	4.569	0.214	11.851	43.00
WSMAN01	0.936	0.936	2.213	5.569	0.143	13.137	362.00
WSMAN02	0.484	1.776	1.499	1.428	0.214	15.064	114.00
WWKAH01	0.387	0.226	0.357	5.497	0.143	11.851	418.00
WWKAH01 (DUP)	0.42	0.291	0.357	5.712	0.428	29.058	449.00
KBRS01	0.517	3.551	3.713	6.64	0.357	16.492	62.00
WSHAI02 (DUP)	1.356	1.291	14.636	35.983	1.999	71.609	363.00
WSHAI02	1.259	1.421	14.993	38.624	1.856	73.036	289.00
KS171226	0.807	1.227	0.357	10.995	0.286	70.466	203.00
WWJPR01	0.969	1.421	0.286	2.713	0.071	2.285	456.00

SAMPLE	PO_4^{3-} (µM)	TP (µM)	NH_3 (µM)	$NO_3^- + NO_2^-$ (µM)	NO_2^- (µM)	TN (µM)	SiO_2 (µM)
WWHYG01	5.973	6.522	4.141	6.211	0.071	8.924	468.00
WWHYG01 (DUP)	6.167	6.393	6.14	8.71	0.071	13.851	452.00
WWHYG02	0.194	4.294	296.287	0.643	0.071	354.83	287.00
WWVOT01	1.873	1.84	0.143	5.212	0.071	12.066	291.00
WWFLD01	1.808	1.937	0.428	9.71	0.071	9.353	499.00
WWFLD01 (DUP)	1.776	1.84	0.357	9.638	0.071	10.424	437.00
TANK 1	249.5	262.86	4620.85	0.88		5484.71	469.00
TANK 1 DUP	253.46	262.58	4719.85	1.06		5606.22	500.00
TANK 2	290.94	341.91	5506.23	3.34		5878.75	389.00
Ahuimanu Head 1	1.187	1.43	0.07	11.279		12.872	601.00
Ahuimanu Head 1 (DUP)	1.187	1.43	0.07	11.279		12.872	601.00
Ahuimanu Head 2	1.031	1.12	0.06	8.671		9.859	572.00
Ahuimanu Head 3	0.775	0.98	0.05	5.094		6.727	570.00
DSLAG20	0.55	0.64	1.8	10.83		18.51	361.00
DSLAG21	0.7	0.78	2.1	14.75		23.04	373.00
DSLAG22	0.73	0.8	3.8	14.16		24.18	323.00
DSLAG23	0.71	0.85	2.55	14.37		23.03	359.00
DSKFS02	3.08	3.43	8.64	49.6		107.77	216.00
DSKAH01DIC	0.72	0.78	0.07	16.1		21.88	452.00

Table A1.4. Dissolved ion concentrations for Chapter 2.

SAMPLE	F^- (µM)	Cl^- (µM)	Br^- (µM)	SO_4^{2-} (µM)	Li^+ (µM)	Na^+ (µM)	K^+ (µM)	Mg^{2+} (µM)	Ca^{2+} (µM)
Ahuimanu Head 1		691.1		45.8		717.7	30.7	345.6	366.8
Ahuimanu Head 1 (DUP)		682.7	1.3	43.7		704.7	30.7	341.5	359.3
Ahuimanu Head 2		682.7	1.3	42.7		700.3	30.7	341.5	356.8
Ahuimanu Head 3		631.9		41.6		639.4	28.1	320.9	324.4
DPCON02	1.1	631.9		57.3		778.6	28.1	320.9	314.4

SAMPLE	F^- (µM)	Cl^- (µM)	Br^- (µM)	SO_4^{2-} (µM)	Li^+ (µM)	Na^+ (µM)	K^+ (µM)	Mg^{2+} (µM)	Ca^{2+} (µM)
DPCON03	1.6	696.8	1.3	210.3		887.3	25.6	646.0	591.3
DPCON05	1.6	730.6	1.3	170.7		930.8	30.7	691.2	658.7
DPKAH01		493.4		37.5		613.3	18.7	318.9	309.9
DPKAH05	3.2	842.6	11.5	31.2		1526.3	162.9	1107.2	1767.3
DPKAH09	1368.6				2389.0	2.0	355.8	584.2	
DPKAH11	1.1	547.2	0.4	67.7		642.9	13.6	318.5	360.5
DPKAH12	0.5	481.2	0.5	34.4		593.7	19.7	306.9	299.4
DPLAG01		333750.9	479.7	17213.2	7.1	279491.5	5565.5	41721.5	7323.7
DPLAG01 (DUP)		339991.5	455.8	17515.9	7.3	284459.3	5702.3	42308.6	7435.0
DPLAG02		219081.5	360.3	11111.6		186406.3	3614.0	25647.4	5506.3
DPLAG04		56109.4	61.8	3303.3		54502.4	1069.1	6996.9	3372.4
DPLAG05		84426.8	129.2	3918.5		78868.2	1501.4	9864.6	2432.0
DPLAG06		227754.9	356.3	11414.5		202211.0	3973.1	23238.0	4724.0
DPLAG07		273833.6	372.1	13368.8	2.5	234802.5	6692.4	32254.7	5954.4
DPMAN01		303036.4	460.6	14693.6	9.7	246756.9	4962.7	40306.9	9774.7
DPMAN03		104961.6	165.1	4744.2	2.8	87730.3	1985.3	14949.6	3621.7
DPMAN04		291115.1	456.5	15279.8	9.7	248494.1	5088.2	38513.1	8595.2
DPMAN06		341475.0	516.4	17736.2	11.3	289951.7	6287.8	42036.6	7455.5
DPMAN07	2.6	958.3	2.1	345.1	0.2	2724.7	17.1	1044.2	610.8
DPMAN08	3.2	363.9	2.0	63.5		624.2	26.6	873.5	901.5
DPWEE01	1.1	516.5	1.1	39.6		662.0	24.8	428.3	554.7
DPWEE02	0.5	476.7	0.3	31.2		554.2	20.5	292.1	301.9
DPWEE05	6.3	635.5	1.3	248.8		1009.6	139.4	1143.8	982.1
DPWEE12	1.1	547.2	0.9	43.7		612.0	7.7	456.7	304.4
DPWOL01	1.6	372.9	1.1	3.1		473.2	28.4	415.6	367.0
DPWOL04	1.6	400.6	0.4	17.7		484.1	12.0	352.2	283.9
DPWOL07	1.1	523.0	0.6	34.4		628.1	16.6	487.1	394.2
DSCON01	1.1	533.1	1.3	37.5		691.6	30.7	296.2	311.9
DSCON03	1.1	454.2		36.4		578.5	33.2	242.7	282.0

SAMPLE	F^- (µM)	Cl^- (µM)	Br^- (µM)	SO_4^{2-} (µM)	Li^+ (µM)	Na^+ (µM)	K^+ (µM)	Mg^{2+} (µM)	Ca^{2+} (µM)
DSCON04	1.1	502.1	1.3	46.8		652.5	33.2	275.7	321.9
DSCON06	1.1	524.7	1.3	47.9		661.2	33.2	283.9	306.9
DSCON07	1.1	586.7	1.3	64.5		678.6	33.2	275.7	314.4
DSCON08	1.1	536.0	1.3	47.9		665.5	33.2	288.0	306.9
DSCON09	1.6	4623.4	6.3	255.1		4310.6	107.4	670.6	356.8
DSKAH01		488.0	0.5	37.5		609.0	38.4	308.6	336.8
DSKAH01 (DUP)		490.8	0.5	36.4		652.5	38.4	312.7	341.8
DSKAH01DIC									
DSKAH02		490.8		36.4		652.5	38.4	316.8	344.3
DSKAH03		490.8	0.6	35.4		652.5	38.4	316.8	344.3
DSKAH04		490.8		36.4		609.0	38.4	316.8	344.3
DSKAH05		488.0		35.4		652.5	38.4	312.7	341.8
DSKAH06		488.0		36.4		609.0	38.4	312.7	339.3
DSKAH07		1407.6	1.8	87.4		1348.4	56.3	403.2	399.2
DSKAH08		504.9		35.4		652.5	38.4	312.7	336.8
DSKAH10		493.7		35.4		609.0	38.4	308.6	334.3
DSKAH11		547.2		62.5		652.5	30.7	325.0	404.2
DSKAH12		479.5		33.3		609.0	38.4	304.5	329.4
DSKFS02	63.2	345444.3	619.5	18176.9		299347.5	4644.7	42044.8	6774.3
DSLAG01		188230.2	288.5	9668.6	5.7	159390.2	3225.2	22610.6	4129.9
DSLAG02		130785.6	208.5	6379.9	2.9	110418.0	2245.1	17117.1	3267.9
DSLAG03	2.6	2967.6	4.1	167.7	0.1	2729.4	75.7	541.5	339.3
DSLAG04		33831.0		1681.0		28140.9	606.7	6084.3	1667.7
DSLAG20	10.5	77066.3	125.2	4070.5		66463.7	1220.0	9586.5	1908.8
DSLAG21	10.5	62313.1	111.4	3248.1		53806.0	1018.0	8397.4	1821.4
DSLAG22	15.8	89083.2	161.4	4487.0		76511.5	1286.5	12347.3	2280.6
DSLAG23		81918.2	166.4	4101.8		69378.0	1153.5	11359.8	2150.8
DSMAN02	1.1	517.3	0.6	26.0		582.0	20.5	295.0	249.3
DSMAN04	1.1	1052.8	1.6	57.3		1031.8	25.6	344.0	255.0

SAMPLE	F^- (µM)	Cl^- (µM)	Br^- (µM)	SO_4^{2-} (µM)	Li^+ (µM)	Na^+ (µM)	K^+ (µM)	Mg^{2+} (µM)	Ca^{2+} (µM)
DSMAN05		33248.8	51.3	1698.3	1.3	28211.4	626.1	3986.4	1004.0
DSMAN09	3.2	884.6	6.4	5.7	0.0	1467.2	87.5	1554.8	1390.0
DSWEE01		473.9	0.8	30.2		565.5	35.8	283.9	314.4
DSWEE01 (DUP)		473.9		31.2		565.5	35.8	283.9	314.4
DSWEE02	5.3	471.1		30.2		565.5	35.8	279.8	311.9
DSWEE03		473.9		31.2		565.5	40.9	279.8	311.9
DSWEE04	2.1	479.5		31.2		565.5	38.4	288.0	324.4
DSWEE05	5.3	476.7		33.3		565.5	35.8	292.1	331.9
DSWEE08		547.2	0.6	153.0		782.9	40.9	464.9	499.0
DSWEE09	2.1	476.7		34.4		565.5	35.8	292.1	331.9
DSWEE10	14.7	473.9		51.0		565.5	87.0	234.5	336.8
DSWEE11		473.9	0.4	30.2		565.5	35.8	275.7	306.9
DSWEE12	2.1	465.4		29.1		565.5	35.8	263.3	296.9
DSWEE13		465.4		29.1		565.5	35.8	263.3	296.9
DSWEE14		468.3		28.1		565.5	35.8	267.4	299.4
DSWOL01		366.7		20.8		435.0	28.1	251.0	262.0
DSWOL01 (DUP)		369.5		21.9		435.0	28.1	246.9	259.5
DSWOL02		363.9		21.9		435.0	28.1	234.5	254.5
DSWOL03		366.7		20.8		435.0	28.1	242.7	259.5
DSWOL04		366.7		21.9		435.0	28.1	242.7	257.0
DSWOL06		363.9		20.8		435.0	28.1	238.6	257.0
DSWOL07		363.9		20.8		435.0	28.1	238.6	254.5
DSWOL08		363.9		21.9		435.0	28.1	238.6	254.5
DSWOL09		366.7		21.9		435.0	28.1	246.9	259.5
DWKAH01	1.6	540.5	0.9	42.7		660.7	10.0	379.8	346.1
DWWEE01	1.6	519.0	0.6	27.1		649.4	15.3	436.1	925.7
Kahaluu Headwaters	0.5	394.9		26.0		565.5	25.6	267.4	254.5
Kahaluu Well	1.1	536.0		34.4		826.4	25.6	378.5	366.8
KBRS01		392609.3	584.5	20841.0		345715.5	6675.5	46587.1	5743.8
KS171226		327.2		36.4		369.7	33.2	242.7	376.8

SAMPLE	F^- (µM)	Cl^- (µM)	Br^- (µM)	SO_4^{2-} (µM)	Li^+ (µM)	Na^+ (µM)	K^+ (µM)	Mg^{2+} (µM)	Ca^{2+} (µM)
NCOAST-01		459887.2	590.7	24278.5		407003.0	7826.5	52750.5	6018.3
NCOAST-02		475007.1	772.2	24944.8		419399.7	8107.8	54223.4	6128.1
NCOAST-03	94.7	475684.1	735.9	25164.5		420574.2	8107.8	54478.5	6135.5
NCOAST-04		427672.8	637.0	22647.2		377903.4	7289.4	49878.6	6063.2
TANK 1		2973.2	6.3	117.6		2248.8	636.9	658.3	1020.5
TANK 1 DUP		3227.1	5.0	103.1		2457.6	639.4	613.0	766.0
TANK 2		3207.3	3.8	171.8		2435.8	629.2	613.0	758.5
USCON01		789.8	1.3	87.4		913.4	25.6	411.4	401.7
USCON02		536.0		52.1		696.0	25.6	320.9	366.8
USCON03		733.4	2.5	83.3		782.9	25.6	386.8	394.2
USHAI01		1325.8	2.5	117.6		1435.4	51.2	432.0	641.2
USKAH01		536.0		40.6		652.5	25.6	304.5	326.9
USKAH02		507.8	1.3	40.6		609.0	25.6	267.4	274.5
USKAL01	5.3	648.8	1.3	54.1		869.9	25.6	497.8	596.3
USLAG01		205049.4	287.8	10828.1		181339.7	3478.4	24920.8	3690.3
USLAG01 (DUP)		146685.5	216.5	7653.9		129186.6	2480.9	17465.5	2210.7
USWEE01		479.5		31.2		565.5	25.6	267.4	279.5
USWOL01		366.7		20.8		435.0	25.6	238.6	229.6
Waihee Inclined Wells	1.1	366.7		21.9		478.5	25.6	197.5	192.1
Waihee Tunnel	1.1	451.3		62.5		652.5	25.6	308.6	324.4
WOLAE01		549026.8	796.0	28562.5		483819.1	9412.2	61633.4	6991.4
WOLAE02		549929.5	762.2	28806.1		485298.0	9437.8	61777.4	7126.1
WPKAL01	5.3	1410.4	2.5	216.5		1783.4	76.7	929.8	1033.0
WPKAL03	26.3	122736.2	155.2	6297.4		120878.6	2455.4	14190.5	3944.8
WPKAL04		353370.9	595.7	18896.3		275424.1	5805.9	56745.5	12932.3
WPKAL05		4372.4	6.3	338.3		3697.3	51.2	1867.9	583.9
WPKAS01		189252.5	272.8	9607.9		164767.3	3299.4	23999.2	5921.0
WPKAS02									
WPKAS03	10.5	3695.3		487.2		5741.6	102.3	1682.8	3108.9
WSHAI01	5.3	846.3	2.5	111.4		1000.4	51.2	337.4	541.4

SAMPLE	F^- (µM)	Cl^- (µM)	Br^- (µM)	SO_4^{2-} (µM)	Li^+ (µM)	Na^+ (µM)	K^+ (µM)	Mg^{2+} (µM)	Ca^{2+} (µM)
WSHAI02	5.3	789.8	1.3	90.6		913.4	76.7	419.7	536.5
WSHAI02 (DUP)	5.3	733.4	1.3	86.4		869.9	76.7	403.2	519.0
WSHAI03		424259.5	663.3	22318.2		374554.2	7238.2	49380.8	5733.8
WSKAL01		648.8	1.3	70.8		826.4	25.6	473.2	543.9
WSKAL02	5.3	507.8		46.8		652.5	25.6	308.6	301.9
WSKAS01									
WSKAS02		539830.7	689.6	28252.3		475989.6	9258.8	60798.2	7056.2
WSKAS03									
WSKAS04		538392.1	892.3	28012.8		474945.6	9233.2	60748.8	7008.8
WSMAN01		423.1		26.0		522.0	25.6	263.3	249.5
WSMAN02		358730.6	526.9	19043.1		317746.8	6164.0	42007.8	5037.7
WWFLD01		677.0		46.8		739.5	25.6	345.6	286.9
WWFLD01 (DUP)		677.0	1.3	46.8		739.5	25.6	349.7	289.4
WWHYG01	5.3	761.6	1.3	39.6		1261.4	76.7	395.0	351.8
WWHYG01 (DUP)	5.3	761.6	1.3	39.6		1261.4	76.7	395.0	354.3
WWHYG02	5.3	16135.4	30.0	408.1		8438.5	306.9	3785.2	3835.0
WWJPR01		648.8	1.3	46.8		956.9	25.6	362.1	359.3
WWKAH01		564.2		45.8		696.0		366.2	356.8
WWKAH01 (DUP)		592.4		45.8		696.0		370.3	359.3
WWVOT01		507.8		55.2		609.0		246.9	222.1
WWWTPFC		3244.0		297.7		2696.8	281.3	917.5	1018.0
WWWTPIN		3215.8		242.6		2827.3	306.9	987.5	1048.0
WWWTPSF		2933.7		265.5		2479.3	255.8	872.2	990.6

Table A1.5. Carbonate geochemistry for Chapter 2.

SAMPLE	$\delta^{13}C$ of DIC vs. VPDB (‰)	DIC (µmol kg^{-1})	TA (µmol kg^{-1})
Waihee Tunnel	-23.67151252	628.02	--
Kahaluu Well	-19.42295286	676.06	--
Waihee Inclined Well	--	228.71	--
Kahaluu Headwaters	-15.63489523	518.04	--
DPKAH01	-11.66458169	1147.54	1124.39
DWKAH01	-14.69660273	1721.05	1306.14
DPKAH05	-17.00622758	7673.64	6234.88
DPKAH09	-19.34030684	2798.95	1480.97
DPKAH11	-15.81458081	1481.42	1122.83
DPKAH12	-12.95334506	1120.37	1089.70
DPWEE01	-12.21126027	2019.78	1772.54
DWWEE01	-17.45316561	2937.23	2496.94
DPWEE05	-15.96416946	5497.26	4109.08
DPWEE12	-21.23988554	2382.39	1292.56
DPWOL01	-16.58145518	1699.44	1473.61
DPWOL04	-19.0314412	1515.26	1136.77
DPWOL07	-16.69649038	2066.46	1609.47
DPLAG01	-8.185367459	2066.49	1897.86
DPLAG01 (DUP)	-8.453444652	2059.28	1886.81
DPLAG02	-16.24557076	3884.45	3200.05
DPLAG04	-16.45195753	2459.29	1948.92
DPLAG05	-12.64708809	6815.09	4467.18
DPLAG06	-16.27049009	4503.98	3754.58
DPLAG07	-12.24646814	2999.17	2714.27
DPMAN01	-11.3806142	3526.12	3399.12
DPMAN03	-12.26016063	3168.37	3150.51
DPMAN04	-11.45137491	7716.02	7655.84
DPMAN06	-7.33162261	2126.01	2115.94
DPMAN07	-15.71228769	6672.42	4058.43
DPMAN08	-13.99155938	4464.20	3497.12
DPCON02	-18.64425907	1424.57	1105.36
DPCON03	-18.81342677	3307.76	2160.41
DPCON05	-17.06998466	3335.01	2487.13
WPKAL01	-13.91313135	4032.01	3648.62
WPKAL03	-10.50580669	11914.77	11532.77
WPKAL04	-16.23276012	7725.33	7375.57
WPKAL05	-13.79781061	5252.62	3582.47
WPKAS01	-15.56759159	6050.43	5888.77
WPKAS03	-15.7807289	10132.87	8981.75
WWKAH01	-15.29290597	1732.54	1290.78
WWJPR01	-21.89752394	1732.54	1290.78
WWHYG01	-12.79835892	1813.71	1641.05
WWHYG01 (DUP)	-20.61607861	1861.37	1687.10
WWHYG02	-15.64151304	1580.38	1508.83
WWVOT01	-17.81686398	1701.21	798.09

SAMPLE	$\delta^{13}C$ of DIC vs. VPDB (‰)	DIC (µmol kg^{-1})	TA (µmol kg^{-1})
WWFLD01	-16.75944481	1254.07	1073.46

Table A1.6. H and O isotopes for Chapter 2.

SAMPLE	$\delta^{18}O$ (‰) vs. VSMOW	$\delta^{2}H$ (‰) vs. VSMOW
Waihee Tunnel	-3.20	-9.60
Waihee Inclined	-3.20	-9.50
Kahaluu Head	-3.20	-9.30
Kahaluu Wells	-3.30	-10.10
DPKAH01	-3.20	-10.10
DSKAH01	-3.20	-10.80
DSKAH01DUP	-3.20	-10.20
DWKAH01	-3.00	-10.00
DPKAH05	-2.50	-6.80
DSKAH05	-3.00	-9.70
DSKAH08	-2.60	-8.00
DPKAH09	-3.10	-9.70
DPKAH11	-2.80	-9.10
DSKAH11	-2.70	-8.70
DSKAH12	-3.20	-9.90
DPKAH12	-3.20	-9.80
DPWEE01	-3.10	-9.80
DSWEE01	-3.20	-10.10
DSWEE01DUP	-3.20	-10.10
DWWEE01	-3.10	-9.40
DSWEE02	-3.20	-10.00
DPWEE02	-3.10	-9.80
DSWEE05	-3.20	-10.10
DPWEE05	-2.60	-8.10
DSWEE08	-2.80	-8.50
DSWEE12	-3.20	-10.20
DPWEE12	-3.10	-9.70
DSWOL01	-3.10	-8.70
DSWOL01DUP	-3.10	-8.90
DPWOL01	-3.10	-8.90
DSWOL04	-3.10	-8.90
DPWOL04	-3.10	-8.70
DSWOL07	-3.10	-8.80
DPWOL07	-3.10	-9.50
DSLAG01	-1.80	-5.50

SAMPLE	$\delta^{18}O$ (‰) vs. VSMOW	$\delta^{2}H$ (‰) vs. VSMOW
DPLAG01	-0.80	-0.70
DPLAG01DUP	-0.80	-0.70
DPLAG02	-1.60	-3.80
DPLAG04	-2.50	-6.90
DSLAG04	-2.90	-9.70
DSLAG07	-2.00	-6.20
DPLAG05	-2.30	-6.40
DPLAG06	-1.50	-3.40
DPLAG07	-1.20	-2.30
DPMAN01	-1.00	-1.30
DSMAN02	-3.10	-8.90
DPMAN03	-2.30	-5.50
DSMAN04	-3.10	-8.90
DSMAN05	-2.90	-7.90
DPMAN04	-1.10	-0.90
DPMAN06	-0.50	0.60
DPMAN07	-2.30	-6.00
DPMAN08	-3.00	-8.20
DSMAN09	-1.90	-3.40
DSCON01	-3.20	-10.20
DPCON02	-3.10	-10.20
DSCON03	-2.80	-9.50
DPCON03	-2.90	-9.80
DSCON04	-2.90	-9.60
DPCON05	-2.80	-9.10
DSCON06	-3.00	-9.60
DSCON07	-2.50	-9.00
DSCON08	-2.90	-9.60
DSCON09	-2.70	-9.10
Kahaluu Pond Stream	0.20	1.90
USWOL01	-3.10	-8.60
USKALO1	-2.50	-8.00
USHAI01	-2.90	-10.20
USLAG01	-1.80	-5.30
USLAG01DUP	-2.10	-6.20
USWEE01	-3.20	-10.10
USKAH01	-3.20	-9.70
USCON03	-3.00	-10.10
USCON01	-3.00	-9.90

SAMPLE	$\delta^{18}O$ (‰) vs. VSMOW	$\delta^{2}H$ (‰) vs. VSMOW
USCON02	-3.10	-9.80
USKAH02	-2.90	-9.40
WSKAL01	-2.80	-8.40
WPKAL01	-2.70	-8.10
WSKAL02	-2.90	-9.30
WSHAI01	-2.80	-9.50
NCOAST-01	-0.10	2.20
WPKAL03	-1.80	-4.30
WPKAL04	-0.70	-0.40
NCOAST-02	0.00	2.10
WPKAL05	-2.50	-9.30
NCOAST-03	0.00	2.40
NCOAST-04	-0.40	1.30
WOLAE01	0.40	3.60
WOLAE01 DUP	0.40	3.60
WOLAE02	0.40	3.50
WPKAS01	-1.20	-3.10
WSKAS02	0.60	4.20
WPKAS03	-3.10	-11.40
WSKAS04	0.40	3.60
WSHAI03	-0.30	1.00
WSMAN01	-3.10	-8.50
WSMAN02	-0.70	-0.60
WWKAH01	-2.60	-8.10
WWKAH01 (DUP)	-3.20	-9.80
KBRS01	-0.30	1.50
WSHAI02	-2.70	-7.60
WSHAI02 (DUP)	-2.70	-7.50
WWJPR01	-3.40	-13.10
WWHYG01	-3.40	-12.20
WWHYG01 DUP	-3.40	-12.20
WWHYG02	-2.70	-8.80
WWVOT01	-3.30	-11.50
WWFLD01	-3.30	-11.60
WWFLD01 DUP	-3.30	-11.70

Table A1.7. Boron concentrations and isotopes for Chapter 2.

SAMPLE	$\delta^{11}B$	Concentration (ppb)
DSWEE01	47.3	18
DSWEE01 (DUP)	46.8	18
DSKAH05	45.2	20
DSWEE09	46.6	20
DSWEE10	42.8	21
DSCON03	37.4	23
WSKAL01	37.5	27
DPWEE05	43.2	29
DSKAH11	36.8	31
WWJPR01	32.9	31
DPKAH11	36.8	32
WSHAI01	35.5	32
WPKAL05	27.6	141
WWWTPFC	8.6	178
WOLAE02	39.7	255

Table A1.8. Nitrate stable isotopic composition for Chapter 2.

SAMPLE	$\delta^{15}N$ of NO_3^- vs. AIR (‰)	$\delta^{18}O$ of NO_3^- vs. VSMOW (‰)
Kahaluu Special 10	16.49	8.88
Kahaluu Special 10D	16.27	8.51
Kahaluu Special 7	9.74	3.97
Kahaluu Special 7 DUP	9.63	3.67
Kahaluu Special 5	14.51	8.46
Kahaluu Special 8	9.06	2.73
Kahaluu Special 3	9.89	3.99
Kahaluu Special 1	9.51	3.29
Kahaluu Special 6	9.74	3.80
Kahaluu Special 2	9.14	2.95
Kahaluu Special 4	4.44	1.02
Kahaluu Special 4 DUP	4.55	1.06
Kahaluu Special 11	6.20	1.86
Kahaluu Special 18	11.84	7.34
Kahaluu Special 13	4.80	2.34
Kahaluu Special 15	7.09	4.10
Kahaluu Special 15D	6.97	3.69
Kahaluu Special 12	10.14	6.74
Kahaluu Special 9A	1.51	-1.36
Waihee Inclined Wells	2.39	3.20
Waihee Inclined Wells DUP	2.44	3.35
Waihee Tunnel	1.99	1.26
Waihee Tunnel DUP	1.85	1.37
Kahaluu Well	1.60	0.32
Kahaluu Headwaters	2.23	1.79

SAMPLE	$\delta^{15}N$ of NO_3^- vs. AIR (‰)	$\delta^{18}O$ of NO_3^- vs. VSMOW (‰)
Kahaluu Nuts SG	6.93	5.38
Kahaluu Nuts SG DUP	6.95	5.09
Waihee Nuts SG	6.19	5.73
Waihee Nuts SG DUP	6.21	5.44
Kahaluu SR-05	7.49	6.34
Kahaluu SR-01	8.15	6.50
Kahaluu SR-03	7.81	6.16
Kahaluu SR-04	7.76	5.96
Kahaluu SR-02	7.72	6.04
Kahaluu SR-07	6.44	5.68
Kahaluu SR-07 DUP	6.60	5.94
Kahaluu SR-06	7.02	5.66
Kahaluu SW 170320	7.75	4.54
Kahaluu GW 170320	4.87	4.64
Waihee SW 170320	5.20	3.26
Waihee GW 170320	14.47	12.14
Waihee SR-02	4.69	3.02
Waihee SR-03	3.68	1.65
Waihee SR-04	2.41	0.85
Waihee SR-05	2.52	0.63
Waihee SR-04 DUP	2.77	1.36
DPKAH01	6.62	3.30
DSKAH01	6.94	3.93
DSKAH08	6.19	3.49
DSKAH01 (DUP)	7.22	4.16
DSKAH02	6.87	3.94
DSKAH10	5.84	3.66
DSKAH05	6.44	3.39
DPKAH12	5.17	2.88
DSKAH04	6.66	3.51
DSKAH12	5.24	4.13
DWKAH01	4.89	-0.77
DSKAH03	6.87	3.66
DSKAH06	6.61	3.72
DSKAH07	6.67	2.97
DSKAH11	10.27	5.99
DPKAH11	14.20	8.20
DPKAH05	10.04	2.24
DSWEE12	1.72	0.11
DSWEE14	2.60	1.75
DSWEE14 vial DUP	2.64	1.64
DSWEE13	2.09	0.57
DSWEE01	4.60	2.57
DSWEE09	12.20	5.11
DSWEE11	4.29	2.58
DSWEE03	6.14	4.71

SAMPLE	$\delta^{15}N$ of NO_3^- vs. AIR (‰)	$\delta^{18}O$ of NO_3^- vs. VSMOW (‰)
DPWEE02	4.11	1.09
DSWEE04	6.02	4.49
DSWEE01 (DUP)	4.44	2.66
DSWEE02	6.08	4.54
DSWEE02 vial DUP	6.31	4.32
DPWEE05	22.80	9.43
DSWEE10	9.48	8.99
DSWOL01	2.04	0.84
DSWOL02	0.50	-2.03
DSWOL03	3.28	2.94
DSWOL04	3.22	2.12
DSWOL04 (DUP)	2.89	1.92
DSWOL06	-2.94	-0.63
DSWOL07	4.39	4.11
DSWOL08	2.12	1.11
DSWOL09	3.93	2.89
DPLAG04	6.33	-0.59
DSLAG03	7.03	3.88
DSLAG04	8.09	5.11
DSMAN02	1.74	1.38
DSMAN05	1.94	0.87
DSCON03	8.54	7.26
DPCON02	7.17	5.46
DSCON01	7.21	4.72
WWWTPFC	24.05	5.70
WWWTPSF	26.04	11.84
Kahaluu Fishpond Stream	5.62	2.49
USHAI01	8.81	2.77
USKAL01	4.99	-0.32
USKAH01	7.12	5.28
USLAG01 (DUP)	8.21	5.37
USLAG01	7.11	2.57
USWOL01	2.55	1.09
USWOL01 DUP	3.16	1.32
USWEE01	3.89	2.94
USWEE01 DUP	4.21	3.13
USCON02	11.69	8.35
USCON03	15.11	9.01
USCON03 DUP	14.81	9.19
USKAH02	9.03	7.74
USCON01	10.70	9.63
WSHAI01	7.96	3.35
WSKAL02	5.66	3.95
WPKAL01	17.29	9.51
WSKAL01	7.33	2.09
NCOAST-03	6.61	6.35

SAMPLE	$\delta^{15}N$ of NO_3^- vs. AIR (‰)	$\delta^{18}O$ of NO_3^- vs. VSMOW (‰)
WPKAL05	20.62	11.45
WPKAL05 BOT DUP	20.66	11.78
NCOAST-01	5.66	12.62
WSHAI03	5.91	3.00
WPKAS03	33.26	22.06
WSKAS04	6.29	6.45
WOLAE01	4.05	5.14
WSMAN02	3.39	0.16
WSMAN01	1.61	-0.15
WSHAI02 (DUP)	7.41	4.81
WSHAI02	8.78	7.26
WWKAH01	7.57	5.34
WWKAH01 (DUP)	6.67	3.18
KBRS01	7.48	7.52
KS171226	4.32	2.90
WWVOT01	5.93	3.37
WWJPR01	3.92	0.52
WWJPR01 Bottle DUP	3.51	0.24
WWHYG01	4.41	-0.67
WWHYG01 DUP	4.58	0.02
WWFLD01 DUP	2.90	0.68
WWFLD01	2.89	0.59
Ahuimanu Head 3	0.73	-2.38
Ahuimanu Head 2	0.66	-2.99
Ahuimanu Head 1	0.69	-2.95
Ahuimanu Head 1 DUP	0.55	-2.74

Table A1.9. Mangrove leaf analysis for Chapter 2. Coordinates are UTM Zone 4.

Sample	UTM Easting	UTM Northing	Mass (mg)	µg N	$\delta^{15}N$ (‰ vs. AIR)	µg C	$\delta^{13}C$ (‰ vs. VPDB)
BR01	620176	2373510	2.615	30.8	6	1126.2	-29.5
BR02	620125	2373542	2.4728	37.6	6	1075.1	-29.8
BR03	620105	2373548	2.693	36.2	4.5	1193.6	-32
BR03 DUP	620105	2373548	2.4995	33.2	4.5	1091.8	-32.3
BR04	620082	2373595	2.4236	27.5	6.2	1016.9	-30
BR05	620037	2373653	2.6688	32.2	6.3	1157.6	-29.3
BR06	620006	2373712	2.5385	32.8	5.3	1125.3	-30.2
BR07	619983	2373771	2.6679	22.9	6.1	1161.4	-29
BR08	619965	2373812	2.4614	34.5	5.9	1086.4	-26.8
BR09	619953	2373836	2.5983	33.4	6.7	1208.3	-28.2
BR10	619895	2373900	2.4925	44.6	10	1083.6	-28.3
KO01	619904	2373944	2.5171	34.6	4	1075.3	-30.9
KO02	619879	2373980	2.6683	45.5	4.4	1131.4	-31.9
KO03	619859	2373981	2.6555	31.2	6.1	1035.2	-36.1
KO04	619858	2373977	2.4028	37.9	6.1	935.2	-32.9

Sample	UTM Easting	UTM Northing	Mass (mg)	µg N	$\delta^{15}N$ (‰ vs. AIR)	µg C	$\delta^{13}C$ (‰ vs. VPDB)
KO05	619883	2374010	2.5299	37.2	7	1090.6	-29.6
KO06	619870	2374042	2.5143	44.4	4.4	1087.7	-28.9
KO07	619866	2374063	2.5464	50.7	7	1060.5	-32.3
KO07 DUP	619866	2374063	2.5656	51.8	7	1093.3	-32.3
KO08	619881	2374081	2.6542	22.4	8.8	1158.8	-28.9
KL01	620314	2373032	2.6942	47.3	2.8	1148.4	-35.2
KL02	620321	2373037	2.6061	44.6	0.8	1126	-34.6
KL03	620338	2373035	2.4508	42	4.4	1102.4	-32.7
KL04	620338	2373017	2.5402	39.6	4.7	1030.7	-34.6
KL05	620352	2373043	2.5055	41.8	0.4	1086.2	-32.3
KL05DUP	620352	2373043	2.4879	43	-0.4	1086.7	-32.3
KL06	620365	2373040	2.4117	41.6	1.2	991.9	-34.1
KL07	620386	2373037	2.5809	39.1	5.2	1132.1	-31.4
KL08	620354	2373011	2.4796	25.2	4.7	1094.1	-33
KL09	620349	2373001	2.6366	47.8	1.2	1107.8	-32.5
KL10	620372	2373000	2.6306	32.3	2.7	1012.4	-35.4
KL11	620396	2372990	2.6363	37.9	3.6	1116.1	-31.8
KL12	620378	2372959	2.4974	38.2	4.1	1041.1	-33
KL13	620351	2372982	2.6759	50.3	5	1111.7	-33.6
WM01	619692	2376165	2.4537	27.9	3.9	1091.9	-31.2
WM02	619760	2376192	2.4362	37.5	3.9	1017.6	-31.4
WM03	619760	2376192	2.6208	28	4.5	980.7	-29.5
WM04	619809	2376238	2.5205	33.2	2.8	1007.8	-36.4
WM05	619854	2376267	2.5555	22.3	2.5	1120.3	-30.8
WM06	619887	2376239	2.5098	22.5	4.7	1122.4	-31.3
WM07	619911	2376219	2.6134	33	4.4	1139	-29.9
WM08	619966	2376074	2.4781	27.3	5.5	1025.8	-34.1
WM09	619959	2375983	2.5252	31.3	-6.6	1018.5	-31.5
WM09 DUP	619959	2375983	2.4929	29	-6.2	1021.1	-31.3
WM10	619948	2376006	2.587	25.7	5.1	1120.5	-33.3
WM10 DUP	619948	2376006	2.6237	25.9	5	1137.5	-33.3
WM11	619948	2376006	2.4363	37.9	5.7	937.4	-29.9
WM12	619937	2376073	2.6165	42.5	5.5	1078.4	-34.7
WM13	619865	2376256	2.5287	38.5	1.4	1087.6	-31.9

Table A1.10. Error analysis for Chapter 2.

Parameter	Number of Duplicates	Number of Samples (Excluding Duplicates)	Sample Precision (1 Standard Deviation)
$\delta^{15}N$ of NO_3^- (‰)	26	117	0.32
$\delta^{18}O$ of NO_3^- (‰)	26	117	0.63
$\delta^{2}H$ of Terrestrial Water (‰)	10	99	0.45
$\delta^{18}O$ of Terrestrial Water (‰)	10	99	0.15

Parameter	Number of Duplicates	Number of Samples (Excluding Duplicates)	Sample Precision (1 Standard Deviation)
$\delta^{2}H$ of Precipitation (‰)	19	61	0.39
$\delta^{18}O$ of Precipitation (‰)	19	61	0.12
$\delta^{11}B$ of Boron (‰)	1	14	0.39
Boron (ppb)	1	14	0
$\delta^{13}C$ of DIC (‰)	3	46	0.32
DIC (μmol kg^{-1})	3	46	19.74
TA (μmol kg^{-1})	3	42	19.50
PO_4^{3-} (μM)	14	174	0.76
TP (μM)	13	153	0.11
NH_3 (μM)	14	174	0.56
$NO_3^- + NO_2^-$ (μM)	14	174	1.27
NO_2^- (μM)	12	152	0.07
SiO_2 (μM)	14	174	44.45
TN (μM)	11	138	4.86
F^-	2	59	0
Cl^-	11	129	12514.28
Br^-	9	90	17.74
SO_4^{2-}	11	129	679.82
Li^+	1	18	0.11
Na^+	11	130	11169.51
K^+	10	130	225.14
Mg^{2+}	11	130	1594.42
Ca^{2+}	11	129	320.994
Foliar μg N	5	44	1.304
Foliar $\delta^{15}N$	5	44	0.284
Foliar μg C	5	44	34.26
Foliar $\delta^{15}C$	5	44	0.11
Temperature (°C)	11	166	0.21
SpC. (μS/cm)	12	164	5.11
Salinity	12	165	0.20
pH	12	159	0.20
TDS	12	148	3.48
ODO % Sat	11	163	1.28
ODO (mg L^{-1})	12	147	0.21

APPENDIX 2. Chapter 3 Data

Table A2.1. Locations of precipitation collectors for Chapter 3. Coordinates are UTM Zone 4.

Name	UTM Easting	UTM Northing	Elevation	Distance East
Kamehameha Hwy	621325.18	2373115.337	6	29
Ewa Poamoho	605043.8	2378810.3	378	12629
Ewa Waimano	610052.1	2370110.8	291	10671
Haleiwa Wells	593961	2386342	64	18999
Hauʻula	612189.4	2389866.8	24	683
Hawaiʻi Ag. Center	628196.5332	2362395.892	111	5542
HIG UH Mānoa	622760	2355609	22	14456
Honolulu F.R.	618954.3	2365376.5	188	6882
Hoʻomaluhia B.G.	623417.4	2365502	65	3737
Kahaluʻu Ridge	619516	2371546	100	2323
Kaʻena Point	577713.1	2383944.5	11	34176
Kunia III Wells	601295	2366681	98	20019
Lyon Arboretum	624183	2359481	152.4	10329
Mokuleia F.R.	585481	2383614.8	167	27766
Mokuleia F.R. 2	583448.12	2382782.91	610	29826
Nanakuli F.R.	589089.9	2365462.5	51	32235
Wahiawa B.G.	602113	2378146	307.8	16025
Waiāhole F.R.	616351	2375013	190	3744
Waianae Kai	587480.5	2375569.6	262	30438
Waimea Valley	597896	2392848	4	12234

Table A2.2. Error analysis for Chapter 3.

Parameter	Number of Duplicates	Number of Samples (Excluding Duplicates)	Sample Precision (1 Standard Deviation)
$\delta^{18}O$ of Water (‰)	19	61	0.127
$\delta^{2}H$ of Water (‰)	19	61	0.39
Cl^- (µM)	20	61	25.50
$SO4^-$ (µM)	20	61	1.95
Na^+ (µM)	20	61	32.38
K^+ (µM)	20	61	9.94
Mg^{2+} (µM)	20	61	4.55
Ca^{2+} (µM)	20	61	9.30

Table A2.3. Volume collected during sampling for Chapter 3.

Name	Mar 2017	Apr - Jun 2017	Jul - mid-Aug 2017	Jul (L.A. mid-Aug) - Sep 2017	Oct - late-Nov 2017	Oct (L.A. late Nov) - Dec 2017	Jan - mid-Feb 2018	Jan (L.A. mid-Feb) - Mar 2018
	Vol. (mL)	Vol. (mL)	Vol. (mL)	Vol. (mL)	Vol. (mL)	Vol. (mL)	Vol. (mL)	Vol. (mL)
Ewa Waimano		2320		4445		5650		5790
Hawai‘i Ag. Center		7060		5050		12780		9770
HIG UH Mānoa		2240		912		4940		2895
Honolulu F.R.		3420						
Ho‘omaluhia B.G.		12380		5400		4995		9400
Kahalu‘u Ridge	2840	8010		7200		15890		11405
Ka‘ena Point		2820		1270		2280		6470
Lyon Arboretum		18357	3730	5000	10300	5850	10430	5240
Mokuleia F.R.		2980		2090		4380		1950
Nanakuli F.R.		1410						
Waiāhole F.R.	2495	9940.0		10500		7695		16765
Waianae Kai		2490		3998		3300		
Wahiawa B.G.		4820		3345		4240		3515
Waimea Valley		12755		2580		3340		6275
Kamehameha Hwy.						4850		7390
Kunia III Wells						1175		1690
Haleiwa Wells						845		3080
Mokuleia F.R. 2								3250

Table A2.4. Lyon Arboretum minor intervals common ion concentrations for Chapter 3.

Name	Jul - mid-Aug 2017						Oct - late Nov 2017						Jan mid-Feb 2017					
	Cl^- µM	SO_4^{2-} µM	Na^+ µM	K^+ µM	Mg^{2+} µM	Ca^{2+} µM	Cl^- µM	SO_4^{2-} µM	Na^+ µM	K^+ µM	Mg^{2+} µM	Ca^{2+} µM	Cl^- µM	SO_4^{2-} µM	Na^+ µM	K^+ µM	Mg^{2+} µM	Ca^{2+} µM
Lyon Arb.	225.7	22.9	261.0	0.0	41.1	62.4	245.4	14.6	208.8	0.0	32.9	53.5	220.0	13.5	182.7	0.0	82.3	127.6

Table A2.5. H and O isotopes for Chapter 3, reported against VSMOW. *Denotes samples affected by evaporation due to collector vandalism.

Name	Mar 2017		Apr - Jun 2017		Jul - mid-Aug		Jul (mid-Aug for Lyon) - Sep 2017		Oct - late-Nov 2017		Oct (late Nov for Lyon) - Dec 2017		Jan - mid-Feb 2017		Jan (mid-Feb for Lyon) - Mar 2018	
	$\delta^{18}O$ (‰)	δ^2H (‰)	$\delta^{18}O$ (‰)	δ^2H (‰)	$\delta^{18}O$ (‰)	δ^2H (‰)	$\delta^{18}O$ (‰)	δ^2H (‰)	$\delta^{18}O$ (‰)	δ^2H (‰)	$\delta^{18}O$ (‰)	δ^2H (‰)	$\delta^{18}O$ (‰)	δ^2H (‰)	$\delta^{18}O$ (‰)	δ^2H (‰)
Ewa Waimano			-1.5	-1.5			-2.3	-7.0			-3.6	-13.9			-2.7	-9.2
Ewa Waimano DUP															-2.8	-9.1
Hawai‘i Ag. Center			-2.1	-1.1			-2.0	-4.5			-2.8	-7.7			-2.7	-8.7
Hawai‘i Ag. Center DUP											-2.4	-6.3				
HIG UH Mānoa			-1.5	-2.4			-1.6	-4.0			-3.1	-15.5			-3.4	-14.2
HIG UH Mānoa DUP											-3.4	-16.2				
Honolulu F.R.			-1.8	-2.7												
Ho‘omaluhia B.G.			-1.7	-0.2			-2.2	-5.1			-3.3	-11			-3.0	-10.1
Ho‘omaluhia B.G. DUP											-2.9	-10.1				
Kahalu‘u Ridge	-4.4	-22.4	-2.0	-0.5			-2.3	-6.7			-2.9	-8.5			-3.4	-13.6
Kahalu‘u Ridge DUP											-2.7	-7.9				
Ka‘ena Point			-1.3	-0.2			-3.1	-15.7			-2.2	-5.3			-3.0	-11.3
Ka‘ena Point DUP							-3.1	-15.8			-2	-4.1			-2.9	-11.1

Name	Mar 2017		Apr - Jun 2017		Jul - mid-Aug		Jul (mid-Aug for Lyon) - Sep 2017		Oct - late-Nov 2017		Oct (late Nov for Lyon) - Dec 2017		Jan - mid-Feb 2017		Jan (mid-Feb for Lyon) - Mar 2018	
	$\delta^{18}O$ (‰)	$\delta^{2}H$ (‰)	$\delta^{18}O$ (‰)	$\delta^{2}H$ (‰)	$\delta^{18}O$ (‰)	$\delta^{2}H$ (‰)	$\delta^{18}O$ (‰)	$\delta^{2}H$ (‰)	$\delta^{18}O$ (‰)	$\delta^{2}H$ (‰)	$\delta^{18}O$ (‰)	$\delta^{2}H$ (‰)	$\delta^{18}O$ (‰)	$\delta^{2}H$ (‰)	$\delta^{18}O$ (‰)	$\delta^{2}H$ (‰)
Lyon Arboretum			-1.2	0.7	-2.0	-5.8	-2.0	-4.4	-2.1	-3.5	-3.1	-11	-2.2	-7.8	-1.7	-1.4
Lyon Arboretum DUP			-1.2	1.2			-2.0	-4.3								
Mokuleia F.R.			-2.7	-9.9			-4.1	-19.8			-3.5	-13.9			-3.5	-15.0
Mokuleia F.R. DUP															-3.5	-15.0
Nanakuli F.R.			-2.1	-5.9												
Waiāhole F.R.	-3.4	-13.9	-2.2	-1.1			-2.6	-7.4			-2.5	-4.2			-3.2	-11.5
Waiāhole F.R. DUP											-2.5	-4				
Waianae Kai			-1.7	-4.0			-2.9	-11.0			-2.7	-11.4			1.8*	7.6*
Waianae Kai DUP															1.9*	8.1*
Wahiawa B.G.			-2.1	-5.6			-1.9	-3.1			-3.3	-13			-3.1	-11.5
Wahiawa B.G. DUP							-1.9	-3.1								
Waimea Valley			-1.5	-0.6			-2.3	-9.8			-2.7	-8.1			-2.6	-9.1
Waimea Valley DUP			-1.5	-0.5												
Kamehameha Hwy.											-2.8	-9.4			-3.8	-17.8
Kamehameha Hwy. DUP															-3.9	-18.1
Kunia III Wells											-3.9	-20.9			-3.3	-14.2
Kunia III Wells DUP															-3.3	-14.2
Haleiwa Wells											-4	-22.8			-3.8	-17.7
Haleiwa Wells DUP															-3.8	-17.6
Mokuleia F.R. 2															-3.9	-16.6
Mokuleia F.R. 2 DUP															-4.1	-16.9

Table A2.6. Common ions collected for Chapter 3, first half of the year.

Name	Mar 2017						Apr - Jun 2017						Jul (mid-Aug for Lyon) - Sep 2017					
	Cl^- µM	SO_4^{2-} µM	Na^+ µM	K^+ µM	Mg^{2+} µM	Ca^{2+} µM	Cl^- µM	SO_4^{2-} µM	Na^+ µM	K^+ µM	Mg^{2+} µM	Ca^{2+} µM	Cl^- µM	SO_4^{2-} µM	Na^+ µM	K^+ µM	Mg^{2+} µM	Ca^{2+} µM
Ewa Waimano							310.3	31.2	348.0	0.0	57.6	111.1	225.7	17.7	174.0	0.0	24.7	185.2
Hawai‘i Ag. Center							310.3	33.3	391.5	0.1	57.6	115.2	225.7	12.5	217.5	0.0	28.8	144.0
HIG UH Mānoa							592.4	48.9	652.5	0.1	78.2	279.8	761.6	52.1	739.5	0.1	90.5	526.6
Honolulu F.R.							169.3	13.5	217.5		28.8	86.4						
Ho‘omaluhia B.G.							197.5	17.7	261.0	0.0	41.1	156.4	141.0		130.5	0.0	24.7	148.1
Kahalu‘u Ridge	169.3	18.7	174.0	25.6	24.7	69.9	310.3	13.5	304.5	0.1	32.9	148.1	141.0	12.5	130.5	0.0	32.9	94.6
Ka‘ena Point							733.4	76.0	783.0	0.1	82.3	119.3	1213.0	84.3	1043.9	0.1	127.6	345.6
Ka‘ena Point DUP											0.0	0.0	1213.0	84.3	1043.9	0.1	127.6	341.5
Lyon Arboretum							253.9	21.9	261.0	0.0	53.5	144.0	169.3	12.5	130.5	0.0	24.7	74.06
Lyon Arboretum DUP							197.5	19.8	217.5		53.5	127.6	169.3	13.5	130.5		28.8	90.5
Mokuleia F.R.							169.3	19.8	217.5		37.0	90.5	141.0	15.6	174.0	0.1	32.9	94.6
Nanakuli F.R.							141.0	87.5	174.0	0.0	41.1	111.1						
Waiāhole F.R.	225.7	41.6	261	25.6	41.1	109.8	507.8	16.7	565.5	0.1	49.4	127.6	141.0	10.4	130.5	0.0	24.7	152.2
Waianae Kai							310.3	17.7	348.0	0.1	45.3	107.0	197.5	34.4	174.0	0.0	32.9	189.3

Name	Mar 2017						Apr - Jun 2017						Jul (mid-Aug for Lyon) - Sep 2017					
	Cl^- µM	SO_4^{2-} µM	Na^+ µM	K^+ µM	Mg^{2+} µM	Ca^{2+} µM	Cl^- µM	SO_4^{2-} µM	Na^+ µM	K^+ µM	Mg^{2+} µM	Ca^{2+} µM	Cl^- µM	SO_4^{2-} µM	Na^+ µM	K^+ µM	Mg^{2+} µM	Ca^{2+} µM
Wahiawa B.G.							366.7	34.4	391.5	0.1	53.5	119.3	366.7	32.3	348.0	0.1	65.8	214.0
Wahiawa B.G. DUP													366.7	35.4	391.5	0.1	74.1	189.3
Waimea Valley							282.1	15.6	304.5	0.1	45.3	139.9	282.1	17.7	217.5	0.1	61.7	296.2
Waimea Valley DUP							253.9	9.4	261.0	0.1	37.0	176.9						

Table A2.7. Common ions collected for Chapter 3, second half of the year.

Name	Oct (late Nov for Lyon) - Dec 2017						Jan (mid-Feb for Lyon) - Mar 2018					
	Cl^- µM	SO_4^{2-} µM	Na^+ µM	K^+ µM	Mg^{2+} µM	Ca^{2+} µM	Cl^- µM	SO_4^{2-} µM	Na^+ µM	K^+ µM	Mg^{2+} µM	Ca^{2+} µM
Ewa Waimano	284.9	21.9	278.4	15.3	32.9	34.9	397.7	26.0	334.9	35.8	53.5	122.3
Ewa Waimano DUP							366.7	25.0	304.5	20.5	53.5	117.3
Hawai‘i Ag. Center	268.0	17.7	243.6	10.2	28.8	47.4	293.4	17.7	239.2	17.9	41.1	62.4
Hawai‘i Ag. Center DUP	270.8	19.8	256.6	7.7	28.8	44.9						
HIG UH Mānoa	397.7	30.2	395.8	20.5	49.4	52.4	324.4	20.8	269.7	7.7	32.9	20.0
HIG UH Mānoa	380.8	31.2	382.8	10.2	49.4	54.9						
Ho‘omaluhia B.G.	220.0	19.8	230.5	15.3	28.8	34.9	234.1	14.6	191.4	12.8	32.9	54.9
Ho‘omaluhia B.G. DUP	194.6	18.7	208.8	7.7	24.7	37.4						
Kahalu‘u Ridge	231.3	18.7	243.6	10.2	45.3	34.9	166.4	13.5	139.2	10.2	37.0	39.9
Kahalu‘u Ridge DUP	231.3	17.7	243.6	10.2	45.3	34.9						
Ka‘ena Point	2970.4	158.2	2609.8	110.0	279.8	227.1	617.8	39.6	513.3	30.7	82.3	79.8

Name	Oct (late Nov for Lyon) - Dec 2017						Jan (mid-Feb for Lyon) - Mar 2018					
	Cl^- µM	SO_4^{2-} µM	Na^+ µM	K^+ µM	Mg^{2+} µM	Ca^{2+} µM	Cl^- µM	SO_4^{2-} µM	Na^+ µM	K^+ µM	Mg^{2+} µM	Ca^{2+} µM
Kaʻena Point DUP	2882.9	155.1	2496.7	79.3	263.3	222.1	665.7	41.6	561.1	56.3	82.3	92.3
Lyon Arboretum	268.0	25.0	269.7	10.2	45.3	44.9	431.6	26.0	352.3	10.2	61.7	49.9
Mokuleia F.R.	304.7	18.7	269.7	20.5	45.3	62.4	225.7	13.5	204.4	76.7	61.7	109.8
Mokuleia F.R. DUP	0.0	0.0	0.0	0.0	0.0	0.0	293.4	16.7	278.4	107.4	61.7	129.7
Waiāhole F.R.	296.2	19.8	287.1	17.9	41.1	57.4	256.7	16.7	208.8	10.2	41.1	94.8
Waiāhole F.R. DUP	290.6	18.7	278.4	15.3	37.0	52.4						
Waianae Kai	372.4	22.9	304.5	76.7	41.1	89.8	318.8	27.1	304.5	115.1	86.4	209.6
Waianae Kai DUP							273.6	19.8	208.8	104.9	69.9	209.6
Wahiawa B.G.	454.2	6.2	430.6	99.7	86.4	174.7	234.1	0.0	200.1	35.8	24.7	69.9
Waimea Valley	440.1	23.9	417.6	30.7	90.5	286.9	287.7	13.5	221.8	48.6	49.4	217.1
Kamehameha Hwy.	507.8	34.4	435.0	20.5	45.3	29.9	268.0	19.8	217.5	20.5	24.7	22.5
Kamehameha Hwy. DUP	0.0	0.0	0.0	0.0	0.0	0.0	222.8	17.7	187.0	5.1	20.6	12.5
Kunia III Wells	386.5	45.8	326.2	179.0	53.5	64.9	214.4	23.9	182.7	112.5	53.5	127.3
Kunia III Wells DUP							203.1	23.9	169.6	110.0	53.5	129.7
Haleiwa Wells	1097.3	60.4	1048.3	148.3	115.2	59.9	299.0	11.5	243.6	117.7	53.5	92.3
Haleiwa Wells DUP							335.7	10.4	295.8	143.2	53.5	99.8
Mokuleia F.R. 2							242.6	17.7	200.1	38.4	41.1	67.4
Mokuleia F.R. 2 DUP							237.0	18.7	200.1	38.4	37.0	59.9

Table A2.8 Common ion concentrations and H and O isotopic composition of storm samples for Chapter 3 against VSMOW.

Location	Date	Vol (mL)	$\delta^{18}O$ (‰)	$\delta^{2}H$ (‰)	Cl^- µM	SO_4^{2-} µM	Na^+ µM	K^+ µM	Mg^{2+} µM	Ca^{2+} µM
HIG UH Mānoa	2.6.17	3700	-0.7	2.7	70.5	10.4	56.5	5.1	20.6	34.9
HIG UH Mānoa	2.25.18	8395	-1.9	-5.7	239.8	20.8	213.1	7.7	37.0	20.0
HIG UH Mānoa	3.22.18	1500	-5.2	-29.7	355.4	37.5	326.2	10.2	45.3	22.5
HIG UH Mānoa	3.24.18	1000	-6.3	-40	31.0	19.8	52.2	2.6	12.3	15.0
HIG UH Mānoa	3.24.18 (DUP)	1000	-6.3	-40	28.2	17.7	21.7	2.6	4.1	7.5
HIG UH Mānoa	4.2.18	200	-1.5	0.6						

Table A2.9. Sample precision for each volumetric measurement and propagated for the annual volumetric total. “Prec.” represents calculated sample precision for each sampling window and the annual volumetric total.

Sample Name	Mar 2017 Vol. (mL)	Apr - Jun 2017 Vol. (mL)	Prec.	Jul - mid-Aug 2017 Vol. (mL)	Prec.	Jul - Sep 2017 Vol. (mL)	Prec.	Oct - late-Nov 2017 Vol. (mL)	Prec.	Oct - Dec 2017 Vol. (mL)	Prec.	Jan - mid-Feb 2018 Vol. (mL)	Prec.	Jan - Mar 2018 Vol. (mL)	Prec.	Total Vol. (mL)	Total Prec.
Ewa Waimano		2320	28.3			4445	34.6			5650	34.6			5790	34.6	18205	66.3
Hawai‘i Ag. Center		7060	40.0			5050	34.6			12780	52.9			9770	44.7	34660	87.2
HIG UH Mānoa		2240	28.3			912	20.0			4940	34.6			2895	28.3	10987	56.6
Honolulu F.R.		3420	28.3													3420	28.3
Ho‘omaluhia B.G.		12380	52.9			5400	34.6			4995	34.6			9400	44.7	32175	84.9

Sample Name	Mar 2017 Vol. (mL)	Apr - Jun 2017 Vol. (mL)	Prec.	Jul - mid-Aug 2017 Vol. (mL)	Prec.	Jul - Sep 2017 Vol. (mL)	Prec.	Oct - late-Nov 2017 Vol. (mL)	Prec.	Oct - Dec 2017 Vol. (mL)	Prec.	Jan - mid-Feb 2018 Vol. (mL)	Prec.	Jan - Mar 2018 Vol. (mL)	Prec.	Total Vol. (mL)	Total Prec.
Kahaluʻu Ridge	2840	8010	44.7			7200	40.0			15890	56.6			11405	49.0	45345	95.9
Kaʻena Point		2820	28.3			1270	20.0			2280	28.3			6470	40.0	12840	60.0
Lyon Arboretum		18357	63.2	3730	28.3	5000	34.6	10300	49.0	5850	34.6	10430	49.0	5240	34.6	58907	114.9
Mokuleia F.R.		2980	28.3			2090	28.3			4380	34.6			1950	20.0	11400	56.6
Nanakuli F.R.		1410	20.0													1410	20.0
Waiāhole F.R.	2495	9940	44.7			10500	49.0			7695	40.0			16765	60.0	47395	98.0
Waianae Kai F.R.		2490	28.3			3998	28.3			3300	28.3					9788	49.0
Wahiawa B.G.		4820	34.6			3345	28.3			4240	34.6			3515	28.3	15920	63.2
Waimea Valley		12755	52.9			2580	28.3			3340	28.3			6275	40.0	24950	77.5
Kamehameha Hwy.										4850	34.6			7390	40.0	12240	52.9
Kunia III Wells										1175	20.0			1690	20.0	2865	28.3
Haleiwa Wells										845	20.0			3080	28.3	3925	34.6
Mokuleia F.R. 2											0.0			3250	28.3	3250	28.3

REFERENCES

Abaya, L.M., Wiegner, T.N., Colbert, S.L., Beets, J.P., Carlson, K.M., Kramer, K.L., Most, R., and Couch, C.S., 2018, A multi-indicator approach for identifying shoreline sewage pollution hotspots adjacent to coral reefs: Marine Pollution Bulletin, v. 129, p. 70-80. https://doi.org/10.1016/j.marpolbul.2018.02.005

Adame, M.F., and Lovelock, C.E., 2011, Carbon and nutrient exchange of mangrove forests with the coastal ocean: Hydrobiologia, v. 663, p. 23-50. DOI: 10.1007/s10750-010-0554-7.

Adame, M.F., Virdis, B., and Lovelock, C.E., 2010, Effect of geomorphological setting and rainfall on nutrient exchange in mangroves during tidal inundation: Marine and Freshwater Research, v. 61, p. 1197-1206. DOI: 10.1007/s10750-010-0554-7.

Allen, J.A., 1998, Mangroves as alien species: the case of Hawaii: Global Ecology and Biogeography Letters, v. 7, p. 61-71.

Amato, D.W., Bishop, J.M., Glenn, C.R., Dulai, H., and Smith, C.M., 2016, Impact of submarine groundwater discharge on marine water quality and reef biota of Maui: PLoS ONE, 28 p. DOI: 10.1371/journal.pone.0165825.

Anderson, D.M., Glibert, P.M., and Burkholder, J.M., 2002, Harmful algal blooms and eutrophication: nutrient sources, composition, and consequences: Estuaries, v. 25, p. 704-726.

Aravena, R., Evans, M.L., and Cherry, J.A., 1993, Stable isotopes of oxygen and nitrogen in source identification of nitrate from septic systems: Ground Water, v. 31, p. 180-186.

Babcock Jr., R.W., Lamichhane, K.M., Cummings, M.J., and Cheong, G.H., 2014, Condition assessment survey of onsite sewage disposal systems (OSDSs) in Hawaii: Water Science and Technology, v. 70, p. 1083-1089. DOI: 10.2166/wst.2014.336

Bahr, K.D., Jokiel, P.L., and Toonen, R.J., 2015, The unnatural history of Kāneʻohe Bay: coral reef resilience in the face of centuries of anthropogenic impacts: PeerJ, 26 p. DOI: 10.7717/peerj.950.

Bahr, K.D., Rodgers, K.S., and Jokiel, P. L., 2017, Impact of three bleaching events on the reef resiliency of Kāneʻohe Bay, Hawaiʻi: Frontiers in Marine Science, v. 4, p. 1-13. DOI: 10.3389/fmars.2017.00398

Berner, R.A., 1980, Early Diagenesis: Princeton, Princeton University Press.

Bhavya, P.S., Kumar, S., Gupta, G.V.M., Sudharma, K.V., and Sudheesh, V., 2018, Spatio-temporal variation in d13CDIC of a tropical eutrophic estuary (Cochin estuary, India) and adjacent Arabian Sea: Continental Shelf Research, v. 153, p. 75-85. DOI: https://doi.org/10.1016/j.csr.2017.12.006

Billy, C., Billen, G., Sebilo, M., Birgand, F., and Tournebize, J., 2010, Nitrogen isotopic composition of leached nitrate and soil organic matter as an indicator of denitrification in a sloping drained agricultural plot and adjacent uncultivated riparian buffer strips: Soil Biology and Biochemistry, v. 42, p. 108-117. DOI: 10.1016/j.soilbio.2009.09.026.

Bishop, J.M., Glenn, C.R., Amato, D.W., and Dulai, H., 2017, Effect of land use and groundwater flow path on submarine groundwater discharge nutrient flux: Journal of Hydrology: Regional Studies, v. 11, p 194-218. http://dx.doi.org/10.1016/j.ejrh.2015.10.008.

Blumenstock, D.I., 1961, Climates of Hawaii, in Climates of the States: Washington, D.C., U.S. Department of Commerce.

Boonsong, K., Piyatiratitivorakul, S., and Patanaponpaiboon, P., 2003, Potential use of mangrove plantation as constructed wetland for municipal wastewater treatment: Water Science and Technology, v. 48, p. 257-266.

Bowen, J.L., Kroeger, K.D., Tomasky, G., Pabich, W.J., Cole, M.L., Carmichael, R.H., and Valiela, I., 2007, A review of land-sea coupling by groundwater discharge of nitrogen to New England estuaries: Mechanisms and effects: Applied Geochemistry, v. 22, p. 175-191. DOI:10.1016/j.apgeochem.2006.09.002.

Briand, C., Sebilo, M., Louvat, P., Chesnot, T., Vaury, V., Schneider, M., and Plagnes, V., 2017, Legacy of contaminant N sources to the NO_3^- signature in rivers: a combined isotopic ($\delta^{15}N$-NO_3^-, $\delta^{18}O$-NO_3^-, $\delta^{11}B$) and microbiological investigation: Nature Scientific Reports, p. 1-11. DOI: 10.1038/srep41703.

Bruland, G.L., and MacKenzie, R.A., 2010, Nitrogen source tracking with $d^{15}N$ content of coastal wetland plants in Hawaii: Journal of Environmental Quality, v. 39, p. 409-419. DOI:10.2134/jeq2009.0005.

Bruno, J.F., Petes, L.E., Harvell, C.D., and Hettinger, A., 2003, Nutrient enrichment can increase the severity of coral diseases: Ecology Letters, v. 6, p. 1056-1061. DOI: 10.1046/j.1461-0248.2003.00544.x.

Burnett, W.C., Bokuniewicz, H., Huettel, M., Moore, W.S., and Taniguchi, M., 2003, Groundwater and pore water inputs to the coastal zone: Biogeochemistry, v. 66, p. 3-33.

Cesar, H., and van Beukering, P.J.H., 2004, Economic valuation of the coral reefs of Hawaii: Pacific Science, v. 28, p. 231-242.

Chu, P-S., Nash, A.J., and Porter, F-Y., 1993, Diagnostic studies of two contrasting rainfall episodes in Hawaii: Dry 1981 and wet 1982: Journal of Climate, v. 6, 1457-1462.

Clague, D.A., and Sherrod, D.R., 2014, Growth and degradation of Hawaiian volcanoes, in Characteristics of Hawaiian Volcanoes, Poland et al. (Eds.), US Geological Survey Professional Paper 1801, p. 97-146.

Clark, I., and Fritz, P., 1997, Environmental Isotopes in Hydrogeology: New York, CRC Press.

Conley, D.J., Paerl, H.W., Howarth, R.W., Boesch, D.F., Seitzinger, S.P., Havens, K.E., Lancelot, C., and Likens, G.E., 2009, Controlling eutrophication: nitrogen and phosphorus: Science, v. 323, p. 1014-1025.

Cox, D.C., 1954, Notes: Research in ground-water hydrology in Hawaii: Journal Series of the Experiment Station, Hawaiian Sugar Planters' Association, 4 p.

Craig, H., 1961, Isotopic variations in meteoric waters: Science, v. 133, p. 1702–1703.

Dailer, M.L., Knox, R.S., Smith, J.E., Napier, M., and Smith, C.M., 2010, Using $\delta^{15}N$ values in algal tissue to map locations and potential sources of anthropogenic nutrient inputs on the island of Maui, Hawaii, USA: Marine Pollution Bulletin, v. 60, p. 655-671. doi:10.1016/j.marpolbul.2009.12.021

Dansgaard, W., 1964, Stable isotopes in precipitation: Tellus, v. 4, p. 1-33.

Davis, S.E., Childers, D.L., Day Jr., J.W., Rudnick, D.T., and Sklar, F.H., 2003, Factors affecting the concentration and flux of materials in two southern Everglades mangrove wetlands: Marine Ecology Progress Series, v. 253, p. 85-96.

Dawes, L., and Goonetilleke, A., 2003, An investigation into the role of site and soil characteristics in onsite sewage treatment: Environmental Geology, v. 44. P. 467-477.

De Carlo, E.H., Hoover, D.J., Young, C.W., Hoover, R.S., and Mackenzie, F.T., 2007, Impact of storm runoff from tropical watersheds on coastal water quality and productivity: Applied Geochemistry, v. 22, p. 1777-1797. DOI:10.1016/j.apgeochem.2007.03.034.

Deenik, J., 2008, Anammox activity and nitrogen dynamics in flooded taro soils of Hawaii: United States Department of Agriculture Research, Education, and Economics Information System. Online at: https://portal.nifa.usda.gov/web/crisprojectpages/0214753-anammox-activity-and-nitrogen-dynamics-in-flooded-taro-soils-of-hawaii.html

Demopoulos, A.W.J., and Smith, C.R., 2010, Invasive mangroves alter macrofaunal community structure and facilitate opportunistic exotics: Marine Ecology Progress Series, v. 404, p. 51-67. DOI: 10.3354/meps08483.

Ding, J., Xi, B., Gau, R., He, L., Liu, H., Dai, X., and Yu, Y., 2014, Identifying diffused nitrate sources in a stream in an agricultural field using a dual isotopic approach: Science of the Total Environment, v. 484, p. 10-18.

Dore, J.E., Lukas, R., Sadler, D.W., Church, M.J., and Karl, D.M., 2009, Physical and biogeochemical modulation of ocean acidification in the central North Pacific: Proceedings of the National Academy of Sciences, v. 106, p. 12235-12240. DOI: www.pnas.org_cgi_doi_10.1073_pnas.0906044106

Dulai, H., Kleven, A., Ruttenberg, K., Briggs, R., and Thomas, F., 2016, Evaluation of submarine groundwater discharge as coastal nutrient source and its role in coastal groundwater quality and quantity, in Fares, A., ed., Emerging issues in groundwater resources: Switzerland, Spring International Publishing, 39 p.

Earth Justice, July 14, 2006, https://earthjustice.org/news/press/2006/hawai-i-water-commission-splits-over-waiahole-water-case.

Englund, R.A., Preston, D.J., Wolff, R., Coles, S.L., Eldredge, L.G., and Arakaki, K., 2000, Biodiversity of freshwater and estuarine communities in Lower Pearl Harbor, O'ahu, Hawaii with observations on introduced species, Final Report, prepared for the U.S. Navy, Hawaii Biological Survey, Bishop Museum Technical Report No. 16.

Fabricius, K.E., 2005, Effects of terrestrial runoff on the ecology of corals and coral reefs: review and synthesis: Marine Pollution Bulletin, v. 50, p. 125-146. DOI: 10.1016/j.marpolbul.2004.11.028.

Fackrell, J.K., 2016, Geochemical evolution of Hawaiian groundwater [Ph.D. thesis]:Honolulu, University of Hawai'i at Mānoa.

Fackrell, J.K., Glenn, C.R., Popp, B.N., Whittier, R.B., and Dulai, H., 2016, Wastewater injection, aquifer biogeochemical reactions, and resultant groundwater N fluxes to coastal waters: Kā'anapali, Maui, Hawai'i: Marine Pollution Bulletin, v. 110, p. 281-292. DOI: http://dx.doi.org/10.1016/j.marpolbul.2016.06.050

Froelich, P.N., Klinkhammer, G.P., Bender, M.L., Luedtke, N.A., Heath, G.R., Cullen, D., Dauphin, P., Hammond, D., Hartman, B., and Maynard, V., 1979, Early oxidation of organic matter in pelagic sediments of the eastern equatorial Atlantic: suboxic diagenesis: Geochimica et Cosmochimica Acta, v. 43, p. 1075-1090.

Fry, B., Bern, A.L., Ross, M.S., and Meeder, J.F., 2000, $\delta^{15}N$ studies of nitrogen use by the red mangrove, Rhizophora mangle L. in South Florida: Estuarine, Coastal, and Shelf Science, v. 50, p. 291-296. DOI: 10.1006/ecss.1999.0558.

Fujita, M., Suzuki, J., Sato, D., Kuwahara, Y., Yokoki, H., and Kayanne, H., 2013, Anthropogenic impacts on water quality of the lagoonal coast of Fongafale Islet, Funafuti Atoll, Tuvalu: Sustainable Science, v. 3, p. 381-390. DOI: 10.1007/s11625-013-0204-x

Garrison, G.H., Glenn, C.R., and McMurtry, G.M., 2003, Measurement of submarine groundwater discharge in Kahana Bay, O'ahu, Hawai'i: Limnology and Oceanography, v. 48, p. 920-928.

Giambelluca, T.W., Chen, Q., Frazier, A.G., Price, J.P., Chen, Y.-L., Chu, P.-S., Eischeid, J.K., and Delparte, D.M., 2013, Online Rainfall Atlas of Hawai'i: Bull. Amer. Meteor. Soc., v. 94, p. 313-316. DOI: 10.1175/BAMS-D-11-00228.1

Giambelluca, T.W., and Sanderson, M., 1993, The water balance and climatic classification, in Sanderson, M. ed., Prevailing Trade Winds: Weather and Climate in Hawai‘i: Honolulu, University of Hawaii Press, p. 56-72.

Giblin, A.E., and Gaines, A.G., 1990, Nitrogen inputs to a marine embayment: the importance of groundwater: Biogeochemistry, v. 10, p. 309-328.

Gilman, E.L., Ellison, J., Jungblut, V., Lavieren, H.V., Wilson, L., Areki, F., Brighouse, G., Bungitak, J., Dus, E., Henry, M., Kilman, M., Matthews, E., Sauni, I., Teriki-Ruatu, N., Tukia, S., and Yuknavage, K., 2006, Adapting to Pacific Island mangrove responses to sea level rise and climate change. Climate Research, v. 32, p. 161-176.

Gingerich, S.B., and Oki, D.S., 2000, Ground Water in Hawaii: U.S. Geological Survey, 6 p.

Glenn, C.R., Whittier, R.B., Dailer, M.L., Dulaiova, H., El-Kadi, A.I., Fackrell, J., Kelly, J.L., and Waters, C.A., 2012. Lahaina Groundwater Tracer Study – Lahaina, Maui, Hawaii, Interim Report, prepared for the State of Hawaii Department of Health, the U.S. Environmental Protection Agency, and the U.S. Army Engineer Research and Development Center.

Glenn, C.R., Whittier, R.B., Dailer, M.L., Dulaiova, H., El-Kadi, A.I., Fackrell, J., Kelly, J.L., Waters, C.A., and Sevadjian, J., 2013. Lahaina Groundwater Tracer Study – Lahaina, Maui, Hawaii, Final Report, prepared for the State of Hawaii Department of Health, the U.S. Environmental Protection Agency, and the U.S. Army Engineer Research and Development Center.

GWP Consultants, 2007, Integrated water resources management in Pacific island countries: a synopsis, 52 p.

Hartley, T.M., and Chen, Y-L., 2010, Characteristics of summer trade wind rainfall over Oahu: Weather and Forecasting, v. 25, p. 1797-1815. DOI: 10.1175/2010WAF2222328.1

Hawai‘i State Department of Health, 2018. Report to the Twenty-Ninth Legislature, Relating to Cesspools and Prioritization for Replacement. Online. https://health.hawaii.gov/opppd/files/2017/12/Act-125-HB1244-HD1-SD3-CD1-29th-Legislature-Cesspool-Report.pdf.

He, L., and Pacific Climate Team, 2015, ENSO and Season Rainfall Variability over the Hawaiian and US-affiliated Pacific Islands: Science and Technology Infusion Climate Bulletin, p. 89-92.

Hem, J.D., 1985, Study and interpretation of the chemical characteristics of natural water: U.S. Geological Survey Water-Supply Paper 2254, 263 p.

Hirashima, G.T., 1971, Tunnels and dikes of the Ko‘olau Range, O‘ahu, Hawai‘i, and their effect on storage depletion and movement of ground water: Geological Survey Water-Supply Paper 1999-M, 25 p.

Hoover, D.J., 2002, Fluvial nitrogen and phosphorous in Hawaii: storm runoff, land use, and impacts on coastal waters [Ph.D. dissertation]: Mānoa, University of Hawai‘i.

Hoover, D.J., and Mackenzie, F.T., 2009, Fluvial fluxes of water suspended particulate matter, and nutrients and potential impacts on tropical coastal water biogeochemistry: Oahu, Hawai‘i, Aquatic Geochemistry, v. 15, p. 547-570. DOI: 10.1007/s10498-009-9067-2.

Hufen, T.H., Eyre, P.E., and McConachie, W., 1980, Underground residence times and chemical quality of basal groundwater in Pearl Harbor and Honolulu aquifers, Oahu, Hawaii: University of Hawaii Water Resources Research Center Technical Report No. 129, 75 p.

Hunt, C.D., 1996, Geohydrology of the island of O‘ahu, Hawaii, Regional Aquifer-System Analysis: U.S. Geological Survey Professional Paper 1412-B, 63 p.

Hunt, C.D., 2004, Ground-water quality and its relation to land use on Oahu, Hawaii, 2000-01: Water-Resources Investigations Report 03-4305, 67 p.

Hunt, C.D. and Rosa S.N., 2009. A multitracer approach to detecting wastewater plumes at Kihei and Lahaina, Maui, Hawaii: U.S. Geological Survey Scientific Investigations Report 2009-5253, 166 p.

Hunter, C.L., and Evans, C.W., 1995, Coral Reefs in Kāne‘ohe Bay: Two centuries of western influence and two decades of data: Bulletin of Marine Sciences, v. 57, p. 501-515.

Jaeschke, J.B., Scholl, M.A., Cozzarelli, I.M., Masoner, J.R., Christenson, Scott, and Qi, Haiping, 2011, Stable-isotope ratios of hydrogen and oxygen in precipitation at Norman, Oklahoma, 1996–2008: U.S. Geological Survey Scientific Investigations Report, 2011–5262, 22 p.

Johannes, R.E., 1980, The ecological significance of the submarine discharge of groundwater: Marine Ecology, v. 3, p. 365-373.

Johannes, R.E., and Hearn, C.J., 1985, The effect of submarine groundwater discharge on nutrient and salinity regimes in a coastal lagoon off Perth, Western Australia: Estuarine, Coastal and Shelf Science, v. 21, p. 789-800.

Johnson, A.G., Glenn, C.R., Burnett, W.C., Peterson, R.N., and Lucey, P.G., 2008, Aerial infrared imaging reveals large nutrient-rich groundwater inputs to the ocean: Geophysical Research Letters, v. 35, p. 1-15. DOI: 10.1029/2008GL034574.

Kelly, JL., 2012, Identification and quantification of submarine groundwater discharge in the Hawaiian Islands [Ph.D. dissertation]: Mānoa, University of Hawai‘i.

Kelly, J.L., Glenn, C.R, and Lucey, P.G., 2013. High-resolution aerial infrared mapping of groundwater discharge to the coastal ocean: Limnology and Oceanography: Methods, v. 11, p. 262-277.

Kendall, C., Elliott, E.M., and Wankel, S.D., 2007, Tracing anthropogenic inputs of nitrogen to ecosystems, in Stable Isotopes in Ecology and Environmental Science: Blackwell Publishing Ltd, Oxford, UK., p. 375-449.

Kendall, C., and McDonnell, J.J., 1998, Tracing nitrogen sources and cycling in catchments, in Isotope Tracers in Catchment Hydrology: Amsterdam, Elsevier Science B.V., p. 519-576.

Kellman, L.M., and Hillaire-Marcel, C., 2003, Evaluation of nitrogen isotopes as indicators of nitrate contamination sources in an agricultural watershed: Agriculture, Ecosystems, and Environment, v. 95, p. 87-102. PII: S0167-8809(02)00168-8.

Kim, G., and Swarzenski, P.W., 2010, Submarine ground-water discharge (SGD) and associated nutrient fluxes to the coastal ocean, in Liu, K.-K., Atkinson, L., Quinones, R., and Talaue-McManus, L., eds., Carbon and Nutrient Fluxes in Continental Margins: A Global Synthesis: New York, Springer-Verlag, p. 529-538.

Knee, K.L., Layton, B.A., Street, J.H., Boehm, A.B., and Paytan, A., 2008. Sources of nutrients and fecal indicator bacteria to nearshore waters on the north shore of Kaua‘i (Hawai‘i, USA): Estuaries and Coasts 31, 607–622. DOI: 10.1007/s12237-008-9055-6.

Knee, K.L, R. Gossett, A.B. Boehm, and Paytan, A., 2010a, Caffeine and agricultural pesticide concentrations in surface water and groundwater on the north shore of Kaua‘i (Hawai‘i, USA): Marine Pollution Bulletin 60, 1376-1382. DOI:10.1016/j.marpolbul.2010.04.019.

Knee, K.L., Street, J.H., Grossman, E.E., Boehm, A.B., and Paytan, A., 2010b, Nutrient inputs to the coastal ocean from submarine groundwater discharge in a groundwater dominated system: relation to land use (Kona Coast, Hawai’i, USA): Limnology and Oceanography 55, 1105–1122. DOI:10.4319/lo.2010.55.3.1105.

Kroeger, K.D., and Charette, M.A., 2008, Nitrogen biogeochemistry of submarine groundwater discharge: Limnology and Oceanography, v. 53, p. 1025-1039.

Leopold, L.B., 1949, The interaction of trade wind and sea breeze, Hawaii: Journal of Meteorology, v. 6, p. 312-320.

Libes, S., 2009, Introduction to Marine Biogeochemistry: San Diego, Academic Press.

Liu, C.Q., Li, S.L., Lang, Y.C., and Xiao, H.Y., 2006, Using δ15N- δ18O- values to identify nitrate sources in karst ground water, Guiyang, Southwest China: Environmental Science and Technology, v. 40, p. 6928-6933.

Lusk, M.G., Toor, G.S., Yang, Y.Y., Mechtensimer, S., De, M., and Obreza, T.A., 2017, A review of the fate and transport of nitrogen, phosphorus, pathogens, and trace organic chemicals in septic systems: Critical Reviews in Environmental Science and Technology, v. 47, p. 455-541. DOI: 10.1080/10643389.2017.1327787

Lyons, S.W., 1982, Empirical orthogonal function analysis of Hawaiian rainfall: Journal of Applied Meteorology, v. 21, p. 1713-1729.

Maher, D.T., Santos, I.R., Golsby-Smith, L., Gleeson, J., and Eyre, B.D., 2013, Groundwater-derived dissolved inorganic and organic carbon exports from a mangrove tidal creek: The missing mangrove carbon sink?: Limnology and Oceanography, v. 58, p. 475-488. DOI:10.4319/lo.2013.58.2.0475.

Manahan, S.E., 2010, Environmental Geochemistry, 9th Edition: Boca Raton, Taylor & Francis Group.

Mayor, J.R., Wright, S.J., Schuur, E.A.G., Brooks, M.E., and Turner, B.L., 2014, Stable nitrogen isotope patterns of trees and soils altered by long-term nitrogen and phosphorus addition to a lowland tropical rainforest: Biogeochemistry, v. 119, p. 293-306. DOI 10.1007/s10533-014-9966-1.

Macdonald, G.A., Abbott, A.T., and Peterson, F.L., 1983, Volcanoes in the Sea, 2nd Edition: Honolulu, University of Hawaii Press.

McDougall, I., 1985, Age and evolution of the volcanoes of Tutuila, American Samoa: Pacific Science, v. 39, p. 311–320.

Miller, J.A., Whitehead, R.L., Gingerich, S.B., Oki, D.S., and Olcott, P.G., 1999, Ground water atlas of the United States, Segment 13, 36 p.

Mink, J.F., 1960, Distribution pattern of rainfall in the leeward Koolau Mountains, Oahu, Hawaii: Journal of Geophysical Research, v. 65, p. 2869-2876.

Moore, J.G., 1964, Giant submarine landslides on the Hawaiian ridge: U.S. Geological Survey Professional Paper 501-D, p. 95- 98.

Moore, J.G., and Clague D.A., 2002, Mapping the Nuuanu and Wailau Landslides in Hawaii. In: Takahashi E, Lipman PW, Garcia MO, Naka J, Aramaki S (Eds) Hawaiian Volcanoes: Deep Underwater Perspectives, Am. Geophys. Union Monogr. 128, p. 223-244.

Moore, W.S., 2010, The effect of submarine groundwater discharge on the ocean: Annual Review of Marine Science, v. 2, p. 59-88. DOI: 10.1146/annurev-marine-120308-081019

Moosdorf, N., Stieglitz, T., Waska, H., Durr, H.H., and Hartmann, J., 2015, Submarine groundwater discharge from tropical islands: a review: Grundwasser, v. 20, p. 53-67. DOI: 10.1007/s00767-014-0275-3.

Nascimento, C., Atekwana, A., and Krishnamurthy, R.V., 1997, Concentrations and isotope ratios of dissolved inorganic carbon in denitrifying environments: Geophysical Research Letters, v. 24, p. 1511-1514.

Neal, V.E., and Trewick, S.A., 2008, The age and origin of the Pacific islands: a geological review: Philosophical Transactions of the Royal Society B, v. 363, p. 3293-3308. DOI:10.1098/rstb.2008.0119

Nichols, W.D., Shade, P.J., and Hunt, C.D., 1996, Summary of the Oahu, Hawaii regional aquifer-system analysis: U.S. Geological Survey Professional Paper 1412-A, 61 p.

Norton, C.W., Chu, P-S., and Schroeder, T.A., 2011, Projecting changes in future heavy rainfall events for Oahu, Hawaii: A statistical downscaling approach: Journal of Geophysical Research, v. 116, p. 1-9. DOI:10.1029/2011JD015641

O'Connor, C.F., Chu, P.S., Hsu, P.C., and Kodama, K., 2015, Variability of Hawaiian winter rainfall during La Nina event since 1956: American Meteorological Society, v. 28, p. 7809-7823. DOI: 10.1175/JCLI-D-14-00638.1

Ouyang, X., and Guo, F., 2016, Paradigms of mangroves in treatment of anthropogenic wastewater pollution: Science of the Total Environment, v. 544. P. 971-979. DOI: http://dx.doi.org/10.1016/j.scitotenv.2015.12.013

Owor, M., Taylor, R.G., Tindimugaya, C., and Mwesigwa, D., 2009, Rainfall intensity and groundwater recharge: empirical evidence form the Upper Nile Basin: Environmental Research Letters, v. 4, p. 1-6. DOI:10.1088/1748-9326/4/3/035009

Pastorok, R.A. and Bilyard, G.R., 1985, Effects of sewage pollution on coral-reef communities. Marine Ecology Progress Series, 21, p. 175-189.

Paytan, A., Shellenbarger, G.G., Street, J.H., Gonneea, M.E., Davis, K., Young, M.B., and Moore, W.S., 2006, Submarine groundwater discharge: An important source of inorganic nitrogen to coral reef ecosystems, Limnology and Oceanography, v. 51, p. 343-348.

Penton, C.R., Deenik, J.L., Popp, B.N., Bruland, G.L., Engstrom, P., Mueller, J., Worden, A., and Tiedje, J.M., 2014, Assessing nitrogen transformations in a flooded agroecosystem using the isotope pairing technique and nitrogen functional gene abundances: Soil Science, v. 179, p. 1-10. DOI: 10.1097/SS.0000000000000038

Penton, C.R., Deenik, J.L., Popp, B.N., Bruland, G.L., Engstrom, P., St. Louis, D., and Tiedje, J., 2012, Importance of sub-surface rhizosphere-mediated coupled nitrification-denitrification in a flood agroecosystem in Hawaii: Soil Biology and Biochemistry, v. 57, p. 362-373. DOI: http://dx.doi.org/10.1016/j.soilbio.2012.10.018

Peterson, F.L., 1972, Water development of tropic volcanic islands – type example: Hawaii: Groundwater, v. 10, p. 18-23. DOI: 10.1111/j.1745-6584.1972.tb03586.x

Prouty, N.G., Cohen, A., Yates, K.K., Storlazzi, C.D., Swarzenski, P.W., and White, D., 2017, vulnerability of coral reefs to bioerosion from land-based sources of pollution: Journal of Geophysical Research: Oceans, 32 p. DOI: 10.1002/2017JC013264.

Presley, T.K., Sinton, J.M., and Pringle, M., 1997, Postshield volcanism and catastrophic mass wasting of the Waianae Volcano, Oahu, Hawaii: Bulletin of Volcanology, v. 58, p. 597-616.

Quay, P., Sonnerup, R., Westby, T., Stutsman, J., and McNichol, A., 2003, Changes in the $^{13}C/^{12}C$ of dissolved inorganic carbon in the ocean as a tracer of anthropogenic CO_2 uptake: Global Biogeochemical Cycles, v. 17, p. 1-20. DOI:10.1029/2001GB001817

Redding, J.E., Myers-Miller, R.L., Baker, D.M., Fogel, M., Raymundo, L.J., and Kim, K., 2013, Link between sewage-derived nitrogen pollution and coral disease severity in Guam: Marine Pollution Bulletin, v. 73, p. 57-63. http://dx.doi.org/10.1016/j.marpolbul.2013.06.002.

Reef, R., Feller, I.C., and Lovelock, C.E., 2010, Nutrition of mangroves: Tree Physiology, v. 30, p. 1148-1160. DOI:10.1093/treephys/tpq048.

Reppun, F., 2016, Invasive marine algae as a soil amendment for island farmers: agronomic and ethnographic assessment of implications for nutrient management [M.S. thesis]: Columbus, Ohio State University.

Rhodes, A.L., Guswa, A.J., and Newell, S.E., 2006, Seasonal variation in the stable isotopic composition of precipitation in the tropical montane forests of Monteverde, Costa Rica: Water Resources Research, v. 42, 17 p.

Richardson, C.M., Dulai, H., and Whittier, R.B., 2017, Sources and spatial variability of groundwater-derived nutrients in Maunalua Bay, Oʻahu, Hawaiʻi: Journal of Hydrology: Regional Studies, 16 p. http://dx.doi.org/10.1016/j.ejrh.2015.11.006.

Riehl, H., 1949, Some aspects of Hawaiian rainfall, Bulletin of the American Meteorological Society, v. 30, p. 176-187.

Rodellas, V., Garcia-Orellana, J., Masqué, P., Feldman, M., and Weinstein, Y., 2015, Submarine groundwater discharge as a major source of nutrients to the Mediterranean Sea: Proceedings of the National Academy of Sciences, v. 112, p. 3926-3930. DOI: www.pnas.org/cgi/doi/10.1073/pnas.1419049112.

Rouse, J.D., 2013, Sustainability of wastewater treatment and excess sludge handling practices in the Federated States of Micronesia: Sustainability, v. 5, p. 4183-4194. DOI: 10.3390/su5104183

Sadat-Noori, M., Santos, I.R., Tait, D., and Maher, D.T., 2016, Fresh meteoric versus recirculated saline groundwater nutrient inputs into a subtropical estuary: Science of the Total Environment, 14 p. http://dx.doi.org/10.1016/j.scitotenv.2016.06.008.

Sanders, C.J., Eyre, B.D., Santos, I.R., Machado, W., Luiz-Silva, W., Smoak, J.M., Breithaupt, J.L., Ketterer, M.E., Sanders, L., Marotta, H., and Silva-Filho, E., 2014, Elevated rates of organic carbon, nitrogen, and phosphorous accumulation in a highly impacted mangrove wetland: Geophysical Research Letters, p. 2475-2480. DOI: 10.1002/2014GL059789.

Satake, K., Smith, J.R., and Shinozaki, K., 2002, Volume estimate and tsunami modeling for the Nuuanu and Wailau landslides, In: Takahashi E, Lipman PW, Garcia MO, Naka J, Aramaki S (Eds) Hawaiian Volcanoes: Deep Underwater Perspectives, Am Geophys. Union Monogr. 128, p. 333-348.

Scholl, M.A., Giambelluca, T.W., Gingerich, S.B., Nullet, M.A., and Loope, L.L., 2007, Cloud water in windward and leeward mountain forests: the stable isotope signature of orographic cloud water: Water Resources Research, v. 43, p. 1-13. DOI: 10.1029/2007WR006011

Scholl, M.A., Gingerich, S.B., and Tribble, G.W., 2002, The influence of microclimates and fog on stable isotope signatures used in interpretation of regional hydrology: East Maui, Hawaii: Journal of Hydrology, v. 264, p. 170-184.

Scholl, M.A., Ingebritsen, S.E., Janik, C.J., and Kauahikaua, J.P., 1996, Use of precipitation and groundwater isotopes to interpret regional hydrology on a tropical volcanic island: Kilauea volcano area, Hawaii: Water Resources Research, v. 32, p. 3325-3357.

Scholl, M.A., and Murphy, S.F., 2014, Precipitation isotopes link regional climate patterns to water supply in a tropical mountain forest, eastern Puerto Rico: Water Resources Research, v. 50, p. 4305-4322. DOI: 10.1002/2013WR014413

Scholl, M.A., Shanley, J.B. Murphy, S.F., Willenbring, J.K., Occhi, M., and González, G., 2015, Stable-isotope and solute-chemistry approaches to flow characterization in a forested tropical watershed, Luquillo Mountains, Puerto Rico: Applied Geochemistry, v. 63, p. 484-497. http://dx.doi.org/10.1016/j.apgeochem.2015.03.008

Schroeder, T. 1993, Climate Controls, in Sanderson, M. ed., Prevailing Trade Winds: Weather and Climate in Hawai‘i: Honolulu, University of Hawaii Press, p. 12-36.

Sebilo, M., Billen, G., Grably, M., and Mariotti, A., 2003, Isotopic composition of nitrate-nitrogen as a marker of riparian and benthic denitrification at the scale of the whole Seine River system: Biogeochemistry, v. 63, p. 35-51.

Seiler, R.L., 2005, Combined use of ^{15}N and ^{18}O of nitrate and ^{11}B to evaluate nitrate contamination in groundwater: Applied Geochemistry, v. 20, p. 1626-1636.

Shade, P.J., and Nichols, W.D., 1996, Water budget and effects of land-use changes on Groundwater recharge, Oahu, Hawaii: U.S. Geological Survey Professional Paper 1412-C, 48 p.

Shuler, C.K, El-Kadi, A.I., Dulai, H., Glenn, C.R., and Fackrell, J., 2017, Source partitioning of anthropogenic groundwater nitrogen in a mixed-use landscape, Tutuila, American Samoa: Hydrogeology Journal, v. 25, p. 2419-2434. DOI:10.1007/s10040-017-1617-x

Sigman, D.M., Casciotti, K.L., Andreani, M., Barford, C., Galanter, M., and Böhlke, J.K., 2001, A bacterial method for the nitrogen isotopic analysis of nitrate in seawater and freshwater: Analytical Chemistry v. 73, p. 4145-4153.

Simpson, R.H., 1951, Evolution of the Kona storm, a subtropical cyclone: Journal of Meteorology, v. 9, p. 24-35.

Slomp, C.P., and Van Cappellen, P., 2004, Nutrient inputs to the coastal ocean through submarine groundwater discharge: controls and potential impact: Journal of Hydrology, v. 295, p. 64-86. DOI:10.1016/j.jhydrol.2004.02.018

Smith, S.V., Kimmerer, W.J., Laws, E.A., Brock, R.E., and Walsh, T.W., 1981, Kaneohe Bay sewage diversion experiment: perspectives on ecosystem responses to nutritional perturbation: Pacific Science, v. 35, p. 279-395.

Spalding, M., Kainuma, M., and Collins, L, 2010, World Atlas of Mangroves. Earthscan Publ., London, 319p.

Stearns, H.T., and Vaksvik, K.N., 1935, Geology and Groundwater resources of the island of Oahu, Hawaii: Waikuku, Maui Publishing Company, 536 p.

Stearns, H.T., 1944, Geology of the Samoan Islands: Geological Society of America Bulletin, v. 55, p. 1279–1332. DOI:10.1130/GSAB-55-1279

Stidd, CK., and Leopold, L.B., 1948, The geographic distribution of average monthly rainfall, Hawaii: American Meteorological Society Meteorological Monographs, v. 1, p. 23-33.

Stimson, J., Larned, S.T., and Conklin, E., 2001, Effects of herbivory, nutrient levels, and introduced algae on the distribution and abundance of the invasive macroalga Dictyosphaeria cavernosa in Kaneohe Bay, Hawaii: Coral Reefs, v. 19, p. 343-357. DOI: 10.1007/s003380000123.

Street, J.H., Knee, K.L., Grossman, E.E., and Paytan, A., 2008, Submarine groundwater discharge and nutrient addition to the coastal zone and coral reefs of leeward Hawai'i: Marine Chemistry 109, 355–376.

Stumm, W., and Morgan, J.J., 1995, Aquatic Chemistry: Chemical Equilibria and Rates in Natural Waters, 3rd Edition: New York, John Wiley & Sons, Inc.

Takasaki, K.J., Hirashima, G.T., and Lubke, E.R., 1969, Water resources of windward Oʻahu, Hawaiʻi: US Geological Survey Water-Supply Paper 1894, 129 p.

Takasaki, K.J., and Mink, J.F., 1981, Evaluation of major dike-impounded Groundwater reservoirs, Island of Oahu: U.S. Geological Survey Open-File Report 81-1119, 154 p.

Takasaki, K.J., and Mink, J.F., 1982, Water resources of Southeastern Oʻahu, Hawaiʻi: U.S. Geological Survey Water-Resources Investigations 82-628, 97 p.

Terluow, G.J., 2017, Temporal trends in the CO2 content of Hawaiian coastal waters and climatic drivers: an eight year time-series perspective [M.S. Thesis]: Honolulu, University of Hawaiʻi at Mānoa.

U.S. Census Bureau, 2017, www.census.gov/data.

United Nations Environment Programme, 2011, Freshwater under threat Pacific Islands: Vulnerability assessment of freshwater resources to environmental change, 66 p.

U.S. EPA, 2018, National Primary Drinking Water Regulations, 6 p.

van Beukering, P.J.H., and Cesar, H., 2004, Ecological economic modeling of coral reefs: evaluating tourist overuse at Hanauma Bay and algae blooms at the Kīhei Coast, Hawai‘i: Pacific Science, v. 28, p. 243-260.

Vengosh, A., Heumann, K.G., Juraske, S., and Kasher, R., 1994, Boron isotope application for tracing sources of contamination in groundwater: Environmental Science and Technology, v. 28, p. 1968-1974.

Walker, G.P.L., 1986, Koolau Dike Complex, Oahu: intensity and origin of a sheeted-dike complex high in a Hawaiian volcanic edifice: Geology v. 14, p. 310-313.

Walker, G.P.L., 1987, The dike complex of Koolau Volcano, Oahu: Internal structure of a Hawaiian rift zone: U.S. Geological Society Professional Paper 1350, Volcanism In Hawaii, Chapter 4, p. 961-993.

Walker, G.P.L., and Eyre, P.R., 1995, Dike complexes in American Samoa: Journal of Volcanology and Geothermal Research, v. 69, p. 241-254.

Wang, H., Gau, J.E., Zhang, M.J., Li, X.H, Zhang, S.L., and Jia, L.Z., 2015, Effects of rainfall intensity on groundwater recharge based on simulated rainfall experiments and a groundwater flow model: Catena, v. 127, p. 80-91. DOI: 10.1016/j.catena.2014.12.014

Whittier, R.B., and El-Kadi, A.I., 2009, Human Health and Environmental risk ranking of onsite sewage disposal systems: Final Report, prepared for the State of Hawaii Department of Health.

Whittier, R.B., and El-Kadi, A.I., 2014. Human Health and Environmental risk ranking of on-site sewage disposal systems for the Hawaiian Islands of Kauai, Molokai, Maui, and Hawaii: Final Report, prepared for the State of Hawaii Department of Health.

Widory, D., Petelet-Giraud, E., Négrel, P, and Ladouche, B., 2005, Tracking the sources of nitrate in groundwater using coupled nitrogen and boron isotopes: a synthesis: Environmental Science and Technology, v. 39, p. 539-548.

Wiedenmann, J., D’Angelo, C., Smith, E., Hunt, A.N., Legiret, F.-E., Postle, A.D., and Achterberg, E., 2013, Nutrient enrichment can increase the susceptibility of reef corals to leaching: Nature Climate Change 3, p. 160-164. DOI: 10.1038/NCLIMATE1661.

Wiegner, T.N., Mokiau-Lee, A.U., and Johnson, E.E., 2016, Identifying nitrogen sources to thermal tide pools in Kapoho, Hawai‘i, U.S.A. using a multi-stable isotope approach: Marine Pollution Bulletin, v. 103, p. 63-71.

Wong, Y.S., Tam, N.F.Y., and Lan, C.Y., 1997, Mangrove wetlands as wastewater treatment facility: a field trial: Hydrobiologia, v. 352, p. 49-59.

World Health Organization, 2011, Nitrate and nitrite in drinking-water, 31 p.

Wu, Y., Chung, A., Tam, N.F.Y., Pi, N., and Wong, M.H., 2008a, Constructed mangrove wetland as secondary treatment system for municipal wastewater: Ecological Engineering, v. 34, p. 137-146. DOI:10.1016/j.ecoleng.2008.07.010.

Wu, Y., Tam, N.F.Y., and Wong, M.H., 2008b, Effects of salinity on treatment of municipal wastewater by constructed mangrove wetland microcosms: Marine Pollution Bulletin, v. 57, p. 727-734. DOI: 10.1016/j.marpolbul.2008.02.026.

Xue, D., Botte, J., De Baets, B., Accoe, F., Nestler, A., Taylor, P., Van Cleemput, O., Berglund, M., and Boeckx, P., 2009, Present limitations and future prospects of stable isotope methods for nitrate source identification in surface- and groundwater: Water Research, v. 43, p. 1159-1170. DOI: 10.1016/j.watres.2008.12.048.

Yang, Q., Tam, N.F.Y., Wong, Y.S., Luan, T.G., Su, W.S., Lan, C.Y., Shin, P.K.S., and Cheung, S.G., 2008, Potential use of mangroves as constructed wetland for municipal sewage treatment in Futian, Shenzhen, China: Marine Pollution Bulletin, v. 57, p. 735-743. DOI: 10.1016/j.marpolbul.2008.01.037

Zbinden, E.A., and Stinton, J.M., 1988, Dikes and the petrology of Waianae Volcano, Oahu: Journal of Geophysical Research, v. 93, p. 14,856-14,866.

Zeebe, R.E., 2005, Stable boron isotope fractionation between dissolved $B(OH)_3$ and $B(OH)_4^-$: Geochimica et Cosmochimica, v. 69, p. 2753-2766. DOI:10.1016/j.gca.2004.12.011